

อันตรกิริยาของยาต้านมาลาเรียระหว่างผิวของระบบจำลองเนื้อเยื่อ



วิทยานิพนธ์นี้เป็นส่วนหนึ่งของการศึกษาตามหลักสูตรปริญญาวิทยาศาสตรดุษฎีบัณฑิต

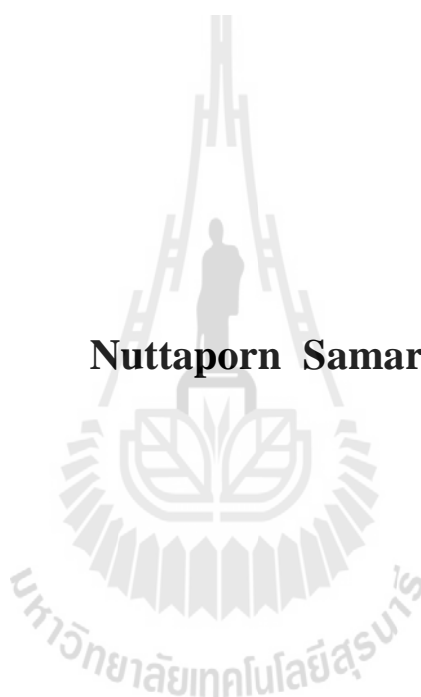
สาขาวิชาเคมี

มหาวิทยาลัยเทคโนโลยีสุรนารี

ปีการศึกษา 2557

**INTERACTION OF ANTIMALARIAL DRUGS WITH
THE INTERFACE OF MODEL MEMBRANE SYSTEMS**

Nuttaporn Samart



**A Thesis Submitted in Partial Fulfillment of the Requirements for the
Degree of Doctor of Philosophy in Chemistry
Suranaree University of Technology
Academic Year 2014**

INTERACTION OF ANTIMALARIAL DRUGS WITH THE INTERFACE OF MODEL MEMBRANE SYSTEMS

Suranaree University of Technology has approved this thesis submitted in partial fulfillment of the requirements for the Degree of Doctor of Philosophy.

Thesis Examining Committee

(Assoc. Prof. Dr. Anan Tongraar)

Chairperson

(Assoc. Prof. Dr. Jatuporn Wittayakun)

Member (Thesis Advisor)

(Prof. Dr. Debbie C. Crans)

Member

(Assoc. Prof. Dr. Jaruwan Siritapetawee)

Member

(Dr. Theeranun Siritanon)

Member

(Prof. Dr. Sukit Limpijumnong)

Vice Rector for Academic Affairs
and Innovation

(Assoc. Prof. Dr. Prapun Manyum)

Dean of Institute of Science

ณัฐพร สามารถ : อันตรกิริยาของยาต้านมาลาเรียระหว่างผิวของระบบจำลองเนื้อเยื่อ
(INTERACTION OF ANTIMALARIAL DRUGS WITH THE INTERFACE OF MODEL
MEMBRANE SYSTEMS) อาจารย์ที่ปรึกษา : รองศาสตราจารย์ ดร.จตุพร วิทยาคูณ,
133 หน้า.

การแทรกซึมผ่านเนื้อเยื่อเป็นสิ่งสำคัญสำหรับการแสดงความมีประสิทธิภาพของยา จึงทำ
การวิเคราะห์ การเกิดอันตรกิริยาระหว่างสารตั้งต้นยามาลาเรียชนิด 1-พีนิลไปกัวไนด์ (PBG) กับ
อันตรกิริยาระหว่างผิว โดยใช้ระบบแบบจำลองรีเวอร์สไมเซลล์ ในการศึกษาด้วย $^1\text{H-NMR}$ โดยค
การข้ามผ่านของ PBG ระหว่างชั้นผิวของเนื้อเยื่อ เพื่อให้เจาะจงมากขึ้น จากการศึกษาด้วยโปรตอน
NMR แสดงให้เห็นว่าสิ่งแวดล้อมของสารประกอบ PBG ในสารละลายที่มีการเปลี่ยนแปลงเมื่อถูก
วางอยู่ใกล้รอยต่อระหว่างชั้น โดยปกติ PBG จะมีพันธะกับไฮโดรเจนของน้ำและถ้าขนาดของไม
เซลล์ที่เกิดจากการผันกลับมีขนาดเปลี่ยนไป จะส่งผลให้การเปลี่ยนแปลงของน้ำในระบบ
เปลี่ยนแปลงไปด้วย นอกจากนี้ยังพบว่า สเปกตรัม NOSEY ของ PBG ใน AOT รีเวอร์สไมเซลล์ มี
สัญญาณที่ปรากฏเหลื่อมล้ำกันระหว่าง โปรตรอนของ PBG และ โปรตรอนของ AOT ซึ่งแสดงให้เห็น
เห็นความสัมพันธ์ PBG ต่อพื้นผิว และในขณะเดียวกันก็มีสัญญาณที่เหลื่อมล้ำกันระหว่างสัญญาณ
ของส่วนที่เป็นไปกัวไนด์ และสัญญาณของ HOD แสดงให้เห็นว่า โปรตรอนของหมู่เอมีน (NH) อยู่
ใกล้กับโปรตรอนของ HOD เป็นการนำหมู่ฟังก์ชันไปกัวไนด์ในก้อนน้ำ จากการศึกษาเบื้องต้น
ยืนยันผลการทดลองโดยการศึกษาด้วยวิธีเฟอเรนเซียลฟูเรียร์ทรานฟอร์มอินฟราเรดสเปกโทรส
โกปี (FTIR) เพื่อยืนยันตำแหน่งดังกล่าว กล่าวโดยสรุปคือ พบว่า PBG สามารถเกิดอันตรกิริยากับ
บริเวณส่วนต่างๆ ของชั้นระหว่างผิว โดยใช้หมู่พีนิลแทรกเข้าไประหว่างผิวในส่วนที่ไม่ชอบน้ำ
ในขณะที่หมู่ไปกัวไนด์ยังอยู่ในส่วนที่เป็นก้อนน้ำ

NUTTAPORN SMART : INTERACTION OF ANTIMALARIAL DRUGS
WITH THE INTERFACE OF MODEL MEMBRANE SYSTEMS.

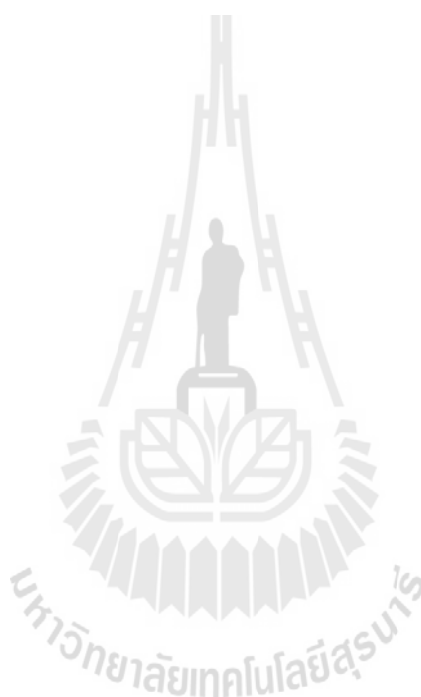
THESIS ADVISOR : ASSOC. PROF. JATUPORN WITTAYAKUN, Ph.D.

133 PP.

BIGUANIDE/1-PHENYLBIGUANIDE/MODEL MEMBRANE SYSTEM/AOT
REVERSE MICELLES/NMR SPECTROSCOPY/INTERFACE INTERACTION

Since membrane penetration is important for drug efficacy, how the antimalarial precursor material 1-phenylbiguanide (PBG) interacts with an interface was characterized using a reverse micelle (RM) model system. ^1H NMR studies show that PBG partitions across the membrane interface. Specifically, the ^1H NMR studies showed that the 1-phenylbiguanide compound in an aqueous environment changed when placed near an interface. PBG is known to affect hydrogen bonding in water, and as the size of the RMs changes, the water organization in the water pool is changed. The Nuclear Overhauser Effect Spectroscopy (NOESY) spectrum of PBG in sodium bis(2-ethylhexyl)sulfosuccinate (AOT) RM contains cross-peak signals between the PBG protons and AOT protons, which is consistent with the penetration of the PBG into the interface. At the same time, there is a cross peak between the biguanide moiety and the HOD signal. This shows that these NH protons are near the HOD protons, placing the biguanide functional group in the water pool. Preliminary differential Fourier transform infrared spectroscopy (FTIR) studies confirmed this location. In summary, we found that PBG interacts with different regions of the

interface, with the phenyl group penetrating the hydrophobic interface while the biguanide remains in the water pool.



School of Chemistry

Student's Signature_____

Academic Year 2014

Advisor's Signature_____

ACKNOWLEDGEMENTS

I would first like to thank my advisors, Assoc. Prof. Dr. Jatuporn Wittayakun and Assoc. Prof. Dr. Kenneth J. Haller, from whom I have learned a great deal. Without their guidance and persistent help and support, this dissertation would not have been possible. I would also like to extend my sincerest gratitude to Prof. Dr. Debbie C. Crans, Colorado State University, USA for her help and assistance as coadvisor. Thank you for chemicals, equipment, support, and inspiring advice during my overseas research in the USA. My appreciation also goes to chairman of the School of Chemistry, Assoc. Prof. Dr. Anan Tongraar and my committee members, Assoc. Prof. Dr. Jaruwan Siritapetawee and Dr. Theeranun Siritanon, for their warm hearted support, encouragement, help, and suggestions.

I would additionally like to thank each member of Crans and Levinger research groups. Without the support from the group members, I would not have been able to finish this work. Their willingness to drop what they were doing to help me out when I was having trouble with an experiment or trying to synthesize something, meant a lot to me. Thanks are also given to my other friends at CSU and SUT for all their support, help, and encouragement throughout the time of my studies.

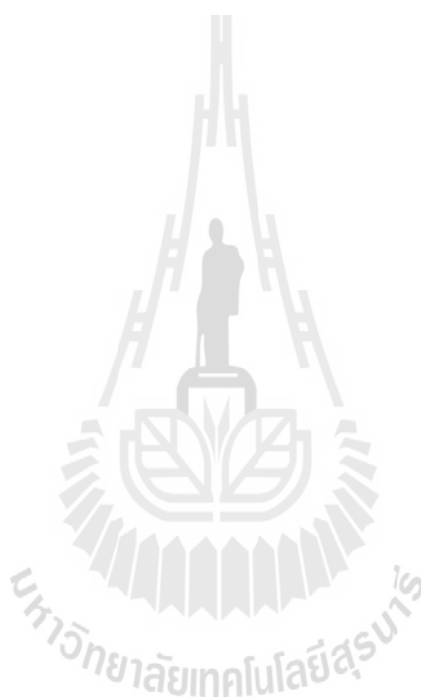
I would also like to thank all lectures at the School of Chemistry, Suranaree University of Technology for their good attitude and advice.

Thank you to the Commission on Higher Education, Thailand for financial support (CHE-PHD-SW-2551) of my Ph.D. program and an overseas travel grant

allowing me to spend one year at CSU as part of my Ph.D. research program, and for opportunities to present parts of my work at international conferences.

Finally, I would like to take this opportunity to express my deepest appreciation and sincerest gratitude to my parents, sister, brother, and my son for their love, devotion, understanding, consolation, and encouragement throughout the long years of my study. Without their love and understanding this work would not have been successful.

Nuttaporn Samart



CONTENTS

	Page
ABSTRACT IN THAI.....	I
ABSTRACT IN ENGLISH	II
ACKNOWLEDGEMENTS.....	IV
CONTENTS.....	VI
LIST OF TABLES	X
LIST OF FIGURES	X
LIST OF SYMBOLS AND ABBREVIATIONS	XIII
CHAPTER	
I INTRODUCTION.....	1
1.1 Malaria	2
1.2 Reverse micelle systems.....	7
1.3 Surfactants.....	10
1.3.1 Anionic surfactants	10
1.3.2 Cationic surfactants.....	11
1.3.3 Nonionic surfactants	13
1.3.4 Zwitterionic surfactants.....	14
1.4 Water pool.....	15
1.5 NMR spectroscopy.....	16
1.5.1 Nuclear Overhauser Effect (NOE).....	16

CONTENTS (Continued)

	Page
1.5.2 2D NMR spectroscopy.....	18
1.6 Probe molecules	19
1.7 Research goals.....	20
1.8 Scope and limitations of the study	21
1.9 References	21
II EXPERIMENTAL	32
2.1 Material	32
2.2 Preparation of samples for analysis.....	32
2.2.1 Anionic reverse micelles	32
2.2.2 Cationic reverse micelles	35
2.2.3 Preparation of AOT/isooctane stock solution and reverse micelle	37
2.2.4 Preparation aqueous stock solutions 1-Phenylbiguanide (PBG)	37
2.2.5 Preparation of AOT/isooctane reverse micelle with 1-phenylbiguanide (PBG) for 1D ¹ H NMR spectroscopic studies.....	37
2.2.6 Preparation of the 2D ¹ H NMR NOESY sample in AOT reverse micelle solution with PBG.....	37
2.2.7 Preparation of the FTIR sample in AOT reverse micelle solution with PBG	38

CONTENTS (Continued)

	Page
2.2.8 Preparation of CTAB reverse micelle solution with 1-phenylbiguanide (PBG)	38
2.3 Methods.....	39
2.3.1 1D NMR spectroscopy	39
2.3.2 2D NMR spectroscopy	39
2.3.2 FTIR spectroscopy	40
2.4 Research procedure	40
2.5 Research procedure	41
III RESULTS	43
3.1 Results.....	43
2.3.1 NMR spectra and properties of 1-phenylbiguanide (PBG).....	43
2.3.2 1-Phenylbiguanide (PBG) in AOT/isooctane RMs: ^1H NMR spectroscopic studies	45
2.3.3 1-Phenylbiguanide (PBG) in AOT reverse micelle 2D NOESY study.....	50
2.3.4 1-Phenylbiguanide (PBG) in AOT/isooctane RMs: FTIR spectroscopic studies	53
2.3.5 1-Phenylbiguanide (PBG) in CTAB/pentanol/cyclohexane RMs: ^1H NMR spectroscopic studies.....	55
3.2 Referencels.....	55

CONTENTS (Continued)

	Page
IV DISCUSSION	61
4.1 References	61
V CONCLUSION	70
APPENDICES	72
APPENDIX A INTERACTION OF BIGUANIDE COMPOUND WITH MODEL MEMBRANE INTERFACE SYSTEM: PROBING PROPERTIES OF ANTIMALARIA AND ANTIDIABETIC COMPOUNDS	73
APPENDIX B GUANYLUREAMETFORMIN DOUBLE SALT OF DECAVANADATE, (HGU ⁺) ₄ (HMet ⁺) ₂ (V ₁₀ O ₂₈ ⁶⁻)·2H ₂ O	84
APPENDIX C INTERACTION OF DECAVANADATE WITH INTERFACES AND BIOLOGICAL MODEL MEMBRANE SYSTEM: CHARACTERIZATION OF SOFT OXOMETALATE SYSTEMS	106
CURRICULUM VITAE.....	114

LIST OF TABLES

Table	Page
2.1 Component volumes in 1 mL samples of 200 mM and 750 mM AOT RMs at various w_0 . ($w_0 = [\text{H}_2\text{O}]/[\text{AOT}]$).....	35
2.2 Component volumes in 1 mL samples of 150 mM CTAB/cyclohexane at various w_0 ($w_0 = [\text{H}_2\text{O}]/[\text{CTAB}]$), ratio Pentanol:CTAB (5:1).....	36
4.1 Content of RMs investigated as determined by w_0 and sizes	64

LIST OF FIGURES

Figure	Page
1.1 Structures of antimalarial drugs a) Chloroquine, b) Atovaquone/Malarone, c) Proguanil and d) Chlorproguanil	5
1.2 Various self-assembled surfactant structures. a) bilayer, b) multilayer, c) micelle, d) reverse micelle, and e) vesicle	8
1.3 Example of anionic surfactant structures	11
1.4 Example of cationic surfactant structures	12
1.5 Example of nonionic surfactant structures	13
1.6 Example of zwitterionic surfactant structure	14
1.7 The cartoon of a) AOT RM and b) CTAB with pentanol co-surfactant RM	16
1.8 Pulse sequence for a 2D NOESY experiment, illustrating the evolution of t_1 during the course of the experiment.....	18
2.1 ^1H NMR of NaAOT in d_6 -DMSO. (2.5 ppm is DMSO, and peak integration values are given below the spectrum)	34
3.1 Partial ^1H NMR spectra were recorded in D_2O of 100 mM PBG in aqueous solution at pH values between 1.0 to 12.3 measured at 400 MHz. Samples were referenced against a solution of DSS using external lock	44

LIST OF FIGURES (Continued)

Figure	Page
3.2 (above) Partial ^1H NMR spectra of 100 mM PBG at pH 1.0 in 750 mM AOT/isooctane RMs recorded at 400 MHz and referenced against the isooctane resonance at 0.904 ppm. (below) A plot of the specific chemical shift of PBG protons, Ha (■), Hb (○) and Hc (▲) as a function of w_0	46
3.3 (above) Partial ^1H NMR spectra of 50 mM PBG at pH 12.3 in 750 mM AOT/isooctane RMs recorded at 400 MHz and referenced against the isooctane resonance at 0.904 ppm. (below) A plot of the apparent specific chemical shifts of PBG, Ha (■), Hb (○) and Hc (▲) as a function of w_0	52
3.4 Partial ^1H NMR NOESY spectrum of 100 mM PBG at pD 7.07 in 750 mM AOT. The spectrum was recorded at 400 MHz using the parameters detailed in the experimental. The F2 or y-axis is zoomed in on the phenyl and nitrogen protons in PBG and the F1 or x-axis is the full spectrum. The diagonal is the solid line and prominent cross peaks are shown as dotted lines along with their respective hydrogen interactions	54
3.5 Absorbance spectra for the O–D stretch in AOT RMs containing PBG recorded at different molarities: 0 mM PBG RMs $w_0 = 10$ (-■-), pH ≈ 7.0 , 10 mM PBG RMs $w_0 = 10$ (-▲-) and 100 mM PBG RMs $w_0 = 10$ (-●-) measured using differential FTIR spectroscopy.	

LIST OF FIGURES (Continued)

Figure	Page
<p>The spectra are obtained by subtraction of AOT/isooctane RMs containing DI water from the corresponding spectra recorded in AOT/isooctane RMs containing 5% HOD for each of the three different concentrations of PBG</p>	55
<p>3.6 A cartoon illustrating the suggested location of 1-phenylbiguanide in the AOT reverse micelle</p>	57
<p>3.7 (above) Partial ^1H NMR spectra of 50 mM PBG at pH 1 in 150 mM CTAB/750 mM pentanol in cyclohexane RMs recorded at 400 MHz and referenced against the cyclohexane resonance at 1.430 ppm (below) A plot of the specific chemical shift of PBG protons, Ha (\blacktriangle), Hb (\blacksquare) and Hc (\circ) as a function of w_0 size</p>	58
<p>3.8 (above) Partial ^1H NMR spectra of 50 mM PBG at pH 1 in 150 mM CTAB/750 mM pentanol in cyclohexane RMs recorded at 400 MHz and referenced against the cyclohexane resonance at 1.430 ppm.(below) A plot of the specific chemical shift of PBG protons, Ha (\blacktriangle), Hb (\blacksquare) and Hc (\circ) as a function of w_0 size</p>	60

LIST OF SYMBOLS AND ABBREVIATIONS

Å	angstrom, non-SI unit of distance commonly used in crystallography
δ	chemical shift
5HT3	5-hydroxytryptamine
AOT	sodium bis(2-ethylhexyl)sulfosuccinate
ATR	attenuated total reflectance
BDBAC	N-benzyl-N-dodecyl-N-bis(2-hydroxy ethyl) ammonium chloride
C10E4	tetraoxyethylene monodecyl ether
COSY	correlation spectroscopy
CPC	cetyl pyridium chloride
CTAB	hexadecyl-trimethyl ammonium bromide
d1	first delay (NMR)
d2	second delay (NMR)
D ₂ O	deuterium oxide
DCl	deuterium chloride
DK-F-110	sugar ester
DLS	dynamic light scattering
DMSO	dimethyl sulfoxide
DOLPA	dioleoyl phosphoric acid
DSS	3-(trimethylsilyl)propanesulfonic

LIST OF SYMBOLS AND ABBREVIATIONS (Continued)

DTAB	dodecyltrimethyl ammonium bromide
DTDPA	di(tridecyl) phosphoric acid
F1	x-axis
F2	y-axis
FID	free induction decay
FTIR	fourier transform infrared spectroscopy
HIV	human immunodeficiency virus
HPA-23	sodium hexaoctacontaoxononaantimonateheneicosa tungstate
IDDM	insulin dependent diabetes mellitus
Met	neutral molecule form of metformin
mM	millimolar
NaDEHP	sodium ethyl hexyl phosphate
NaOD	sodium deuterioxide
n_{avg}	surfactant aggregation number
n_c	number of carbon atoms in the surfactant tail
NOE	nuclear overhauser effect
NOESY	nuclear overhauser effect spectrscopy or nuclear overhauser enhancement spectroscopy
NMR	nuclear magnetic resonance
PBG	phenylbiguanide
r	average micelle radius
r_h	radius of micelle

LIST OF SYMBOLS AND ABBREVIATIONS (Continued)

RM _s	reverse micelles
r_w	radius of water pool
SDBS	sodium dodecylbenzene sulfonate
SDS	sodium dodecyl sulfate
t	acquisition time (NMR)
t_1	first relaxation time
t_2	second relaxation time
T_1	spin-lattice relaxation (NMR)
T	temperature (K)
TMS	tetramethylsilane
TOMAC	trioctylmethyl ammonium chloride
Triton X-100	polyoxyethylene- <i>p-t</i> -octyl phenol
TTAB	tetradecyltrimethyl ammonium bromide
Tween 85	polyoxyethylene sorbitan trioleate
w_0	molar ratio of concentration of water and surfactant

CHAPTER I

INTRODUCTION

Drug uptake is critical for action of any drug, but particularly important for diseases such as malaria in which cell membrane properties are important for infection (de Souza Santos, de Morais Del Lama, Ito, and Zumstein Georgetto Naal, 2014; Fendler, 1987; Ginsburg, Famin, Zhang, and Krugliak, 1998; Griffith, Lewis, Mali, and Parise, 2007; Hindley, Ward, Storr, Searle, Bray, Park, Davies, and O'Neill, 2002; Mather, Darrouzet, Valkova-Valchanova, Cooley, McIntosh, Daldal, and Vaidya, 2005; Moura, Dame, and Fidock, 2009; Pudney, Gutteridge, Zeman, Dickins, and Woolley, 1999; Singh, Kaur, Smith, de Kock, Chibale, and Balzarini, 2014). One of the successful drugs against malaria is proguanil, Figure 1.1 (de Souza Santos, de Morais Del Lama, Ito, and Zumstein Georgetto Naal, 2014; Ginsburg, Famin, Zhang, and Krugliak, 1998; Radloff, Philipps, Nkeyi, Hutchinson, and Kremsner, 1996). Proguanil is a biguanide and is metabolized to cycloguanil, which is a dihydrofolate reductase inhibitor (Fidock, Nomura, and Wellems, 1998; Plowe, Djimde, Bouare, Doumbo, and Wellems, 1995; Pudney, Gutteridge, Zeman, Dickins, and Woolley, 1999; Ryley, 1953). Another biguanide, which is a common drug used for treatment of diabetes, is metformin (Graham, Punt, Arora, Day, Doogue, Duong, Furlong, Greenfield, Greenup, Kirkpatrick, Ray, Timmins, and Williams, 2011; Krentz, and Bailey, 2005; Scarpello, and Howlett, 2008; Tajima, Hirata, Taniguchi, Kondo, Kato, Saito-Hori, Ishimoto, and Yamamoto, 2011). Metformin can dramatically impact the

properties of other compounds, facilitate their solubility (Chatkon, Chatterjee, Sedgwick, Haller, and Crans, 2013), and is often co-administered with other drugs to help improve their uptake (Graham, Punt, Arora, Day, Doogue, Duong, Furlong, Greenfield, Greenup, Kirkpatrick, Ray, Timmins, and Williams, 2011; Scarpello, and Howlett, 2008; Tajima, Hirata, Taniguchi, Kondo, Kato, Saito-Hori, Ishimoto, and Yamamoto, 2011). No common mechanism of action for these biguanide drugs has been described (Sweeney, Raymer, and Lockwood; 2003, Wallace, Ong, and Heard, 2012). Although, it is not known if the properties of the biguanide functionality is important for the mode of action, the possibility that metal complexation is involved has been proposed (Sweeney, Raymer, and Lockwood, 2003). The amphiphilic nature and special properties of these compounds encouraged us to investigate 1-phenylbiguanide (abbreviated PBG), which is structurally related to both proguanil and metformin. Specifically, we are interested in how the properties of biguanides and associated compounds are affected near interfaces. To investigate this question, we examined the interaction of 1-phenylbiguanide with surfactant interfaces in reverse micelles (RMs) using methods that would allow identification of molecular interactions.

1.1 Malaria

Malaria is the most devastating disease afflicting humans, having been so since the dawn of history and continuing today. Malaria is a major cause of morbidity and mortality, responsible for 200 million infections and 1-3 million deaths annually, especially in Africa, and contributes significantly to economic underdevelopment. Malaria is caused by an infection of the body by Plasmodia protozoa, a type of single-

cell animal microorganism. There are many types of Plasmodia; at least ten varieties affect humans, causing the disease symptoms collectively referred to as malaria. The four principal strains infecting humans are *Plasmodium falciparum*, *vivax*, *malariae* and *ovale*. *Falciparum* causes the most fatalities, its infections leading to the often-fatal cerebral malaria. Although, plasmodia are very simple organisms, they have a complex life cycle with many different forms (Egan, 2003; Egan, Mavuso, and Ncokazi, 2001).

Antimalarial drugs, also known as antimalarials, are designed to prevent or cure malaria. Such drugs may be used for some or all of the following:

- Treatment of malaria in individuals with suspected or confirmed infection
- Prevention of infection in individuals visiting a malaria-endemic region who have no immunity (Malaria prophylaxis)
- Routine intermittent treatment of certain groups in endemic regions (Intermittent preventive therapy)

One of the most successful drugs against malaria is chloroquine (de Souza Santos, de Morais Del Lama, Ito, and Zumstein Georgetto Naal, 2014; Ginsburg, Famin, Zhang, and Krugliak, 1998; Hoyer, Nguon, Kim, Habib, Khim, Sum, Christophel, Bjorge, Thomson, Kheng, Chea, Yok, Top, Ros, Sophal, Thompson, Mellor, Arie, Witkowski, Yeang, Yeung, Duong, Newman, and Menard, 2012; Radloff, Philipps, Nkeyi, Hutchinson, and Kremsner, 1996). Chloroquine is known to accumulate in the parasite's food vacuole and inhibits heme crystallization which results in increased amounts of membrane-associated heme (Bray, Mungthin, Ridley, and Ward, 1998; de Souza Santos, de Morais Del Lama, Ito, and Zumstein Georgetto Naal, 2014; Ginsburg, Famin, Zhang, and Krugliak, 1998). Chloroquine therefore

alters the membrane properties and upsets ion homeostasis. Recently, chloroquine was also found to associate with the membrane interface in model membrane systems (Kirk, 2001). Unfortunately, chloroquine, chlorproguanil and proguanil (as shown in Figure 1.1) treatment can both result in drug resistance. Proguanil in combination with atovaquone (Figure 1.1) is available under the trade name Malarone in many countries for treatment of acute malaria caused by *Plasmodium falciparum* (Looareesuwan, Chulay, Canfield, Hutchinson, and Malarone, 1999; Ryley, 1953). Atovaquone is an ubiquinone antagonist that inhibits mitochondrial electron transport and collapses mitochondrial membrane potential (Srivastava, and Vaidya, 1999). Although proguanil converted to cycloguanil is an inhibitor for dihydrofolate reductase, genetically altered human dihydrofolate reductase did not result in resistance to proguanil (Fidock, and Wellems, 1997).



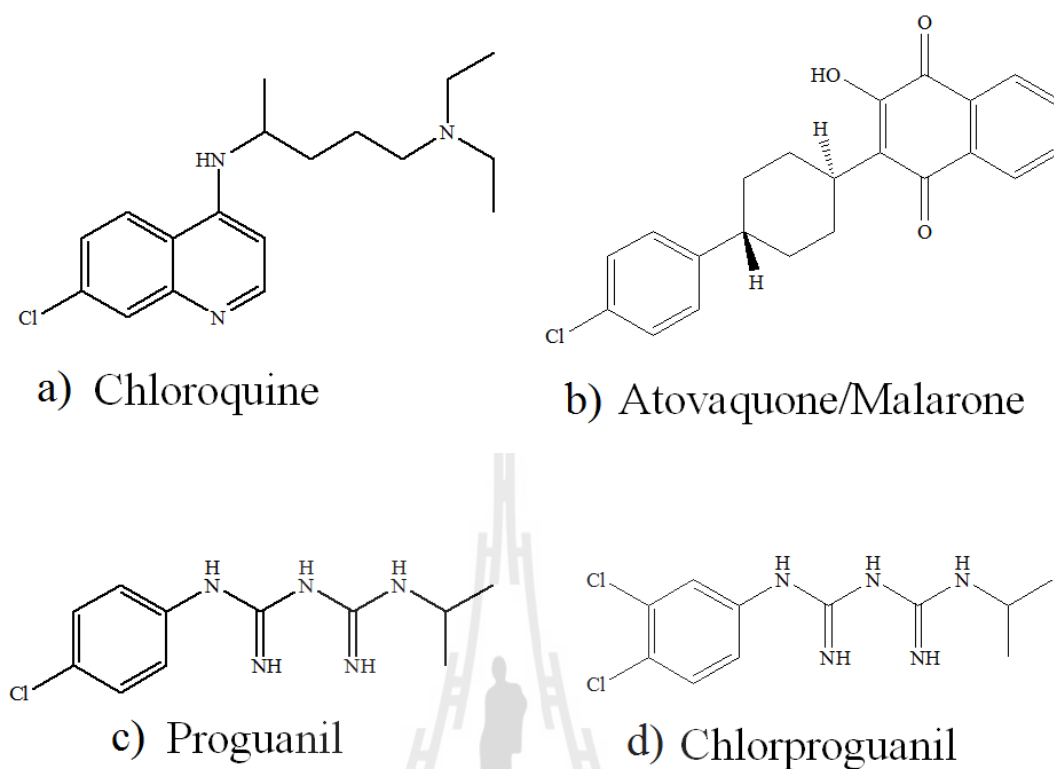


Figure 1.1 Structures of antimalarial drugs.

Proguanil is a biguanide and structurally closely related to the 1-phenylbiguanide and metformin as shown in Figure 1.1. The mode of action of metformin is poorly understood because several enzymes are inhibited by this compound (Graham, Punt, Arora, Day, Doogue, Duong, Furlong, Greenfield, Greenup, Kirkpatrick, Ray, Timmins, and Williams, 2011; Scarpello, and Howlett, 2008; Sweeney, Raymer, and Lockwood, 2003) and its physical properties could impact other compounds, membrane proteins, and membrane signaling. However, by simple structural perturbation both proguanil and metformin can form PBG, which is investigated in this study. PBG has been reported to be a selective 5-hydroxytryptamine (5HT3) receptor agonist (Chen, Vanpraag, van Praag, and

Gardner, 1991; Dukat, Abdel-Rahman, Ismaiel, Ingher, Teitler, Gyermek, and Glennon, 1996). With the exception of the possibility that metal complexation is involved (Sweeney, Raymer, and Lockwood, 2003) no mechanistic connections involving the biguanide functionality have been reported between these drugs and their modes of action. However, the simple structural modification of metformin replacing the dimethyl group with a phenyl group produced a compound able to engage in much more directed interface intercalation than reported for metformin (Chatkon, Chatterjee, Sedgwick, Haller, and Crans, 2013).

Many of the known antimalarial drugs are hydrophobic basic amines, both features which are likely to be important to their mode of action. Here we investigate how drugs containing the biguanide functionality associate with lipids or lipid-like interfaces. Such studies will allow us to evaluate whether membrane association or interactions could play a role in how these drugs work. To this end we describe here the investigation of PBG and its interaction with the sodium bis(2-ethylhexyl) sulfosuccinate (Aerosol-OT or AOT) surfactant interface as well as the cetyltrimethylammonium bromide (CTAB) interface in RMs using fourier transform infrared spectroscopy (FTIR), ^1H -Nuclear magnetic resonance (^1H NMR), and 2D-Nuclear Overhauser Effect Spectroscopy or Nuclear Overhauser Enhancement Spectroscopy (2D- NOESY) (Crans, Trujillo, Bonetti, Rithner, Baruah, and Levinger, 2008; Sedgwick, Cole, Rithner, Crans, and Levinger, 2012; Vermathen, Stiles, Bachofer, and Simonis, 2002).

1.2 Reverse micelle systems

Amphiphiles can spontaneously assemble into a range of interesting and useful structures, such as those displayed in Figure 1.2 (Luzzati, and Tardieu, 1974; Kunieda, and Shinoda, 1979). Most commonly we are familiar with lipid bilayer structures that form the basis for biological membranes (Luzzati, and Tardieu, 1974). Within these structures water exists at both the interfaces and in localized, nanoscopic pockets. It is well established that when water is confined, it has drastically different properties than it does in the bulk.

In ternary mixtures of polar, nonpolar, and amphiphilic molecules, self-assembly of the polar solvent to form nano-droplets surrounded by an amphiphilic surfactant and the nonpolar organic solvent result in the formation of RMs, Figure 1.2 (Correa, Biasutti, and Silber, 1995; De, and Maitra, 1995; Eastoe, Robinson, Steytler, and Thornleeson, 1991; Lawrence, and Rees, 2000; Maitra, 1984; Palazzo, Lopez, Giustini, Colafemmina, and Ceglie, 2003). RMs have been used for many different applications including modeling biological reactions and serving as drug delivery vessels. RMs can be prepared from a variety of surfactants, giving rise to different types of interfaces classified by the charge of their polar head groups (Correa, Durantini, and Silber, 1998; Moilanen, Levinger, Spry, and Fayer, 2007; Zingaretti, Correa, Boscatto, Chiacchiera, Durantini, Bertolotti, Rivarola, and Silber, 2005). The four classes of surfactants are anionic, cationic, zwitterionic, and nonionic (De, and Maitra, 1995; Maitra, 1984). AOT, and CTAB, that are commonly used surfactants to make RMs (Baruah, Roden, Sedgwick, Correa, Crans, and Levinger, 2006; Crans, Rithner, Baruah, Gourley, and Levinger, 2006; Lang, Jada, and Malliaris, 1988; Zulauf, and Eicke, 1979; Crans, Trujillo, Pharazyn, and Cohen, 2011; Zingaretti,

Correa, Boscatto, Chiacchiera, Durantini, Bertolotti, Rivarola, and Silber, 2005; Zulauf, and Eicke, 1979). Combining organic solvent, CTAB, a short chain alcohol and water results in a RMs with a positive interface (Gaidamauskas, Cleaver, Chatterjee, and Crans, 2010; Giustini, Palazzo, Colafemmina, Della Monica, Giomini, and Ceglie, 1996; Zulauf, and Eicke, 1979). The CTAB system is unlike the AOT reverse micelle system, as it requires the use of a cosurfactant (Gaidamauskas, Cleaver, Chatterjee, and Crans, 2010; Palazzo, Lopez, Giustini, Colafemmina, and Ceglie, 2003).

The different types of aggregates are monolayer, bilayer, lamellar (liquid crystalline phase), liposome (vesicles), micelle (in aqueous solutions), and reverse micelle (in apolar/organic solvent).

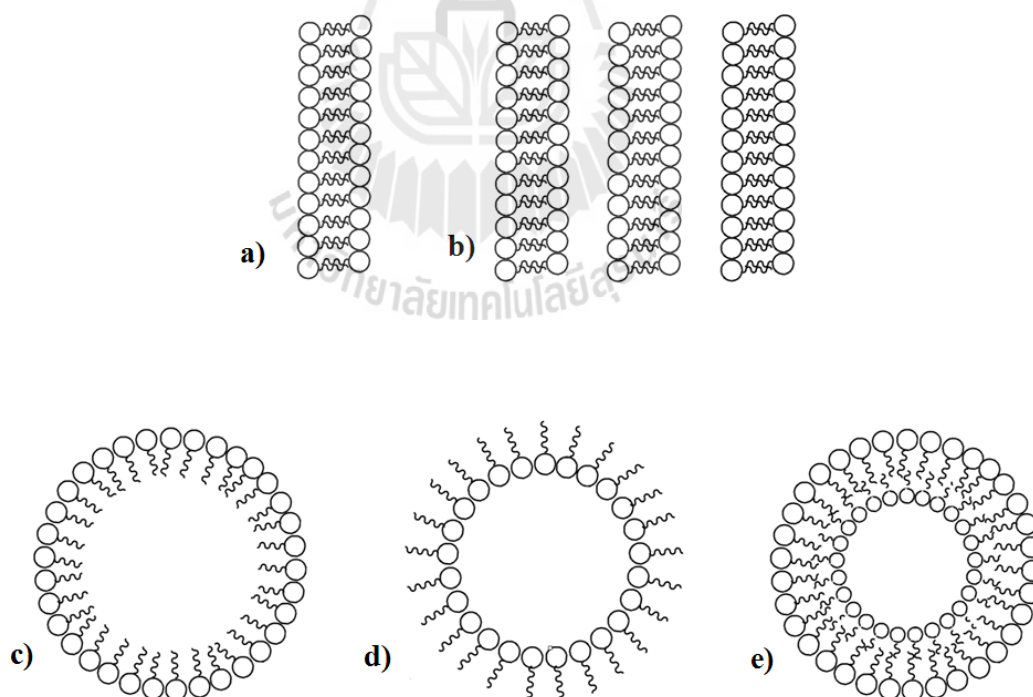


Figure 1.2 Various self-assembled surfactant structures. a) bilayer, b) multilayer, c) micelle, d) reverse micelle, and e) vesicle.

RMs form in ternary systems, comprising of a polar solvent, nonpolar solvent, and a surfactant, where the polar solvent forms a nanodroplet surrounded by surfactant, Figure 1.2 (Kumar, and Brooks, 2005; Levinger, 2002; Muller, 2004; Nave, Eastoe, Heenan, Steytler, and Grillo, 2000; Piletic, Moilanen, Spry, Levinger, and Fayer, 2006; Schubel, and Ilgenfritz, 1997; Sedgwick, Crans, and Levinger, 2009; Zhu, Feng, and Schelly, 1992). In some case, a cosurfactant is needed for reverse micelle formation (Palazzo, Lopez, Giustini, Colafemmina, and Ceglie, 2003; Shinoda, and Lindman, 1987), and typically a straight chain alcohol.

Common nonpolar solvents that are used include isooctane, cyclohexane, benzene, *n*-hexane, carbon tetrachloride and dichloroethane (Abuin, Lissi, Duarte, Silber, and Biasutti, 2002; Comiskey, Albert, Yoshizawa, and Jacobson, 1998; Kunieda, and Shinoda, 1978; Lang, Jada, and Malliaris, 1988; Lawrence, 1994; Lawrence, and Rees, 2000; Naoe, Takeuchi, Kawagoe, Nagayama, and Imai, 2007; Nave, Eastoe, Heenan, Steytler, and Grillo, 2000; Palazzo, Lopez, Giustini, Colafemmina, and Ceglie, 2003; Parent, Yang, Jeon, Toney, Zhou, and Henze, 2011; Pileni, 2003; Roberts, and Thompson, 1998; Zhu, Feng, and Schelly, 1992; Zhu, Wu, and Schelly, 1992).

In general, reverse micelles are defined by the molar ratio of the amount of water to the amount of surfactant present,

$$w_0 = \frac{[H_2O]}{[Surfactant]}$$

Reverse micelles can be made from a variety of different surfactants. One focus of the work reported in this dissertation is using anionic and cationic surfactants and the location of various probe molecules inside various reverse micelle systems.

1.3 Surfactants

A special group of lipids that possess both hydrophilic and hydrophobic parts are termed as amphiphiles or amphipathics and are also referred to as surfactants. They adsorb at surfaces or interfaces and change the interfacial free energy associated with the building of an interface. Surfactants are classified based on the composition of their polar head groups. There are four different classes of surfactants that are commonly used anionic, cationic, nonionic, and zwitterionic (Falcone, Biasutti, Correa, Silber, Lissi, and Abuin, 2004).

1.3.1 Anionic surfactants

In solution, the head group is negatively charged. This is the most widely used type of surfactant for laundering, dishwashing liquids, and shampoos because of its excellent cleaning properties and high potential. The surfactant is particularly good at keeping the dirt away from fabrics, and removing residues of fabric softener from fabrics.

Anionic surfactants are particularly effective at oily soil cleaning and oil/clay soil suspension. Still, they can react in the wash water with the positively charged water hardness ions (calcium and magnesium), which can lead to partial deactivation. The more calcium and magnesium molecules in the water, the more the anionic surfactant system suffers from deactivation. To prevent this, the anionic surfactants need help from other ingredients such as builders (Ca/Mg sequestrants) and more detergent should be dosed in hard water.

An example of anionic surfactants are alkyl sulphate, AOT, sodium dodecylbenzene sulfonate (SDBS), sodium ethyl hexyl phosphate (NaDEHP), dioleyl

phosphoric acid (DOLPA), di(tridecyl) phosphoric acid (DTDPA), and sodium dodecyl sulfate (SDS). Shown in Figure 1.3.

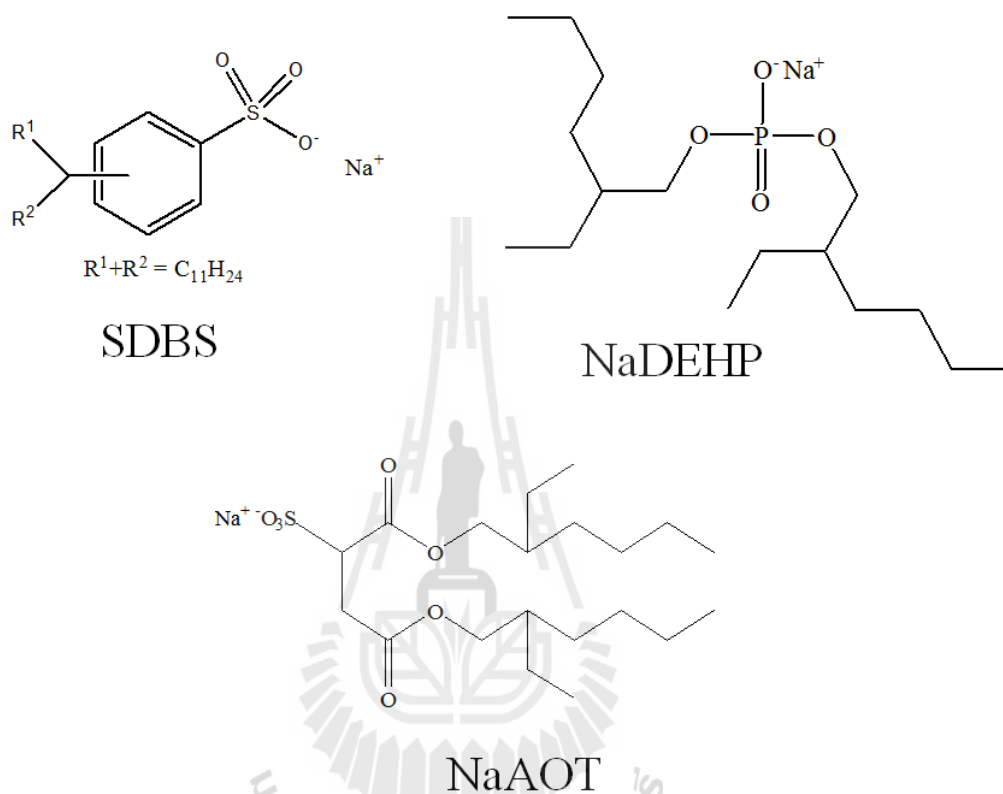


Figure 1.3 Example of anionic surfactant structures.

1.3.2 Cationic surfactants

In solution, the head group is positively charged. There are 3 different categories of cationics each with their specific application.

In fabric softeners and in detergents with built-in fabric softener, cationic surfactants provide softness. Their main use in laundry products is in rinse added fabric softeners, such as esterquats, one of the most widely used cationic surfactants in rinse added fabric softeners.

Examples of cationic surfactants are CTAB, dodecyltrimethyl ammonium bromide (DTAB), tetradecyltrimethyl ammonium bromide (TTAB), trioctylmethyl ammonium chloride (TOMAC), N-benzyl-N-dodecyl-N-bis(2-hydroxy ethyl) ammonium chloride (BDBAC), and cetyl pyridium chloride (CPC). Shown in Figure 1.4.

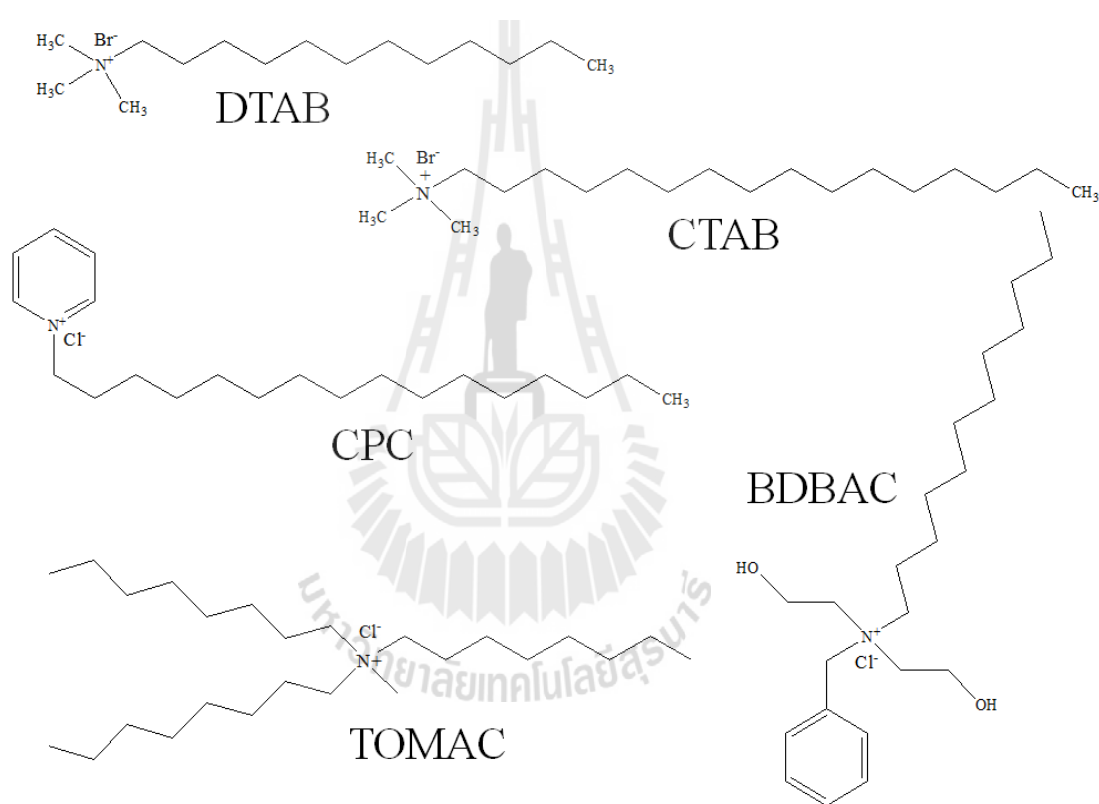


Figure 1.4 Example of cationic surfactant structures.

In laundry detergents, cationic surfactants (positive charge) improve the packing of anionic surfactant molecules (negative charge) at the stain/water interface. This

helps to reduce the water interfacial tension in a very efficient way, leading to a more robust dirt removal system. They are especially efficient at removing greasy stains.

1.3.3 Nonionic surfactants

These surfactants do not have an electrical charge, which makes them resistant to water hardness deactivation. They are excellent grease removers that are used in laundry products, household cleaners, and hand dishwashing liquids.

Most laundry detergents contain both nonionic and anionic surfactants as they complement each other's cleaning action. Nonionic surfactants contribute to making the surfactant system less hardness sensitive.

The most commonly used nonionic surfactants are polyoxyethylene sorbitan trioleate (Tween 85), sugar ester (DK-F-110), tetraoxyethylene monodecyl ether ($C_{10}E_4$), polyoxyethylene-*p*-*t*-octyl phenol (Triton X-100). Shown in Figure 1.5.

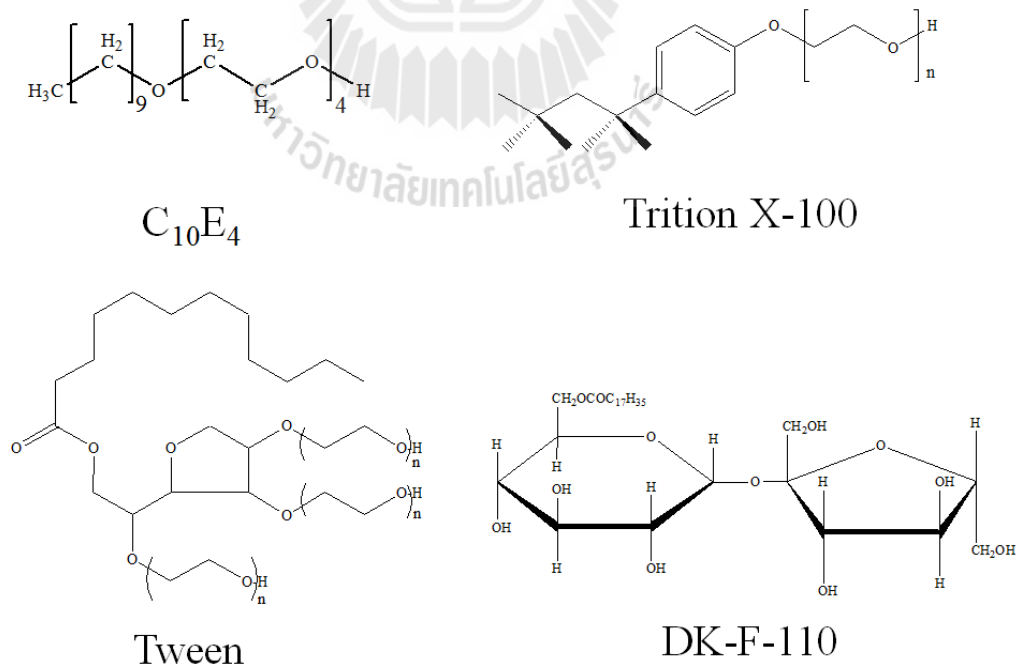
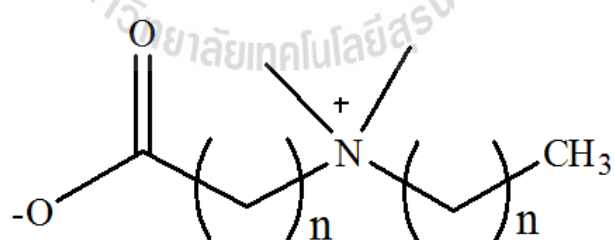


Figure 1.5 Example of nonionic surfactant structures.

1.3.4 Zwitterionic surfactants

These surfactants contain two charged groups of different sign. Whereas the positive charge is almost always ammonium, the source of the negative charge may vary such as carboxylate, sulphate, sulphonate, and phosphate). These surfactants have excellent dermatological properties. The specific zwitterionic surfactants that are being studied here are a series of molecules called trimethylammoniocarboxylates, commonly known as betaines. Betaines are a simpler zwitterionic surfactant model (Savle, Doncel, Bryant, Hubieki, Robinette, and Gandour, 1999). They have a carboxylate as a negative charge and a quaternary ammonium nitrogen as a positive charge. This characteristic yields a large dipole moment, which makes the zwitterion soluble in solutions over a wide range of pH's, salinities, and concentrations. Betaines are also assumed to be less irritating than other surfactants (Nicander, Rantanen, Rozell, Soderling, and Ollmar, 2003). Shown in Figure 1.6.



Betaine.

Figure 1.6 Example of zwitterionic surfactant structure.

1.4 Water pool

The nature of the water in the core of the reverse micelle is of great importance since proteins/enzymes (Menger, and Yamada, 1979) and other biomaterials reside in this water pool. The water pool is generally regarded to be composed of two different types of water, the bound water (lining the interior wall of the reverse micelle) and the (remaining) free water. Further subdivisions of the water pool have also been proposed. It should be stressed that water entrapped in RMs is different from bulk water and similar to water present in the vicinity of biological membranes or proteins in that it has restricted mobility, depressed freezing point, and characteristic spectroscopic properties. The unusual behavior of this water has been attributed to its strong interaction with the head groups of the surfactant as well as to overall disruption of the 3-D hydrogen bonded network usually present in bulk water.

There are a few different types of anionic surfactants that can be used to make reverse micelles. The most commonly used anionic reverse micelle system is Aerosol OT (AOT) in isooctane (Baruah, Roden, Sedgwick, Correa, Crans, and Levinger, 2006; Lang, Jada, and Malliaris, 1988; Naoe, Takeuchi, Kawagoe, Nagayama, and Imai, 2007; Zulauf, and Eicke, 1979). This system also has a large accessible w_0 range, from $w_0 = 6 \sim 30$. The surfactant AOT was used for the work reported in chapter 2-5. CTAB is one of the most commonly used cationic surfactants and is one of the surfactants used for studies reported in this work. Unlike AOT, CTAB requires the use of a cosurfactant, typically a straight chain alcohol such a 1-pentanol to make stable reverse micelles, the molar ratio of cosurfactant to surfactant used was 5:1.

Understanding the nature of the reverse micelle systems is key to understanding and predicting the behavior of other molecules in the reverse micelles. The work

presented in this dissertation focuses on the differences between anionic, and cationic reverse micelles. Details for how to make reverse micelle solutions are presented in chapter 2.

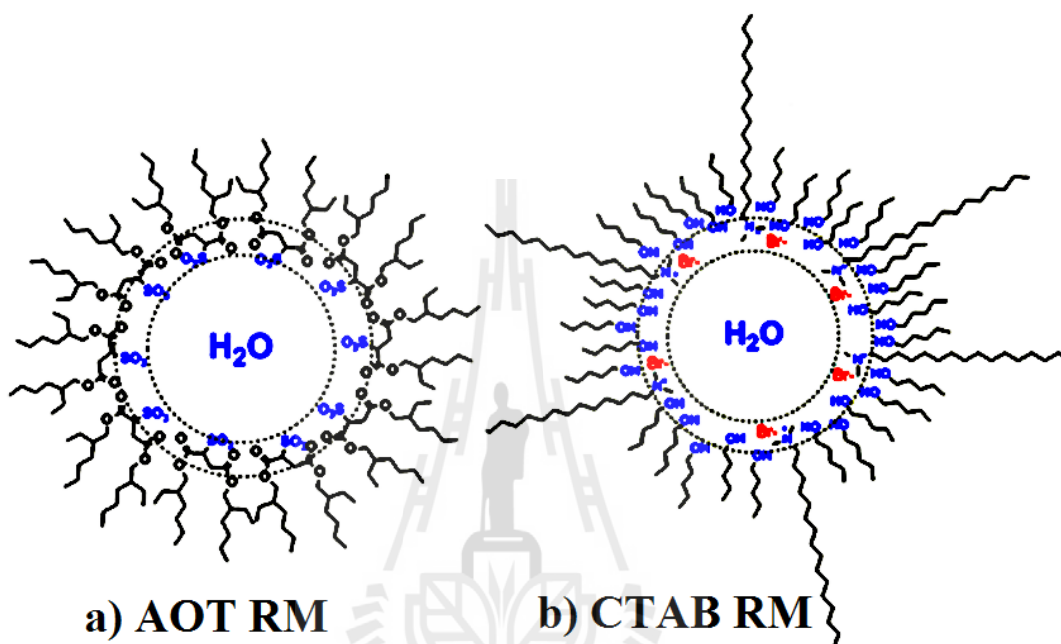


Figure 1.7 Cartoon schematic drawings of characteristic RMs.

1.5 Nuclear Magnetic Resonance (NMR) Spectroscopy

^1H NMR solution spectra were recorded on a INOVA 400 MHz spectrometers (Varian, USA). Tetramethylsilane (TMS) was used as an internal reference (0.00 ppm) for PBG in organic solvent.

1.5.1 Nuclear Overhauser Effect (NOE)

When one nuclear spin in a system is perturbed, the net intensities of other spins in the system may be affected. When this perturbation is brought about by dipole-dipole cross relaxation, it is known as the nuclear Overhauser effect, NOE. (Neuhaus, and Williamson, 1995). The benefit of this type of interaction is that it does occur

through space as well as through bond. This implies that one can identify spins on atoms that are located spatially close to each other that are not close to each other on a molecule through bond. Typically this technique is used to elucidate conformational changes or folding for macromolecules and proteins (Neuhaus, and Williamson, 1995). To describe the NOE, for convenience; if we consider a two spin $\frac{1}{2}$ systems (nuclei like H), the NOE interaction adds two more energy levels to the energy level diagram. The pulse sequence starts as usual with a 90° pulse followed by an relaxation time t_1 . This delay is varied systematically as usual to provide chemical shift information in the F1 domain. Then a 90° pulse transmits some of the magnetization to the Z axis and during the following mixing period, the nonequilibria Z component will exchange magnetization through relaxation (dipole-dipole mechanism). This exchange of magnetization is known as NOE. After some time (shorter than the relaxation time t_1), the transverse magnetization is restored and detected. If relaxation exchange (or chemical exchange) have taken place during the mixing time, cross peaks will be observed in the spectra as shown in Figure 1.8.

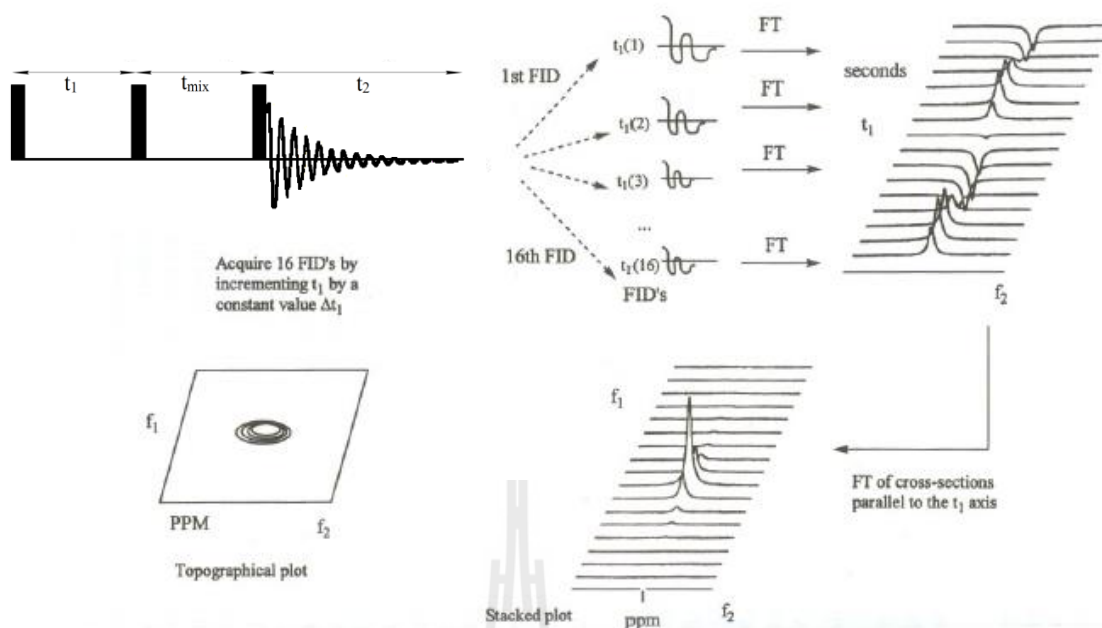


Figure 1.8 Pulse sequence for a 2D NOESY experiment, illustrating the evolution of t_1 during the course of the experiment.

1.5.2 2D NMR Spectroscopy

NOESY is a method in which all the nuclei that are spatially close can be observed simultaneously. This can be a powerful tool in elucidating the structure and conformation of certain molecules and systems. This type of experiment is not without its disadvantages, mainly the time requirement to acquire a decent spectrum. Experiments can take hours to complete depending on how many transients are collected. These methods establish correlations between nuclei which are physically close to each other regardless of whether there is a bond between them. They use the NOE by which nearby atoms (within about 5 Å) undergo cross relaxation by a mechanism related to spin-lattice relaxation.

In NOESY, the nuclear overhauser cross relaxation between nuclear spins during the mixing period is used to establish the correlations. The spectrum obtained is similar to correlation spectroscopy (COSY), with diagonal peaks and cross peaks, however the cross peaks connect resonances from nuclei that are spatially close rather than those that are through-bond coupled to each other. NOESY spectra also contain extra *axial peaks* which do not provide extra information and can be eliminated through a different experiment by reversing the phase of the first pulse. One application of NOESY is in the study of large biomolecules such as in protein NMR, which can often be assigned using sequential walking.

The NOESY experiment can also be performed in a one-dimensional fashion by preselecting individual resonances. The spectra are read with the preselected nuclei giving a large, negative signal while neighboring nuclei are identified by weaker, positive signals. This only reveals which peaks have measurable NOEs to the resonance of interest but takes much less time than the full 2D experiment. In addition, if a preselected nucleus changes environment within the time scale of the experiment, multiple negative signals may be observed.

1.6 Probe molecules

Biguanide is the organic compound with the formula $\text{HN}(\text{C}(\text{NH})\text{NH}_2)_2$. It is a colorless solid that dissolves in water to give highly basic solution. These solutions slowly hydrolyse to ammonia and urea. A variety of derivatives of biguanide are used as pharmaceutical drugs, including for treatment of hyperglycemia, malaria, and

microbial and viral infections. Biguanide is a strong organic base with $pK_1 = 12.8$ and $pK_2 = 3.1$ at 25 °C.

a) Metformin is a biguanide derivative with two methyl groups substituted for the H atoms of one terminal $-NH_2$ group. Metformin has the strong basic character of a biguanide moiety; $pK_1 = 2.8$ and $pK_2 = 11.5$.

b) Proguanil is of synthetic origin and is a biguanide derivative with a $CH(CH_3)_2$ group substituted for one H atom of one terminal $-NH_2$ group and a 4-chlorophenyl group substituted for one H atom of the other terminal $-NH_2$ group (see Figure 1.1). It belongs to dihydrofolate reductase inhibitor pharmacological group on the basis of mechanism of action and is also classified in the antimalarial agent pharmacological group. When taken, it is converted to the active metabolite cycloguanil. The molecular weight of proguanil HCl is 290.20. It has $pK_1 = 2.3$ and $pK_2 = 10.4$.

c) Phenylbiguanide is a biguanide derivative with phenyl groups substituted for the H atoms of one terminal $-NH_2$ group (see Figure 1.1). It is a 5-HT₃ (serotonin) receptor agonist, and has been used in many studies as a “selective” agonist to elicit reflex bradycardia and hypotension through activation of cardiac and pulmonary vagal afferents. Because have reported that endogenous 5-HT stimulates is chemically sensitive abdominal sympathetic afferents through 5-HT₃ receptors. Phenylbiguanide has the strong basic character of a biguanide moiety; $pK_1 = 2.13$ and $pK_2 = 10.76$.

1.7 Research goals

- (a) Malaria is a problem in Thailand. Difficult illness to treat; a few successful drugs.

- (b) Study how drugs is taken up and enter cells. Important to know how effective it is.
- (c) A better understanding will help develop new and more effective drug delivery.

1.8 Scope and limitations of the study

- (a) To study the spectroscopy and interaction of antimalarial drug and drug-like compounds in AOT and CTAB RMs.
- (b) Investigation parameters may include w_0 , pH, and concentration system, additives or other parameters affecting the reverse micelle system.
- (c) Characterization of the systems will begin with 1D and 2D NMR and FTIR spectroscopies technique to elucidate parameters of the interaction of the drug or drug-like probe with the environment in the reverse micelle systems.

1.9 References

- Abuin, E., Lissi, E., Duarte, R., Silber, J. J., and Biasutti, M. A. (2002). Solubilization in AOT–Water Reverse Micelles. Effect of the External Solvent. **Langmuir**. 18: 8340-8344.

- Baruah, B., Roden, J. M., Sedgwick, M., Correa, N. M., Crans, D. C., and Levinger, N. E. (2006). When Is Water Not Water? Exploring Water Confined in Large Reverse Micelles Using a Highly Charged Inorganic Molecular Probe. **Journal of the American Chemical Society**. 128: 12758-12769.
- Bray, P. G., Mungthin, M., Ridley, R. G., and Ward, S. A. (1998). Access to hematin: The basis of chloroquine resistance. **Molecular Pharmacology**. 54: 170-179.
- Chatkon, A., Chatterjee, P. B., Sedgwick, M. A., Haller, K. J., and Crans, D. C. (2013). The antidiabetic compound formed from metformin and decavanadate complex: Counterion affects interaction with interfaces. **Inorganic Chemistry**. 1859-1868.
- Chen, J. P., Vanpraag, H. M., van Praag, H. M., and Gardner, E. L. (1991). Activation of 5-HT₃ receptor by 1-phenylbiguanide increases dopamine release in the rat nucleus accumbens. **Brain Research**. 543: 354-357.
- Comiskey, B., Albert, J. D., Yoshizawa, H., and Jacobson, J. (1998). An electrophoretic ink for all-printed reflective electronic displays. **Nature**. 394, 253-255.
- Correa, N. M., Biasutti, M. A., and Silber, J. J. (1995). Micropolarity of reverse micelles of aerosol-OT in *n*-hexane. **Journal of Colloid and Interface Science**. 172: 71-76.
- Correa, N. M., Durantini, E. N., and Silber, J. J. (1998). Binding of nitrodiphenylamines to reverse micelles of AOT in *n*-hexane and carbon tetrachloride: Solvent and substituent effects. **Journal of Colloid and Interface Science**. 208: 96-103.

- Crans, D. C., Rithner, C. D., Baruah, B., Gourley, B. L., and Levinger, N. E. (2006). Molecular Probe Location in Reverse Micelles Determined by NMR Dipolar Interactions. **Journal of the American Chemical Society**. 128: 4437-4445.
- Crans, D. C., Trujillo, A. M., Bonetti, S., Rithner, C. D., Baruah, B., and Levinger, N. E. (2008). Penetration of Negatively Charged Lipid Interfaces by the Doubly Deprotonated Dipicolinate. **The Journal of Organic Chemistry**. 73: 9633-9640.
- Crans, D. C., Trujillo, A. M., Pharazyn, P., and Cohen, M. (2011). How environment affects drug activity: Localization, compartmentalization and reactions of a vanadium insulin-enhancing compound, dipicolinatooxovanadium(V). **Coordination Chemistry Reviews**.
- De, T., and Maitra, A. (1995). Solution behavior of Aerosol OT in nonpolar solvents. **Advances in Colloid and Interface Science**. 59: 95-193.
- de Souza Santos, M., de Morais Del Lama, M. P. F., Ito, A., and Zumstein Georgetto Naal, R. M. (2014). Binding of chloroquine to ionic micelles: Effect of pH and micellar surface charge. **Journal of Luminescence**. 147: 49-58.
- Dukat, M., Abdel-Rahman, A. A., Ismaiel, A. M., Ingher, S., Teitler, M., Gyermek, L., and Glennon, R. A. (1996). Structure Activity Relationships for the Binding of Arylpiperazines and Arylbiguanides at 5-HT₃ Serotonin Receptors. **Journal of Medicinal Chemistry**. 39: 4017-4026.
- Durfor, C. N., Bolin, R. J., Sugasawara, R. J., Massey, R. J., Jacobs, J., and Schultz, P. G. (1988). **Journal of the American Chemical Society**. 110: 8713.

- Eastoe, J., Robinson, B. H., Steytler, D. C., and Thornleeson, D. (1991). Structural Studies of Microemulsions Stabilized by Aerosol-OT. **Advances in Colloid and Interface Science**. 36: 1-31.
- Egan, T. J. (2003). Haemozoin (malaria pigment): A unique crystalline drug target. **Target**. 2: 115-124.
- Egan, T. J., Mavuso, W. W., and Ncokazi, K. (2001). The mechanism of β -hematin formation in acetate solution. Parallels between hemozoin formation and biomineralization processes. **Biochemistry**. 40: 204-213.
- Falcone, R. D., Biasutti, M. A., Correa, N. M., Silber, J. J., Lissi, E., and Abuin, E. (2004). Effect of the Addition of a Nonaqueous Polar Solvent (Glycerol) on Enzymatic Catalysis in Reverse Micelles. Hydrolysis of 2-Naphthyl Acetate by α -Chymotrypsin. **Langmuir**. 20: 5732-5737.
- Fendler, J. H. (1987). Atomic and molecular clusters in membrane mimetic chemistry. **Chemical Reviews**. 87: 877-899.
- Fidock, D.A., Nomura, T., and Wellem, T. E. (1998). Cycloguanil and its parent compound proguanil demonstrate distinct activities against Plasmodium falciparum malaria parasites transformed with human dihydrofolate reductase. **Molecular Pharmacology**. 54: 1140-1147.
- Gaidamauskas, E., Cleaver, D. P., Chatterjee, P. B., and Crans, D. C. (2010). Effect of Micellar and Reverse Micellar Interface on Solute Location: 2,6-Pyridinedicarboxylate in CTAB Micelles and CTAB and AOT Reverse Micelles. **Langmuir**. 26: 13153-13161.
- Ginsburg, H., Famin, O., Zhang, J. M., and Krugliak, M. (1998). Inhibition of glutathione-dependent degradation of heme by chloroquine and amodiaquine as

a possible basis for their antimalarial mode of action. **Biochemical Pharmacology**. 56: 1305-1313.

Giustini, M., Palazzo, G., Colafemmina, G., Della Monica, M., Giomini, M., and Ceglie, A. (1996). Microstructure and Dynamics of the Water-in-Oil CTAB/*n*-Pentanol/*n*-Hexane/Water Microemulsion: A Spectroscopic and Conductivity Study. **The Journal of Physical Chemistry**. 100: 3190-3198.

Graham, G. G., Punt, J., Arora, M., Day, R. O., Doogue, M. P., Duong, J. K., Furlong, T. J., Greenfield, J. R., Greenup, L. C., Kirkpatrick, C. M., Ray, J. E., Timmins, P., and Williams, K. M. (2011). Clinical Pharmacokinetics of Metformin. **Clinical Pharmacokinetics**. 50: 81-98.

Griffith, K. S., Lewis, L. S., Mali, S., and Parise, M. E. (2007). Treatment of malaria in the United States - A systematic review. **The Journal of the American Medical Association**. 297: 2264-2277.

Hindley, S., Ward, S. A., Storr, R. C., Searle, N. L., Bray, P. G., Park, B. K., Davies, J., and O'Neill, P. M. (2002). Mechanism-based design of parasite-targeted artemisinin derivatives: Synthesis and antimalarial activity of new diamine containing analogues. **Journal of Medicinal Chemistry**. 45: 1052-1063.

Hoyer, S., Nguon, S., Kim, S., Habib, N., Khim, N., Sum, S., Christophel, E.-M., Bjorge, S., Thomson, A., Kheng, S., Chea, N., Yok, S., Top, S., Ros, S., Sophal, U., Thompson, M. M., Mellor, S., Arie, F., Witkowski, B., Yeang, C., Yeung, S., Duong, S., Newman, R. D., and Menard, D. (2012). Focused Screening and Treatment (FSAT): A PCR-Based Strategy to Detect Malaria Parasite Carriers and Contain Drug Resistant *P. falciparum*, Pailin, Cambodia. **Plos One**. 7.

- Kirk, K. (2001). Membrane Transport in the Malaria-Infected Erythrocyte. **Physiological Reviews**. 81: 495-537.
- Krentz, A. J., and Bailey, C. J. (2005). Oral antidiabetic agents - Current role in type 2 diabetes mellitus. **Drugs**. 65: 385-411.
- Kumar, K. R., and Brooks, D. E. (2005). Comparison of Hyperbranched and Linear Polyglycidol Unimolecular Reverse Micelles as Nanoreactors and Nanocapsules. **Macromolecular Rapid Communications**. 26: 155-159.
- Kunieda, H., and Shinoda, K. (1978). Solution behavior of aerosol-OT/water/oil system. **Journal of Colloid and Interface Science**. 70: 577-583.
- Lang, J., Jada, A., and Malliaris, A. (1988). Structure and dynamics of water-in-oil droplets stabilized by sodium bis(2-ethylhexyl)sulfosuccinate. **The Journal of Physical Chemistry**. 92: 1946-1953.
- Lawrence, M. J. (1994). Surfactant systems: Microemulsions and vesicles as vehicles for drug delivery. **European Journal of Drug Metabolism and Pharmacokinetics**. 19: 257-269.
- Lawrence, M. J., and Rees, G. D. (2000). Microemulsion-based media as novel drug delivery systems. **Advanced Drug Delivery Reviews**. 45: 89-121.
- Levinger, N. E. (2002). Water in Confinement. **Science**. 298: 1722-1723.
- Looareesuwan, S., Chulay, J. D., Canfield, C. J., and Hutchinson, D. B. A. (1999). Malarone Clinical Trials Study, G. Malarone (R) (atovaquone and proguanil hydrochloride): A review of its clinical development for treatment of malaria. **The American Journal of Tropical Medicine and Hygiene**. 60: 533-541.
- Luzzati, V., and Tardieu, A. (1974). Lipid Phases: Structure and Structural Transitions. **The Annual Review of Physical Chemistry**. 25: 79-94.

- Maitra, A. (1984). Determination of Size Parameters of Water-Aerosol OT-Oil Reverse Micelles from Their Nuclear Magnetic Resonance Data. **The Journal of Physical Chemistry**. 88: 5122-5125.
- Mather, M. W., Darrouzet, E., Valkova-Valchanova, M., Cooley, J. W., McIntosh, M. T., Daldal, F., and Vaidya, A. B. (2005). Uncovering the molecular mode of action of the antimalarial drug atovaquone using a bacterial system. **Journal of Biological Chemistry**. 280: 27458-27465.
- Menger, F. M., and Yamada, K. (1979). Enzyme catalysis in water pools. **Journal of the American Chemical Society**. 101: 6731-6734.
- Moilanen, D. E., Levinger, N. E., Spry, D. B., and Fayer, M. D. (2007). Confinement or the nature of the interface? Dynamics of nanoscopic water. **Journal of the American Chemical Society**. 129: 14311-14318.
- Moura, P. A., Dame, J. B., and Fidock, D. A. (2009). Role of Plasmodium falciparum Digestive Vacuole Plasmepsins in the Specificity and Antimalarial Mode of Action of Cysteine and Aspartic Protease Inhibitors. **Antimicrobial Agents and Chemotherapy**. 53: 4968-4978.
- Müller, G. C. C. (2004). Physicochemical characterization of colloidal drug delivery systems such as reverse micelles, vesicles, liquid crystals and nanoparticles for topical administration. **European Journal of Pharmaceutics and Biopharmaceutics**. 58: 343-356.
- Naoe, K., Takeuchi, C., Kawagoe, M., Nagayama, K., and Imai, M. (2007). Higher order structure of Mucor miehei lipase and micelle size in cetyltrimethyl ammonium bromide reverse micellar system. **Journal of Chromatography B**. 850: 277-284.

- Nave, S., Eastoe, J., Heenan, R. K., Steyler, D., and Grillo, I. (2000). What Is So Special about Aerosol-OT? 2. Microemulsion Systems. **Langmuir**. 16: 8741-8748.
- Neuhaus, D., and Williamson, M. (1989). The Nuclear Overhauser Effect in Structure and Conformational Analysis, VCH Publishers, Inc: New York, New York.
- Nicander, I., Rantanen, I., Rozell, B., Soderling, E., and Ollmar, S. (2003). The Ability of Betaine to Reduce the Irritating Effects of Detergents Assessed Visually, Histology and by Bioengineering Methods. **Skin Research and Technology**. 9: 50-58.
- Palazzo, G., Lopez, F., Giustini, M., Colafemmina, G., and Ceglie, A. (2003). Role of the Cosurfactant in the CTAB/Water/*n*-Pentanol/*n*-Hexane Water-in-Oil Microemulsion. 1. Pentanol Effect on the Microstructure. **The Journal of Physical Chemistry B**. 107: 1924-1931.
- Parent, M. E., Yang, J., Jeon, Y., Toney, M. F., Zhou, Z.-L., and Henze, D. (2011). Influence of Surfactant Structure on Reverse Micelle Size and Charge for Nonpolar Electrophoretic Inks. **Langmuir**. 27: 11845-11851.
- Pileni, M. P. (2003). The role of soft colloidal templates in controlling the size and shape of inorganic nanocrystals. **Nature Materials**. 2: 145-150.
- Piletic, I. R., Moilanen, D. E., Spry, D. B., Levinger, N. E., and Fayer, M. D. (2006). Testing the Core/Shell Model of Nanoconfined Water in Reverse Micelles Using Linear and Nonlinear IR Spectroscopy. **The Journal of Physical Chemistry A**. 110: 4985-4999.
- Plowe, C. V., Djimde, A., Bouare, M., Doumbo, O., and Wellems, T. E. (1995). Pyrimethamine and proguanil resistance-conferring mutations in plasmodium-

- falciparum dihydrofolate-reductase-polymerase chain-reaction methodes for surveillance in africa. **The American Journal of Tropical Medicine and Hygiene**. 52: 565-568.
- Pudney, M., Gutteridge, W., Zeman, A., Dickins, M., and Woolley, J. L. (1999). Atovaquone and proguanil hydrochloride: A review of nonclinical studies. **Journal of Travel Medicine**. 6: S8-S12.
- Radloff, P. D., Philipps, J., Nkeyi, M., Hutchinson, D., and Kremsner, P. G. (1996). Atovaquone and proguanil for Plasmodium falciparum malaria. **The Lancet**. 347: 1511-1514.
- Roberts, C. B., and Thompson, J. B. (1998). Investigation of Cosolvent Effects on the Solvation of AOT Reverse Micelles in Supercritical Ethane. **The Journal of Physical Chemistry B**. 102: 9074-9080.
- Ryley, J. F. (1953). The mode of action of proguanil and related antimalarial drugs. **British Journal of Pharmacology and Chemotherapy**. 8: 424-430.
- Savle, P., Doncel, G., Bryant, S., Hubieki, M., Robinette, R., and Gandour, R. (1999). Acylcarnitine Analogues as Topical, Microbicidal Spermicides. **Bioorganic Medicinal Chemistry Letters**. 9: 2545-2548.
- Scarpello, J. H. B., and Howlett, H. C. S. (2008). Metformin therapy and clinical uses. **Diabetes and Vascular Disease Research**. 5: 157-167.
- Schubel, D., and Ilgenfritz, G. (1997). Influence of Polyethylene Glycols on the Percolation Behavior of Anionic and Nonionic Water-in-Oil Microemulsions. **Langmuir**. 13: 4246-4250.
- Sedgwick, M., Cole, R. L., Rithner, C. D., Crans, D. C., and Lvinger, N. E. (2012). Correlating Proton Transfer Dynamics To Probe Location in Confined

- Environments. **Journal of the American Chemical Society**. 134: 11904-11907.
- Sedgwick, M. A., Crans, D. C., and Levinger, N. E. (2009). What Is Inside a Nonionic Reverse Micelle? Probing the Interior of Igepal Reverse Micelles Using Decavanadate. **Langmuir**. 25: 5496-5503.
- Shinoda, K., and Lindman, B. (1987). Organized surfactant systems: Microemulsions. **Langmuir**. 3: 135-149.
- Singh, K., Kaur, H., Smith, P., de Kock, C., Chibale, K., and Balzarini, J. (2014). Quinoline-Pyrimidine Hybrids: Synthesis, Antiplasmodial Activity, SAR, and Mode of Action Studies. **Journal of Medicinal Chemistry**. 57: 435-448.
- Solomon, I. (1955). Relaxation Processes in a System of Two Spins. **Physical Review**. 99: 559-566.
- Srivastava, I. K., and Vaidya, A. B. (1999). A mechanism for the synergistic antimalarial action of atovaquone and proguanil. **Antimicrobial Agents and Chemotherapy**. 43: 1334-1339.
- Sweeney, D., Raymer, M. L., and Lockwood, T. D. (2003). Antidiabetic and antimalarial biguanide drugs are metal-interactive antiproteolytic agents. **Biochemical Pharmacology**. 66: 663-677.
- Tajima, A., Hirata, T., Taniguchi, K., Kondo, Y., Kato, S., Saito-Hori, M., Ishimoto, T., and Yamamoto, K. (2011). Combination of TS-021 with metformin improves hyperglycemia and synergistically increases pancreatic β -cell mass in a mouse model of type 2 diabetes. **Life Sciences**. 89: 662-670.

- Vermathen, M., Stiles, P., Bachofer, S. J., and Simonis, U. (2002). Investigations of monofluoro-substituted benzoates at the tetradecyltrimethylammonium micellar interface. **Langmuir**. 18: 1030-1042.
- Wallace, E., Ong, C. M. Y., and Heard, C. M. (2012). Delivery of atovaquone and proguanil across sublingual membranes, in vitro. **Pharma Development Technology**. 17: 770-776.
- Zhu, D. M., Feng, K. I., and Schelly, Z. A. (1992). Reverse micelles of Triton X-100 in cyclohexane: Effects of temperature, water content, and salinity on the aggregation behavior. **The Journal of Physical Chemistry**. 96, 2382-2385.
- Zhu, D. M., Wu, X., and Schelly, Z. A. (1992). Reverse micelles and water in oil microemulsions of Triton X 100 in mixed solvents of benzene and *n*-hexane. Dynamic light scattering and turbidity studies. **Langmuir**. 8: 1538-1540.
- Zingaretti, L., Correa, N. M., Boscatto, L., Chiacchiera, S. M., Durantini, E. N., Bertolotti, S. G., Rivarola, C. R., and Silber, J. J. (2005). Distribution of amines in water/AOT/*n*-hexane reverse micelles: influence of the amine chemical structure. **Journal of Colloid and Interface Science**. 286: 245-252.
- Zulauf, M., and Eicke, H. F. (1979). Inverted micelles and microemulsions in the ternary system water/aerosol-OT/isooctane as studied by photon correlation spectroscopy. **The Journal of Physical Chemistry**. 83: 480-486.

CHAPTER II

EXPERIMENTAL

2.1 Materials

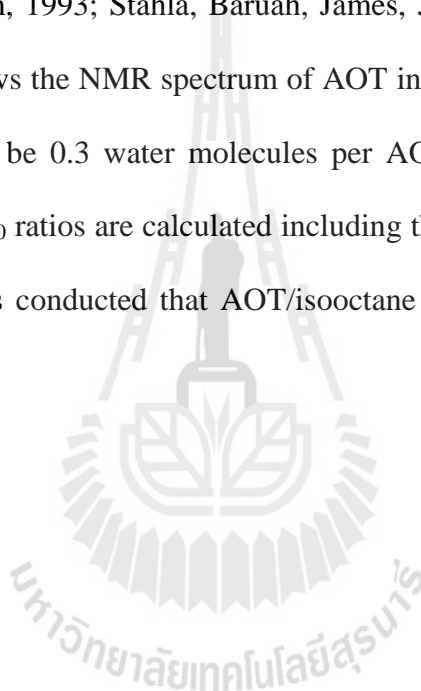
1-Phenylbiguanide, PBG (Aldrich, 98.0%), activated charcoal (carbon 6-12 mesh, Fisher Scientific), sodium bis(2-ethylhexyl)sulfosuccinate, AOT (Sigma-Aldrich, 98.0%), deuterated dimethyl sulfoxide, d_6 -DMSO, tetramethylsilane, TMS (Cambridge Isotope Laboratories), methanol (Sigma-Aldrich, 98.0%), isooctane (Sigma-Aldrich, 99.0%), deuterium oxide, D_2O (Aldrich, 99.9% deuterium), sodium deuterioxide, NaOD (Aldrich, 99% deuterium), deuterium chloride, DCl (Aldrich, 99% deuterium), cetyltrimethylammonium bromide CTAB (Sigma-Aldrich, 99%), cyclohexane (Sigma-Aldrich, 99%), 1-pentanol, (Sigma-Aldrich, 99%), phosphorus pentoxide, (Aldrich, 95%) were used as received unless noted otherwise in the procedures.

2.2 Preparation of samples for analysis

2.2.1 Anionic Reverse Micelles

Aerosol OT (sodium bis(2-ethylhexyl) sulfosuccinate) was the anionic surfactant that was used. The AOT was purified by dissolving a large amount (50-150 g) in methanol. The amount of methanol is not important, just that there is enough methanol to dissolve all the AOT and the sample is nonviscous. After the AOT is dissolved, activated charcoal is placed in the bottom of the flask and stirred overnight.

After stirring, the AOT/methanol solution is vacuum filtered 3 times, to ensure that all the charcoal is removed. If this is not the case, the resultant purified AOT will be yellow in color and will need to be purified again. After filtration, the methanol was removed by evaporation under vacuum for at least 12 hrs, and this the AOT stored in a vacuum desiccator. Purified AOT was dissolved in d_6 -DMSO for ^1H NMR and peak positions for the AOT protons were compared with those previously reported (Eastoe, Robinson, and Heenan, 1993; Stahla, Baruah, James, Johnson, Levinger, and Crans, 2008). Figure 2.1 shows the NMR spectrum of AOT in d_6 -DMSO. The residual water content was found to be 0.3 water molecules per AOT molecule. When preparing reverse micelles the w_0 ratios are calculated including the 0.3 water already present in AOT, the experiments conducted that AOT/isooctane concentration is 200 and 750 mM.



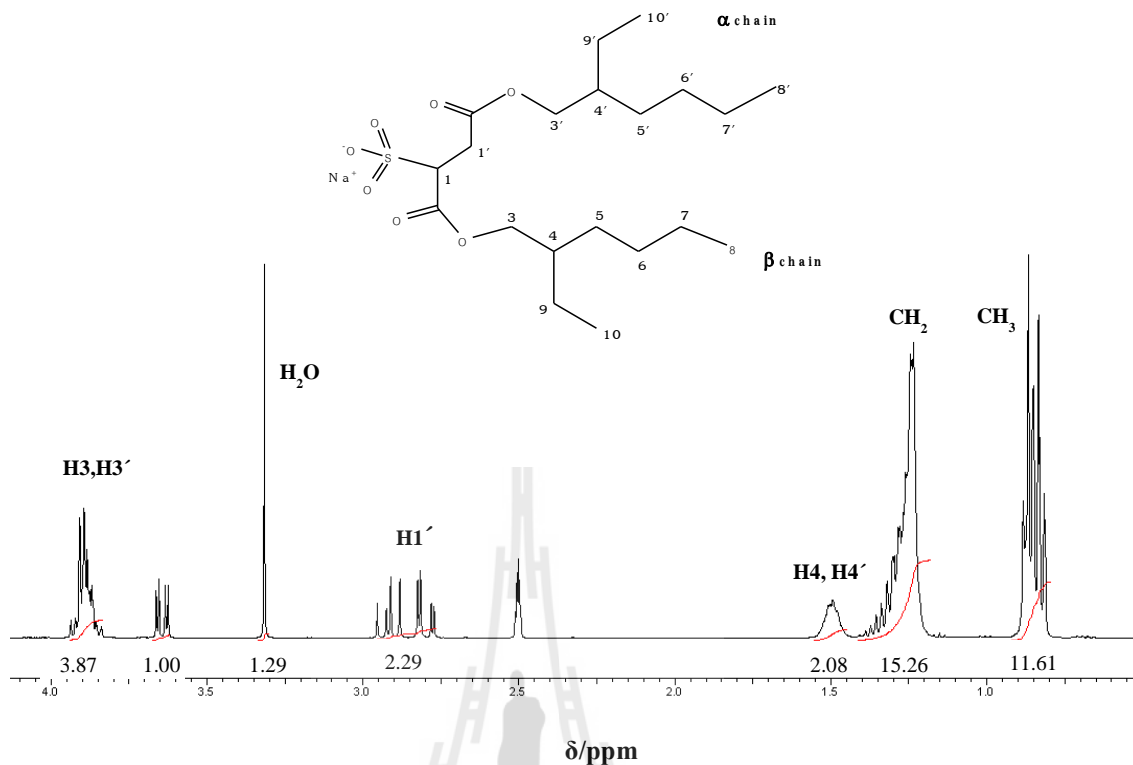


Figure 2.1 ¹H NMR of NaAOT in *d*₆-DMSO. (2.5 ppm is DMSO, and peak integration values are given below the spectrum).

The range of w_0 values that can be achieved is dependent highly on the nonpolar solvent. In isooctane, AOT can form reverse micelles to an upwards of $w_0 = 6, 8, 10, 14, 16, 20, 30$. Preparation of AOT/isooctane stock solution and reverse micelle by using 200 and 750 mM AOT/isooctane stock solution by dissolving 2.223 g (5.0 mmol), 8.340 g (18.8 mmol) of AOT in 25 mL isooctane, respectively together with vortex mixed until the solution cleared. Samples of various w_0 sizes were prepared using different amounts of AOT and D₂O. A range of RMs was prepared, with w_0 ranging from 6 to 20, by pipetting a specific volume of stock solution to aliquots of 200 and 750 mM AOT/isooctane and vortexed until the solution was clear and suitable for ¹H, 2D NMR, and FITR analysis.

Table 2.1 Component volumes in 1 mL samples of 200 mM and 750 mM AOT RMs at various w_0 . ($w_0 = [\text{H}_2\text{O}]/[\text{AOT}]$).

w_0	200 mM AOT/isooctane		750 mM AOT/isooctane	
	Aqueous stock	AOT/isooctane	Aqueous stock	AOT/isooctane
	μL	μL	μL	μL
6	21	979	75	925
8	28	972	98	902
10	35	965	119	881
12	42	959	140	860
14	48	952	159	841
16	55	945	178	822
20	67	933	213	787

2.1.2 Cationic reverse micelles

The cationic surfactant used was CTAB. To be used to make reverse micelles, CTAB must first be purified by double recrystallization from anhydrous ethanol, dried over phosphorus pentoxide for 48 h under reduced pressure, and stored over dried silica gel under vacuum (Giustini, Palazzo, Colafemmina, Della Monica, Giomini, and Ceglie, 1996). Unlike AOT, CTAB does not form reverse micelles as easily. CTAB requires a co-surfactant in order to form stable reverse micelles as well as having a narrower concentration range for forming stable emulsions. The cosurfactant is typically a straight chain alcohol and for the work reported herein we used 1-pentanol. RM solutions are made by dissolving CTAB into the nonpolar solvent,

usually cyclohexane. Once dissolved, the co-surfactant is added in a ratio range of 5:1 cosurfactant to surfactant ratio. Water is then added to make the appropriate w_0 . The CTAB/1-pentanol/cyclohexane system has a w_0 range from 6 to about 30.

Each sample was prepared separately by combining purified solid CTAB, 1-pentanol, cyclohexane, and aqueous 50 mM PBG stock solution. CTAB and 1-pentanol concentrations in cyclohexane before the addition of aqueous phase were 150 and 750 mM, respectively, and the molar ratios $[\text{H}_2\text{O}]/[\text{CTAB}]$ (w_0) were equal to 6, 8, 10, 14, 16, 20, and 30. All experiments were carried out using transparent, single-phase solution sample (Gaidamauskas, Cleaver, Chatterjee, and Crans, 2010).

Table 2.2 Component volumes in 1 mL samples of 150 mM CTAB/cyclohexane at various w_0 ($w_0 = [\text{H}_2\text{O}]/[\text{CTAB}]$), ratio Pentanol:CTAB (5:1).

150 mM CTAB/cyclohexane				
w_0	CTAB (mg)	Pentanol (μL)	Aqueous stock (μL)	Cyclohexane (μL)
6	55	82	16	902
8	55	82	22	897
10	55	82	27	891
14	55	82	38	881
16	55	82	43	875
20	55	82	54	864
30	55	82	81	837

2.2.3 Preparation of AOT/isooctane stock solution and reverse micelles.

The 750 mM AOT/isooctane stock solution was prepared by dissolving 8.34 g (18.8 mmol) of AOT in 25 mL isooctane and vortex mixed until the solution cleared. Samples of various w_0 sizes were prepared using different amounts of AOT and D₂O. A range of RMs was prepared, with w_0 ranging from 6 to 20, by pipetting a specific volume of stock solution to aliquots of 750 mM AOT/isooctane and vortexed until the solution was clear and suitable for ¹H, 2D NMR, and FITR analysis.

2.2.4 Preparation of aqueous stock solutions of 1-Phenylbiguanide (PBG).

The 500 mM PBG (0.886 g, 5.00 mmol) stock solution was prepared in deuterium oxide, D₂O (10 mL) in a volumetric flask. The solution was stirred until clear and the pH of the suspension was adjusted using DCl and NaOD when needed. The pH of the solutions was measured at 25°C on a Orion 720A+ pH meter and these readings were converted to pD by the formula $pD = pH + 0.4$ (Glasoe, and Long, 1960) and adjusted values are reported in this thesis.

2.2.5 Preparation of AOT/isooctane reverse micelle with PBG for 1D ¹H NMR spectroscopic studies. The solution containing 50 mM PBG was acidified using DCl and NaOD for pH values ranging from 1.21 to 12.3, where $pD = pH + 0.4$, and were used to make AOT RMs. A range of RMs were prepared with w_0 ranging from 6 to 20 by pipetting a specific volume of stock solution to aliquots of 750 mM AOT/isooctane. Upon mixing these solutions as prescribed, a cloudy solution resulted, which cleared after vigorous vortexing and then the solutions were suitable for ¹H NMR analysis.

2.2.6 Preparation of the 2D ¹H NMR NOESY sample in AOT reverse micelle solution with PBG. The $w_0 = 10$ sample of PBG in AOT/isooctane was

prepared with 100 mM PBG in D₂O solution with a pD = 7.07 using NaOD and DCl to adjust pH, where pD = pH + 0.4. The samples were lightly heated in a water bath up to 60°C in order to dissolve precipitated PBG during the titration at this neutral pH. Purified AOT was used to make a 750 mM AOT solution in isooctane. Once the aqueous PBG and AOT in isooctane were mixed, the suspension was vortexed until the solution became transparent.

2.2.7 Preparation of the FTIR sample in AOT reverse micelle solution with PBG. For IR spectroscopy experiments, two sets of aqueous solutions for each 10 mM and 100 mM of PBG with a pH range of 6.59 to 7.07 were prepared. One set of solutions for each concentration was prepared by using 5% HOD in H₂O and a second set of solutions for each concentration was prepared using only 100% H₂O. The pH was adjusted to be in this range by using DCl and NaOD in the sample containing D₂O and HCl and NaOH for the samples containing only H₂O. Purified AOT was used to make a 750 mM AOT solution in isooctane. The RM samples, having a w_0 of 10, were prepared by mixing the aqueous PBG with the AOT in isooctane and vortexed until the solution was transparent. This RM preparation was carried out with 5% HOD and with 100% H₂O solutions for each concentration.

2.2.8 Preparation of CTAB reverse micelle solution with PBG. Each sample was prepared separately by combining purified solid CTAB, 1-pentanol, cyclohexane, and aqueous 50 mM PBG stock solution. CTAB and 1-pentanol concentrations in cyclohexane before the addition of aqueous phase were 150 and 750 mM, respectively, and the molar ratios [H₂O]/[CTAB] (w_0) were equal to 8, 10, 16, 20, and 30. All experiments were carried out using transparent and single-phase solution sample (Gaidamauskas, Cleaver, Chatterjee, and Crans, 2010).

2.3 Methods

2.3.1 1D NMR spectroscopy The ^1H NMR spectra of RM solutions were recorded using an Agilent Inova spectrometer operating at 400 MHz at ambient temperature ($25 \pm 0.2^\circ\text{C}$) in the unlocked mode using routine parameters. Spectra were initially referenced against internal TMS ($\delta = 0.00$ ppm) and then routinely against the isooctane resonance ($\delta = 0.904$ ppm) for AOT RM as reported previously (Chatkon, Chatterjee, Sedgwick, Haller, and Crans, 2013; Crans, Rithner, Baruah, Gourley, and Levinger, 2006; Crans, Trujillo, Bonetti, Rithner, Baruah, and Levinger, 2008; Sedgwick, Cole, Rithner, Crans, and Levinger, 2012).

RM samples for NMR spectroscopy were prepared from 750 mM AOT stock solutions in isooctane, and 10, 50, and 100 mM PBG in D_2O at the desired pH values. The PBG stock solutions were adjusted near the desired pH using DCl and NaOD before the final dilutions were made. The chemical shift was referenced against an external sample of 3-(trimethylsilyl)propanesulfonic acid (DSS). Data analysis was conducted using MestReC V.4.5.9.1 NMR spectroscopic data processing software and ACD/NMR Processor Academic Edition for Windows.

2.3.2 2D NMR spectroscopy. ^1H - ^1H NOESY NMR experiments were performed on a 400 MHz Agilent Inova NMR spectrometer. The NOESY data were acquired with a 4500 Hz window for protons in t_2 and t_1 . The NOESY mixing time was 200 ms and 32 transients were acquired per increment. The total recycle time between transients was 1.85 s. The data set consisted of 1332 complex points in t_2 by 200 complex points in t_1 using States-TPPI. Cosine-squared weighting functions were matched to the time domain in both t_1 and t_2 , and the time domains were zero-filled prior to the Fourier transform. The final resolution was 3.2 Hz/pt in F2 and 8.8 Hz/pt

in F1. Data processing was done using the Agilent VNMRJ-3.2D software (Chen, Vanpraag, van Praag, and Gardner, 1991; Crans, Trujillo, Bonetti, Rithner, Baruah, and Levinger, 2008; Sedgwick, Cole, Rithner, Crans, and Levinger, 2012).

2.3.3 FTIR Spectroscopy. Differential FTIR data were collected using a Thermo Scientific Nicolet iS50 attenuated total reflectance (ATR) FTIR. Spectra were obtained from samples with 5% HOD in H₂O and with pure deionized water which allowed us to explore the OD (and OH, data not shown) stretching regions. Spectra that arose only from the OD stretching signal were obtained by subtracting the normalized spectra with RMs that contained only deionized water as the polar solvent from the normalized spectra of RMs that contained 5% HOD in H₂O (Moilanen, Levinger, Spry, and Fayer, 2007). The highest peak positions are shown in the OD regions. A 100 μ L aliquot of the freshly made RM suspension was directly added onto the IR beam transmitting through the diamond ATR crystal window of the ATR adaptor. Data were collected using the following parameters: 32 scans, 4 cm^{-1} resolution, at 25°C, while in absorbance mode. The diamond ATR crystal was cleaned after each data collection using a kimwipe wetted with ethanol. A minimum of three trials were run for all samples.

The work up for the data was performed using OMNIC, Microsoft Excel, and/or Origin 7. Note, we observed no difference in the FTIR spectra obtained from a 20 min old solution or from a 1 week old sample.

2.4 Research procedure

This research aimed at investigation how biguanide compounds such as Metformin 1-phenylbiguanide and proguanil drug interact with the model membrane

systems. We study the solution of sample products in AOT and CTAB reverse micelle (synthetic model membrane systems) and investigated how these compounds and affect with the water in water pool and water organization near interface, including the effect on vary pH, concentration and size of reverse micelle system by using ^1H , 2D NMR, and FTIR techniques.

2.5 References

- Chatkon, A., Chatterjee, P. B., Sedgwick, M. A., Haller, K. J., and Crans, D. C. (2013). The antidiabetic compound formed from metformin and decavanadate complex: Counterion affects interaction with interfaces. **The European Journal of Inorganic Chemistry**. 10-11: 1859-1868.
- Chen, J. P., Vanpraag, H. M., van Praag, H. M., and Gardner, E. L. (1991). Activation of 5-HT₃ receptor by 1-phenylbiguanide increases dopamine release in the rat nucleus accumbens. **Brain Research**. 543: 354-357.
- Crans, D. C., Rithner, C. D., Baruah, B., Gourley, B. L., and Lvinger, N. E. (2006). Molecular probe location in reverse micelles determined by NMR dipolar interactions. **Journal of the American Chemical Society**. 128: 4437-4445.
- Crans, D. C., Trujillo, A. M., Bonetti, S., Rithner, C. D., Baruah, B., and Lvinger, N. E. (2008). Penetration of Negatively Charged Lipid Interfaces by the Doubly Deprotonated Dicolinate. **The Journal of Organic Chemistry**. 73: 9633-9640.
- Eastoe, J., Robinson, B. H., and Heenan, R. K. (1993). Water-in-oil microemulsions formed by ammonium and tetrapropylammonium salts of Aerosol OT. **Langmuir**. 9: 2820-2824.

- Gaidamauskas, E., Cleaver, D. P., Chatterjee, P. B., and Crans, D. C. (2010). Effect of Micellar and Reverse Micellar Interface on Solute Location: 2,6-Pyridinedicarboxylate in CTAB Micelles and CTAB and AOT Reverse Micelles. **Langmuir**. 26: 13153-13161.
- Giustini, M., Palazzo, G., Colafemmina, G., Della Monica, M., Giomini, M., and Ceglie, A. (1996). Microstructure and Dynamics of the Water-in-Oil CTAB/*n*-Pentanol/*n*-Hexane/Water Microemulsion: A Spectroscopic and Conductivity Study. **The Journal of Physical Chemistry**. 100: 3190-3198.
- Glasoe, P., and Long, F. A. (1960). Use of glass electrodes to measure acidities in deuterium oxide. **The Journal of Physical Chemistry**. 64: 188-190.
- Moilanen, D. E., Levinger, N. E., Spry, D. B., and Fayer, M. D. (2007). Confinement or the nature of the interface? Dynamics of nanoscopic water. **Journal of the American Chemical Society**. 129: 14311-14318.
- Sedgwick, M., Cole, R. L., Rithner, C. D., Crans, D. C., and Levinger, N. E. (2012). Correlating Proton Transfer Dynamics To Probe Location in Confined Environments. **Journal of the American Chemical Society**. 134: 11904-11907.
- Stahla, M. L., Baruah, B., James, D. M., Johnson, M. D., Levinger, N. E., and Crans, D. C. (2008). ¹H NMR Studies of Aerosol-OT Reverse Micelles with Alkali and Magnesium Counterions: Preparation and Analysis of MAOTs. **Langmuir**. 24: 6027-6035.

CHAPTER III

RESULTS

3.1 Results

3.1.1 NMR spectra and properties of 1-phenylbiguanide (PBG). For investigation of the interaction of biguanide compounds with model interfaces, firstly the spectroscopic properties of the different protonation states need to be determined in aqueous solution as the reference system at hand.

The ^1H NMR signals for PBG in aqueous solution are dependent on the pH of the solution as shown in Figure 3.1. The diprotonated, monoprotated, and neutral forms of PBG can readily be distinguished based on the location of the ^1H NMR signals. The signals for the deprotonated form are 0.05 to 0.15 ppm downfield from the monoprotated form that exists in solutions with pH 2 through 11. At basic pH the shifts continue to move upfield as is generally observed upon deprotonation (Gaidamauskas, Cleaver, Chatterjee, and Crans, 2010). These observations are in agreement with the reported pKa values for this complex of 3.13 and 10.76 (Woo, Yuen, Thompson, McNeill, and Orvig, 1999).

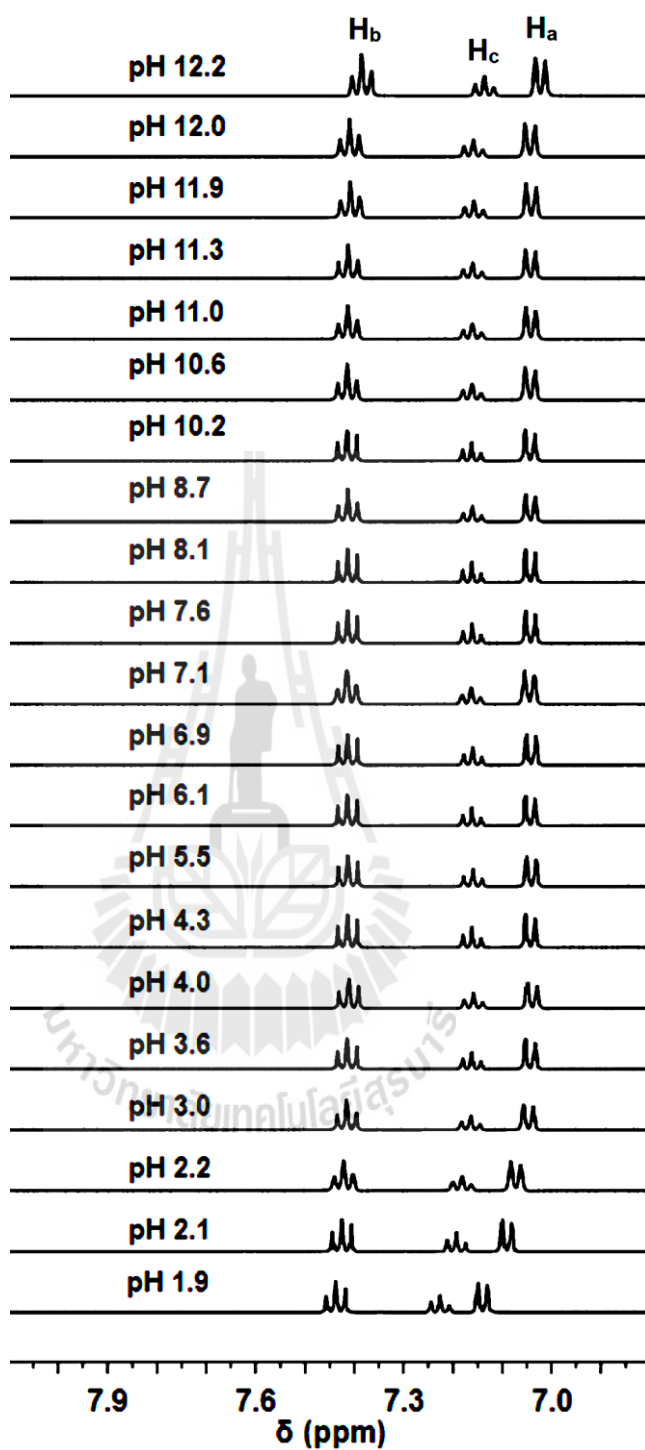


Figure 3.1 Partial ^1H NMR spectra were recorded in D_2O of 100 mM PBG in aqueous solution at pH values between 1.9 to 12.2 measured at 400 MHz. Samples were referenced against a solution of DSS using external lock.

3.1.2 PBG in AOT/isooctane RMs: ^1H NMR spectroscopic studies. The interaction of PBG with the anionic surfactant layer in AOT RMs was studied using ^1H NMR spectroscopy. In Figure 3.1 the ^1H NMR spectra are shown for 50 mM PBG aqueous stock solution containing the double protonated form of the PBG (at pH 1.0) in 750 mM AOT/isooctane at w_0 ratios from 6 to 16. The ^1H NMR chemical shifts for the aqueous solution of the Ha proton is at 7.415 ppm (a doublet signal), the Hb proton at 7.576 ppm (the larger triplet signal), and the Hc protons are at 7.498 ppm (the small triplet signal). When comparing the spectra of the RMs systems with the spectra of the aqueous stock solution (Figure 3.1), an upfield shift is observed for all three protons. The Hb and Hc protons are most shifted by the addition into the RMs. Both these protons shift by 0.2-0.3 ppm upfield. A smaller but downfield shift is observed for Ha. Overall, these spectra show a change in the order of the signals because Ha is the most upfield proton in aqueous solution but the most downfield proton in the RM system. The observed shifts therefore do not correspond to deprotonation of the diprotonated species because none of the RM proton signals approach the spectra observed in aqueous solution at any pH values. The observed shifting is consistent with an environmental change upon placement of PBG into the RMs and a modest but observable change as the w_0 decreases.

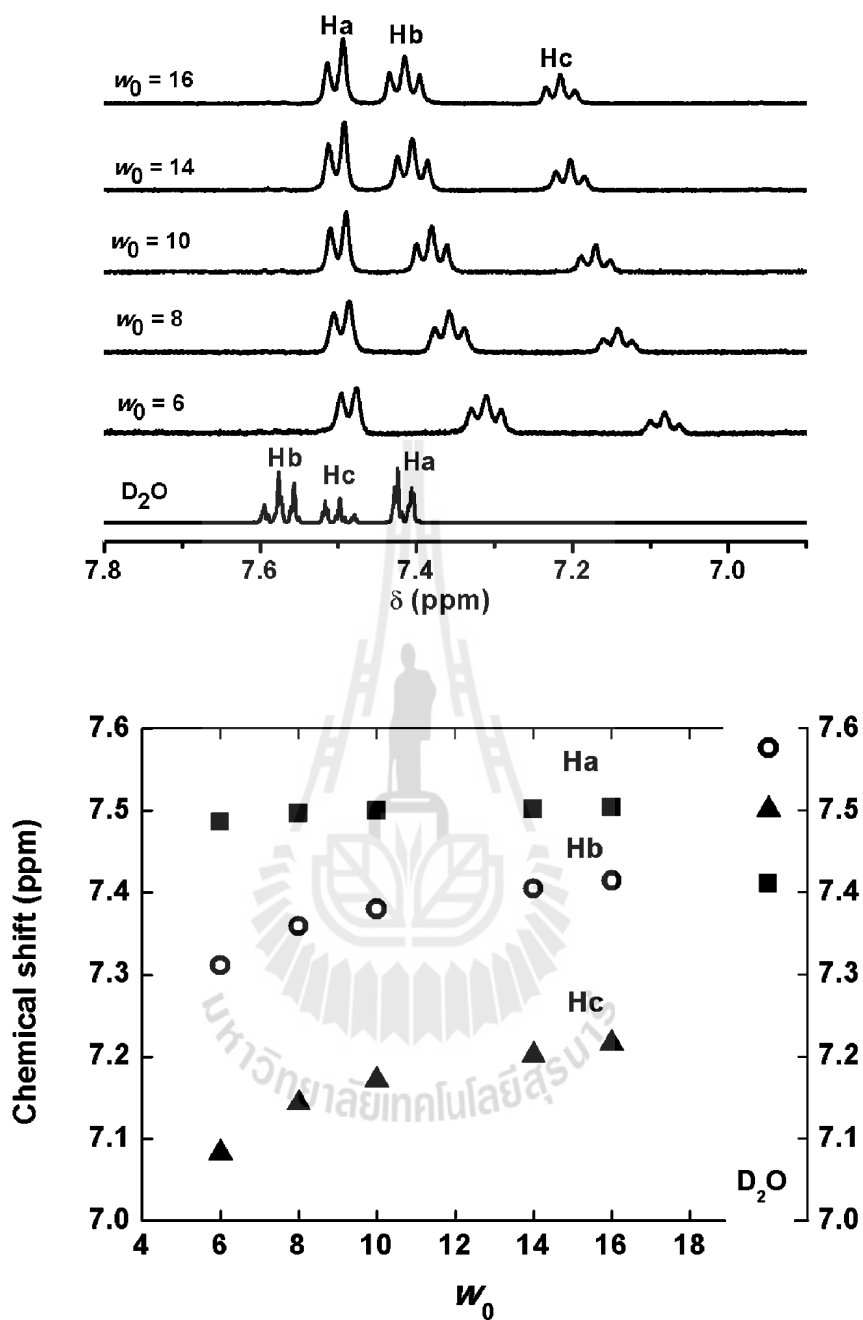
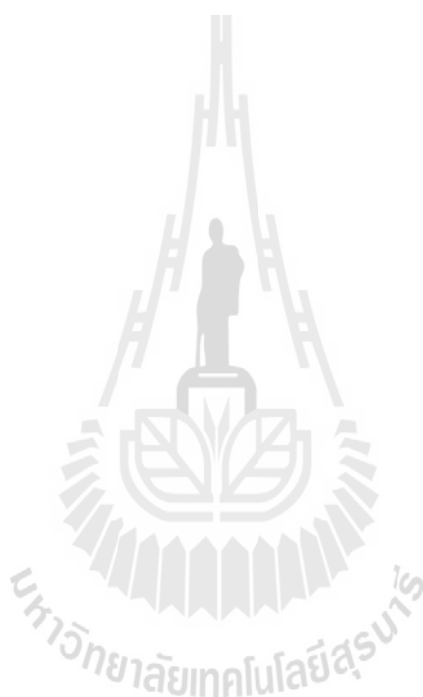


Figure 3.2 (above) Partial ^1H NMR spectra of 100 mM PBG at pH 1.0 in 750 mM AOT/isooctane RMs recorded at 400 MHz and referenced against the isooctane resonance at 0.904 ppm. (below) A plot of the specific chemical shift of PBG protons, Ha (■), Hb (○) and Hc (▲) as a function of w_0 size.

In Figure 3.3 the ^1H NMR spectra are shown for 50 mM PBG aqueous stock solution containing deprotonated PBG (at pH 12.2) added to 750 mM AOT/isooctane in w_0 from 6 to 20. The ^1H NMR chemical shifts for the aqueous solution of the Ha proton is at 7.023 ppm (doublet), the Hb proton at 7.385 ppm (triplet) and Hc protons is at 7.136 (triplet). When comparing the spectra of the RM systems with aqueous stock solution, an upfield shift is observed for two of the protons and one proton shifts downfield, although the amount by which each peak shifted varied. The Ha protons are most shifted by the addition into the RMs (by 0.4 ppm). These spectra show a change in the order of the signals; that is, Ha is the most upfield proton in aqueous solution but the most downfield proton in the RMs system. The observed shifts therefore do not correspond to a simple change in protonation state. The largest shifts are observed in the smaller w_0 values; however, none of the RM proton spectra approached the spectra observed in aqueous solution at any pH value. This is consistent with a definite environmental change upon placement into the RMs and significant is found as the w_0 decrease.

Comparing the spectral series at low (Figure 3.2) and high pH (Figure 3.3), the shifting as the w_0 size changes varies significantly. Perhaps most important, is the fact that all three protons shifted downfield as the w_0 size decreased at low pH, whereas at higher pH only two out of the three protons shifted downfield, and the third proton, Ha, shifted upfield. Such patterns of some protons shifting one direction and the other protons a different direction has been attributed to the specific location at the interface in literature (Chen, Vanpraag, van Praag, and Gardner, 1991; Crans, Schoeberl, Gaidamauskas, Baruah, and Roess, 2011; Crans, Trujillo, Bonetti, Rithner, Baruah, and Levinger, 2008; Sedgwick, Cole, Rithner, Crans, and Levinger, 2012; Vermathen,

Stiles, Bachofer, and Simonis, 2002). The different multidirectional shifting patterns ruled out the possibility that the same protonation stage of the PBG is involved in these spectra and supports the variation in the environment consistent with changing location of the compound depending on the protonation state.



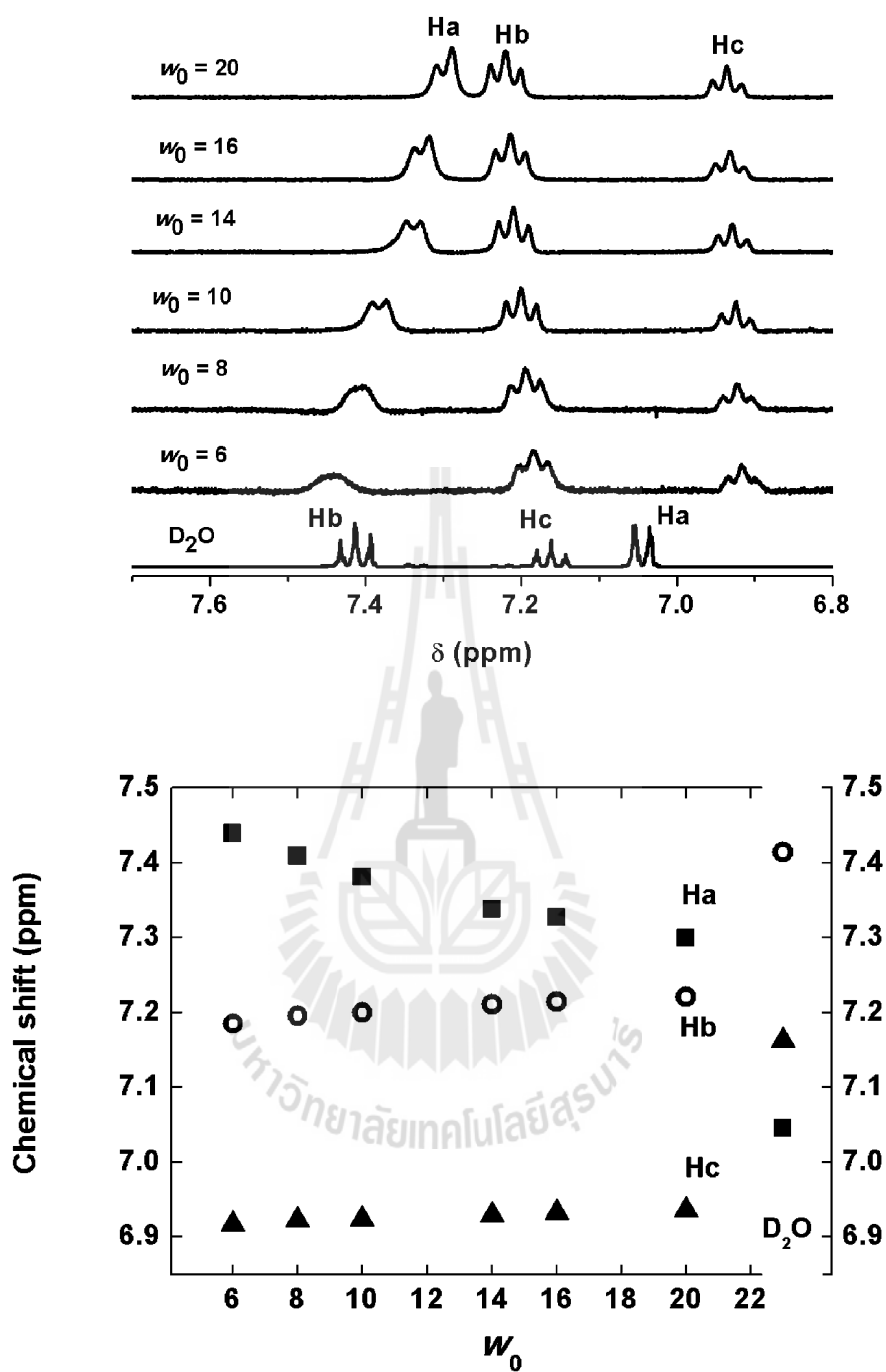


Figure 3.3 (above) Partial ^1H NMR spectra of 50 mM PBG at pH 12.2 in 750 mM AOT/isooctane RMs recorded at 400 MHz and referenced against the isooctane resonance at 0.904 ppm. (below) A plot of the apparent specific chemical shifts of PBG, Ha (■), Hb (○) and Hc (▲) as a function of w_0 .

3.1.3 PBG in AOT RM: 2D NOESY study. To further characterize the interactions of PBG with AOT/isooctane in this model membrane system we employed 2D NMR NOESY to investigate the location of the drug in the RM system (Chen, Vanpraag, van Praag, and Gardner, 1991; Crans, Trujillo, Bonetti, Rithner, Baruah, and Levinger, 2008, Sedgwick, Cole, Rithner, Crans, and Levinger, 2012). Specifically, we characterized the interaction of the solution of 100 mM PBG at neutral pH (pD = 7.07) in 750 mM AOT using 2D ^1H NOESY.

As shown in Figure 3.4, the partial 2D spectrum in the F2-frame is a close up of the phenyl protons Ha (2H, 7.57 ppm), Hb (2H, 7.32 ppm), and Hc (1H, 7.06 ppm) along with a broad H peak, which is the N-H signal (6.82 ppm) in PBG. The F1 frame is the full spectrum including a HOD peak (1H, 4.60 ppm), a broad and large peak of isooctane at 1.01 ppm and especially the methylene protons of AOT, which show at an overlapping signal in AOT (1.41 ppm, 9, 9' as labeled in Figure 1.7). The diagonal (solid line) is present to emphasize the two different scales of the sides on the 2D spectrum. As expected, there are intense cross peaks between Ha and Hb as well as Hb and Hc from PBG and these signals demonstrate that the protons near each other. A weaker cross peak between Ha and Hc was also observed. The cross peak between Ha and Hc is weak in comparison to the cross peak with Ha and Hc indicating that these protons are not as close.

The intense cross peaks of Ha and Hb as well as Hb and Hc show that these protons are close together, which is expected. The phenyl protons Ha, Hb, and Hc all have weak cross peaks with the methylene protons of AOT. Prominent cross peaks between the PBG and signals in AOT are indicated with dashed lines. The Hb and Ha protons can interact with the methylene protons in the backbone of the AOT tails, this

peak is at approximately 1.41 ppm, on AOT. As shown in Figure 3.4, the weak cross peak with the methylene AOT protons with Ha and Hb indicate the positioning of the molecule in the interface; Hc will interact less with these methylene protons. The lack of a cross peak of Ha, Hb, and Hc with the HOD signal at approximately 4.60 ppm shows that the phenyl group is less likely interacting with the water pool. Presumably, the phenyl group protons are mainly interacting with the AOT methylene protons because since there is a defined cross peak with AOT. Thus, this portion of the PBG is nestled high in the interface of the RMs.

Finally, an intense cross peak to the NH signal was observed and traced to HOD. The PBG has multiple NH groups and their signal is very broad; which is an indication that the relaxation time (T1 and T2) is very short and different than that of the phenyl protons. However, in the 2D spectrum we see a very intense NH signal along the diagonal and an intense cross peak with HOD indicating the NH protons are very close to the HOD protons in the water pool. Although it is possible that some water molecules could penetrate the interface, the interaction observed between the NH and HOD protons is very strong suggesting that this interaction of HOD and NH protons is very close as is expected to occur only if these groups are in or very near the water pool. The lack of a NH cross peak with any AOT methylene protons also suggested that this part of PBG is nestled inside the water pool.

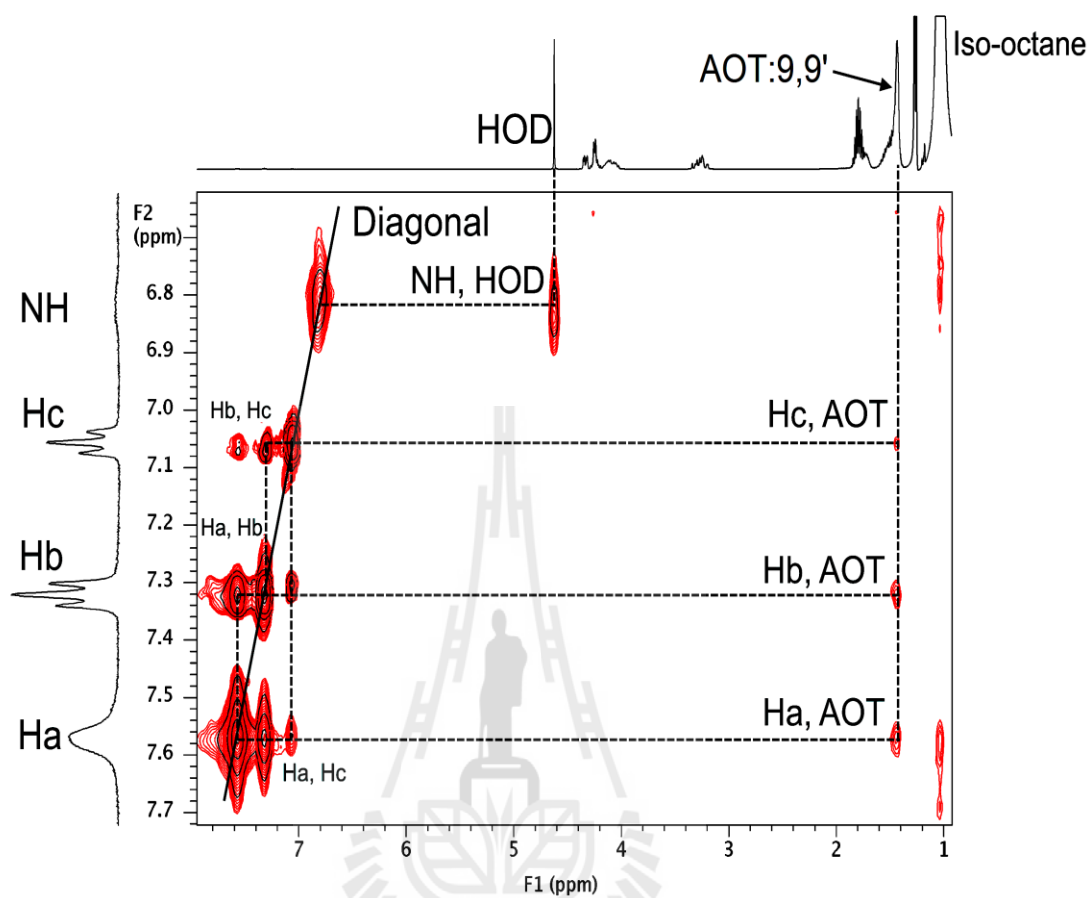


Figure 3.4 Partial ^1H NMR NOESY spectrum of 100 mM PBG at pD 7.07 in 750 mM AOT. The spectrum was recorded at 400 MHz using the parameters detailed in the experimental. The F2 or y-axis is zoomed in on the phenyl and nitrogen protons in PBG and the F1 or x-axis is the full spectrum. The diagonal is the solid line and prominent cross peaks are shown as dotted lines along with their respective hydrogen interactions.

In conclusion, the PBG interacts both with the hydrophobic and hydrophilic parts of the interface as well the HOD in the water pool. Combined, this study showed an example of a probe that extended into both the interface and the water pool.

3.1.4 PBG in AOT/isooctane RMs: FTIR spectroscopic studies. Since the 2D NOESY studies suggested that part of the PBG resided in the water pool, we were interested in confirming that PBG affects the H-bonding in the water pool of the RMs using differential FTIR spectroscopy (Moilanen, Levinger, Spry, and Fayer, 2007). These studies characterized AOT/isooctane RMs comparing spectra in the absence and presence of 5% HOD. Differential FTIR spectra were recorded for samples of the RM with 100% H₂O and RMs containing 5% HOD. These spectra were then subtracted to produce the resultant spectrum of the OD stretching. Such differential FTIR spectra served as the benchmark for spectra of RM solutions containing PBG in H₂O subtracted from spectra of RMs solutions with 5% HOD. The results are shown in Figure 3.5.

In Figure 3.5 we show the FTIR spectra of RMs, $w_0 = 10$, made from AOT/isooctane containing two different concentrations of PBG, 10 mM and 100 mM. Figure 3.5 shows the two spectra at different concentrations of PBG result in shifting; suggesting there are small but statistically distinct differences in the solvation of the PBG when the concentration of PBG changes. These data further more show that in the AOT/RM system the water pool is impacted by the presence of PBG because the OD signal shifts in its presence. These findings show that although the nature of the water pool changes as the RMs size changes, the presence of PBG also impacts the O-D stretch. By comparing the RMs with and without probe we see that as the concentration of the PBG increases, changes occur in the H-bonding in the water pool reflecting the changes that increasing PBG concentration has on the water pool.

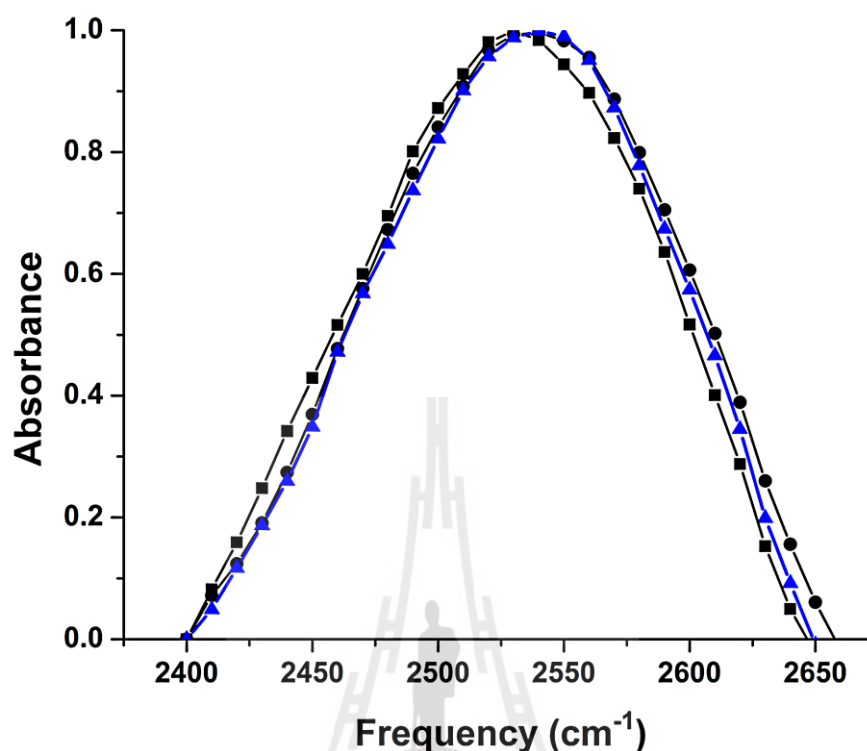


Figure 3.5 Absorbance spectra for the O–D stretch in AOT RMs containing PBG recorded at different molarities: 0 mM PBG RMs $w_0 = 10$ (–■–), pH ≈ 7.0 , 10 mM PBG RMs $w_0 = 10$ (–▲–) and 100 mM PBG RMs $w_0 = 10$ (–●–) measured using differential FTIR spectroscopy. The spectra are obtained by subtraction of AOT/isooctane RMs containing DI water from the corresponding spectra recorded in AOT/isooctane RMs containing 5% HOD for each of the three different concentrations of PBG.

NMR spectroscopic results show that the chemical shift for the phenyl proton in PBG changes, which is consistent with penetration into the interface. The NOESY experiments furthermore show that the NH-groups on the biguanide interact consistent with the PBG molecule residing at the interface and extending deep into the

hydrophobic part as well as in the water pool at the same time. The IR spectroscopic results show that biguanide group in PBG significantly affects the hydrogen-bonding present among the water molecules in the water pool. In summary, the results are consistent with the model illustrated in Figure 3.6.

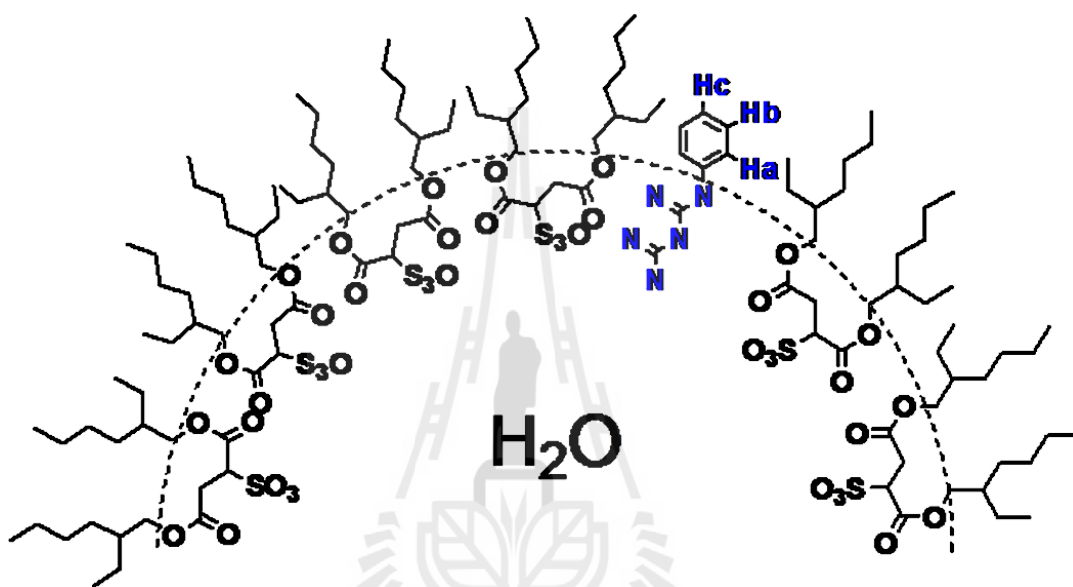
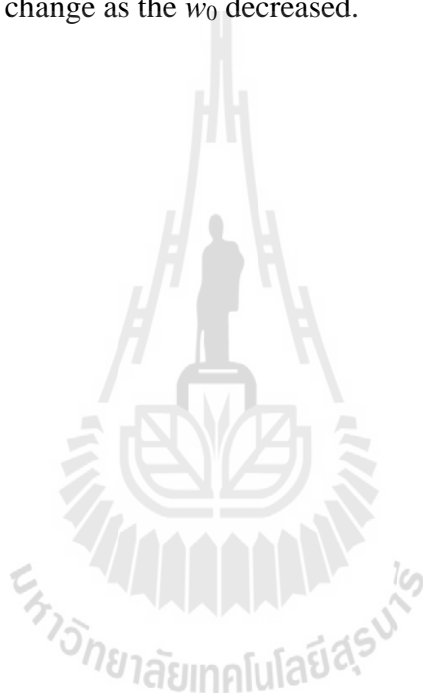


Figure 3.6 A cartoon illustrating the suggested location of PBG in the AOT RM.

3.1.5 PBG in CTAB/pentanol/cyclohexane RMs: ^1H NMR spectroscopic studies. In the following we determined the differences in cell loading if the charge on the RM interface changed. The interaction of PBG with the cationic surfactant layer in CTAB RMs was studied using ^1H NMR spectroscopy. In Figure 3.7 the ^1H NMR spectra are shown for 50 mM PBG aqueous stock solution containing the double protonated form of PBG (at pH 1.9) in 150 mM CTAB/750 mM pentanol in cyclohexane at w_0 ratios from 8 to 30. The ^1H NMR chemical shifts for the aqueous solution of the Ha proton is at 7.415 ppm (a doublet signal), the Hb proton at 7.576

ppm (the larger triplet signal) and Hc protons is at 7.498 ppm (the small triplet signal). All three protons were observed to shift upfield when compared with the spectra of the RM system in the aqueous stock solution (Figure 1.7). The Ha proton is most shifted by the addition into the RM and the proton shifted by 1.0-1.5 ppm upfield. No shifting was observed for Hb and Hc. A little observed shifting is consistent with an environmental change upon placement of PBG into the RMs and a modest but observable change as the w_0 decreased.



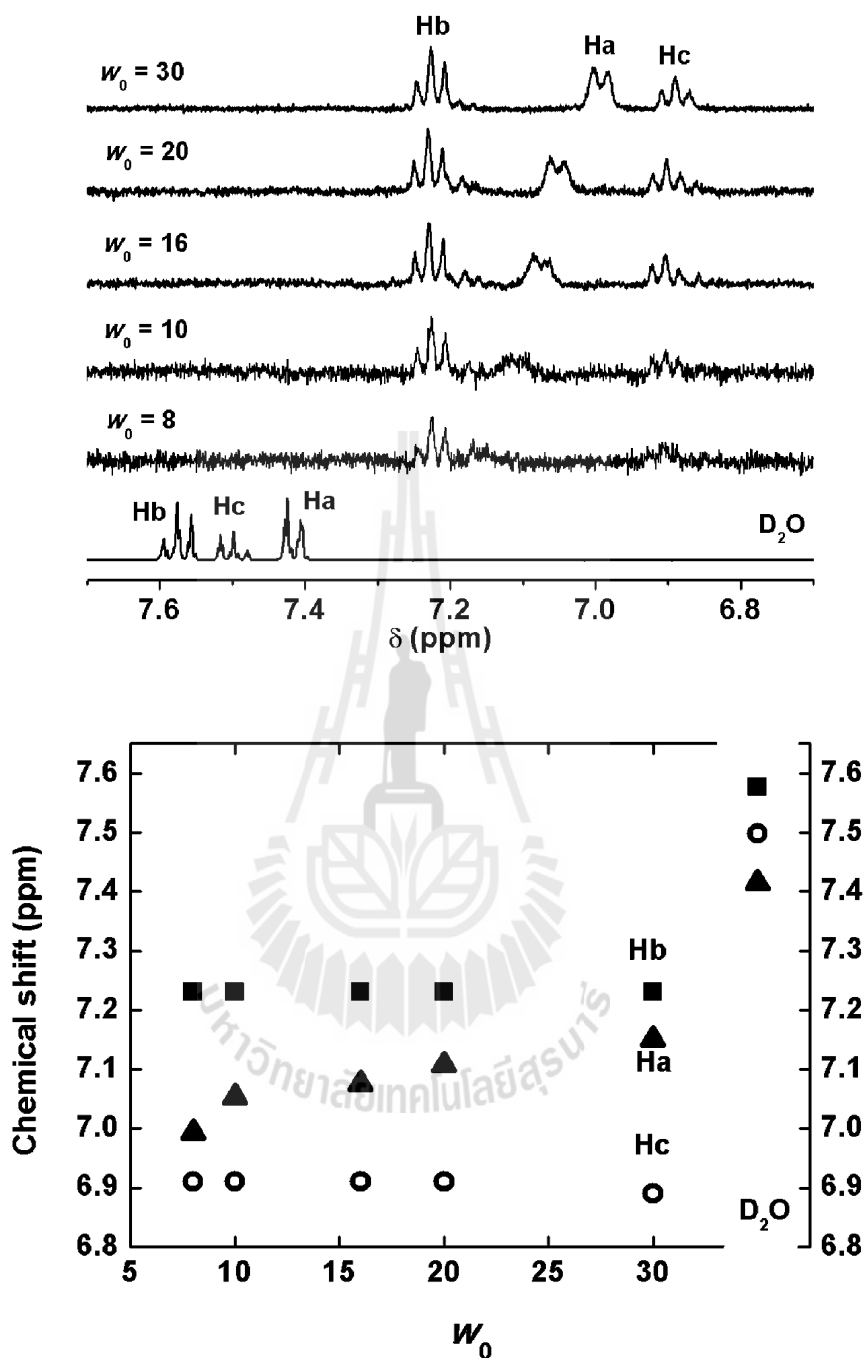


Figure 3.7 (left) Partial ^1H NMR spectra of 50 mM PBG at pH 1 in 150 mM CTAB/750 mM pentanol in cyclohexane RMs recorded at 400 MHz and referenced against the cyclohexane resonance at 1.430 ppm. (right) A plot of the specific chemical shift of PBG protons, Ha (▲), Hb (■) and Hc (○) as a function of w_0 size.

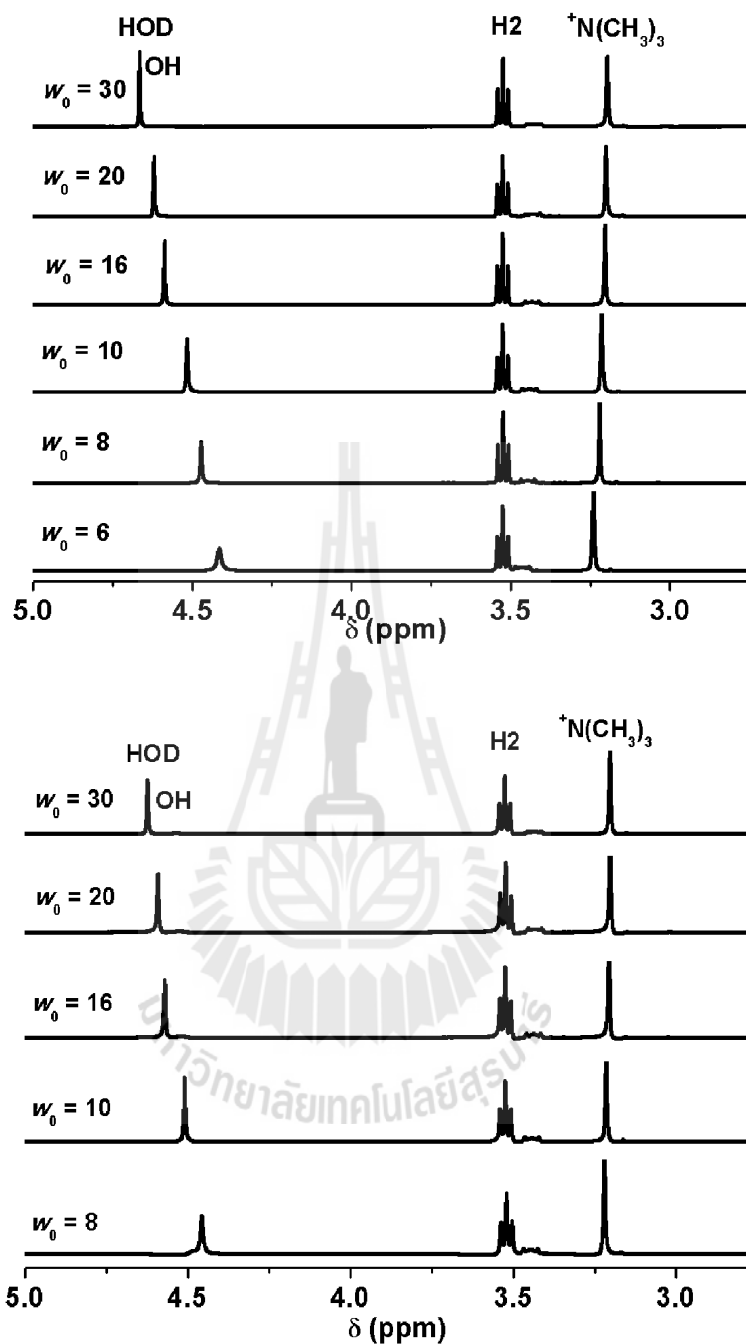


Figure 3.8 (above) Partial ^1H NMR spectra of 50 mM PBG at pH 1 in 150 mM CTAB/750 mM pentanol in cyclohexane RMs recorded at 400 MHz and referenced against the cyclohexane resonance at 1.430 ppm. (below) A plot of the AOT/cyclohexane RMs in the absence of PBG probe.

The spectra in Figure 3.8. shows the shifts that were observed in the region of the CTAB head group and chains. The above panel contains a probe and is to be compared to the panel on the below that was run with no probe in it. As observed, the CTAB protons do not shift as a function of w_0 size which suggested that there is no change in the environment of the surfactant. However, as seen from the comparison of the two panels, there is a small but distinct upfield shift in the water signal. This suggests that the H-bonding and properties of the water pool are changing in the presence of the probe. These results show that the observations made for the AOT/isooctane system and location of the probe at the interface is also observed when the charges on the interface changes. This is particularly interesting because the charge on the PBG is positive and so is the interface. These results suggest that the location of the PBG is not only determined by Columbic forces but that hydrophobic forces are likely to be important for determination of the probe location, as well.

3.2 References

- Chen, J. P., Vanpraag, H. M., van Praag, H. M., and Gardner, E. L. (1991). Activation of 5-HT₃ receptor by 1-phenylbiguanide increases dopamine release in the rat nucleus accumbens. **Brain Research**. 543: 354-357.
- Crans, D. C., Schoeberl, S., Gaidamauskas, E., Baruah, B., and Roess, D. A. (2011). Antidiabetic vanadium compound and membrane interfaces: interface-facilitated metal complex hydrolysis. **Journal of Biological Inorganic Chemistry**. 16: 961-972.
- Crans, D. C., Trujillo, A. M., Bonetti, S., Rithner, C. D., Baruah, B., and Levinger, N. E. (2008). Penetration of Negatively Charged Lipid Interfaces by the Doubly

- Deprotonated Dipicolinate. **The Journal of Organic Chemistry**. 73: 9633-9640.
- Gaidamauskas, E., Cleaver, D. P., Chatterjee, P. B., and Crans, D. C. (2010). Effect of Micellar and Reverse Micellar Interface on Solute Location: 2,6-Pyridinedicarboxylate in CTAB Micelles and CTAB and AOT Reverse Micelles. **Langmuir**. 26: 13153-13161.
- Moilanen, D. E., Levinger, N. E., Spry, D. B., and Fayer, M. D. (2007). Confinement or the nature of the interface? Dynamics of nanoscopic water. **Journal of the American Chemical Society**. 129: 14311-14318.
- Sedgwick, M., Cole, R. L., Rithner, C. D., Crans, D. C., and Levinger, N. E. (2012). Correlating Proton Transfer Dynamics To Probe Location in Confined Environments. **Journal of the American Chemical Society**. 134: 11904-11907.
- Vermathen, M., Stiles, P., Bachofer, S. J., and Simonis, U. (2002). Investigations of monofluoro-substituted benzoates at the tetradecyltrimethylammonium micellar interface. **Langmuir**. 18: 1030-1042.
- Woo, L. C. Y., Yuen, V. G., Thompson, K. H., McNeill, J. H., and Orvig, C. (1999). Vanadyl-biguanide complexes as potential synergistic insulin mimics. **Journal of Inorganic Biochemistry**. 76: 251-257.

CHAPTER IV

DISCUSSION

Malaria and other infectious diseases represent a major health problem for impacted areas and since people frequently travel, it can impact other areas in the world as well. The quest for development of new treatments and drugs remains a high priority because of the problems associated with resistance development. Many approaches (Biot, Nosten, Fraise, Ter-Minassian, Khalife, and Dive, 2011; Krugliak, Deharo, Shalmiev, Sauvain, Moretti, and Ginsburg, 1995; Plowe, Djimde, Bouare, Doumbo, and Wellems, 1995) and new drugs (Loedige, Lewis, Paulsen, Esch, Pradel, Lehmann, Brun, Bringmann, and Mueller, 2013; Salas, Herrmann, Cawthray, Nimphius, Kenkel, Chen, de Kock, Smith, Patrick, Adam, and Orvig, 2013; Singh, Kaur, Smith, de Kock, Chibale, and Balzarini, 2014) are under various stages of development to combat malarial infections. The studies presented here investigated the interaction of PBG by model membrane interfaces using NMR spectroscopy. By choosing a simple model system for these studies we determined molecular details on the solute interaction with the interface. In these studies we used the AOT/isooctane system as the model interface, because this system is found to be an effective model system providing data that are in line with corresponding biological studies (Crans, Rithner, Baruah, Gourley, and Levinger, 2006). The ^1H NMR studies are informative because they do provide molecular information describing the environment of each H-atom which will identify the molecular positioning very precisely. Studies with more

complex systems require use of spectroscopic probes that provide changes in signals that report on environmental changes without the molecular detail whereas NMR spectroscopy is a powerful method for defining molecular probe positioning (Chen, Vanpraag, van Praag, and Gardner, 1991; Crans, Trujillo, Bonetti, Rithner, Baruah, and Levinger, 2008; Sedgwick, Cole, Rithner, Crans, and Levinger, 2012). The chemical shift changes are consistent with the PBG being located at the membrane interface and that it partially penetrates into the interface. This interpretation was supported by FTIR and 2D NOESY experiments which each confirm the location of the PBG with the water pool and the hydrophobic interface. That is, the phenyl ring interacted with the AOT in the interface of the RMs and biguanide NH groups interacted with the water molecules in the water pool. We illustrated the location of PBG in Figure 3.6.

Using 1D NMR studies (*i.e.* chemical shift changes) we found that the environment changed upon placement of the PBG in the RM environment. Since ^1H NMR gives information with regard to all the different signals in the NMR spectrum of the complex, the shifting of the signals is a measure for how the environment is changing for the molecule. However, interpretation of the shifting is nontrivial because both upfield and downfield shifting can be due to penetration of PBG into the interface, (Crans, Rithner, Baruah, Gourley, and Levinger, 2006; Vermathen, Chodosh, Louie, and Simonis, 1999; Vermathen, Louie, Chodosh, Ried, and Simonis, 2000; Vermathen, Stiles, Bachofer, and Simonis, 2002). For example, previously downfield shifting has been associated with $[\text{VO}_2\text{dipic}]^-$ penetration into the interface, (Crans, Rithner, Baruah, Gourley, and Levinger, 2006) and similarly upfield shifting has been associated with penetration of fluoro-benzoates into the interface

(Vermathen, Stiles, Bachofer, and Simonis, 2002). We attribute these factors to the nature of the effects on shifting a complex matter involving environmental hydrophobicity, charge, solubility and in general complementary interaction between probe and interface. Additional information is therefore desirable and we have been obtaining such information using 2D NMR and FTIR experiments.

The changes observed upon placement into the RM and could potentially be attributed to changes in the pH of the solution. The ^1H NMR spectrum of PBG reported on the pH and protonation state of the probe in addition to placement and environmental changes (Figures. 3.1-3.3). The changes of proton chemical shift of PBG by ^1H -NMR spectroscopy were considered and spectra were run at different pH values (Figure 3.1). Since greater shifts are found for Ha at high pH when placed into the RMs (Figure 3.3), this would suggest that the Ha proton is found to move from H_2O to a charged environment and thus experience the most dramatic environmental change. Ha is near the charged biguanide group and as the molecule penetrates into the hydrophobic interface, Ha will feel this difference in environment more than the Hb and Hc that are not penetrated as far up into the interface. At low pH the biguanide residue is doubly protonated and all three phenyl protons will feel the effect of the protonation when the probe is moved from an aqueous to a hydrophobic environment. In contrast, at high pH only Ha will be affected by this environmental change because it is closer to the polar interface. These observations are in line with what has been observed in the past (Chen, Vanpraag, van Praag, and Gardner, 1991; Crans, Schoeberl, Gaidamauskas, Baruah, and Roess, 2011; Sedgwick, Cole, Rithner, Crans, and Levinger, 2012).

The spectrum in Figure 3.4 shows a 2D NOESY experiment where PBG is interacting with the surfactant AOT. The off-diagonal signals demonstrate interaction of the AOT protons with the PBG protons. In addition, the Ha, Hb and Hc on the phenyl group are associating with the CH₂-groups high up in the hydrophobic part of the interface. This interaction is likely to be sensitive to the specific conditions of the system. The spectrum also showed the interaction of NH protons of PBG with HOD protons in the water pool. We carried out the studies using 0.10 M PBG and as a result of using constant PBG concentration, as the w_0 increased the number of probes as the size of the RMs increased. In Table 4.1 we show how the number of probes increases as the w_0 increase. The NOESY experiments were carried out with 1.8 PBG's in each reverse micelle ($w_0 = 10$), documenting the fact that the interface can accommodate two such molecules per RM. In the systems that were investigated, about two layers of water molecules were solvating the RM (Maitra, 1984). The increasing number of probes as the w_0 increase may be important for the specific distribution of the probes and particularly in the smaller w_0 sizes that are barely large enough to hold the PBG (Dalpiaz, Ferrtti, Gilli, and Bertolasi, 1996) within the boundaries of the water pool. It is therefore to be expected that the interface may saturate as observed for other systems (unpublished data) and thus force some of the probes into the water pool.

Table 4.1 Content of RMs investigated as determined by w_0 and sizes.

w_0	n(agg)	N(probes)	N(AOT)	N(RMs)	probes/RMs	Size (radius)
6	50	4.52×10^{18}	4.18×10^{20}	8.35×10^{18}	0.54	28
8	72	5.88×10^{18}	4.07×10^{20}	5.66×10^{18}	1.0	32

Table 4.1 (Continued).

w_0	n(agg)	N(probes)	N(AOT)	N(RMs)	probes/RMs	Size (radius)
10	98	7.17×10^{18}	3.98×10^{20}	4.06×10^{18}	1.8	34
16	215	1.07×10^{19}	3.71×10^{20}	1.73×10^{18}	6.2	42
20	302	1.28×10^{19}	3.55×10^{20}	1.18×10^{18}	11	44

A. Maitra, J. Phys. Chem. 88 (1984) 5122-5125.

The studies with the CTAB/1-pentanol demonstrated that the biguanide favored bridging the membrane and having parts in the water pool and parts up high at the hydrophobic interfacial environment. Although other compounds could exhibit similar properties, we have not previously observed a molecule with such a clear cut 2D NOESY spectrum bridging compartments. With the dipic ligand, (Crans, Trujillo, Bonetti, Rithner, Baruah, and Levinger, 2008) we found that the probe could move but preferred to reside high up in the interface, however some cross peaks indicated that the ligand moved and that the compound also could be found at some times near the polar head groups of the interface. In the cases of the $[\text{Co}(\text{dipic})]^{2-}$, (Yang, Crans, Miller, la Cour, Anderson, Kaszynski, Godzala, Austin, and Willsky, 2002) the ascorbic acid, $\text{Cr}(\text{pic})_3$, and BMOV (Crans, Schoeberl, Gaidamauskas, Baruah, and Roess, 2011) all were found near the interface. In contrast, the decavanadate (Samart, Saeger, Haller, Aureliano, and Crans, 2014) and HTPS (Sedgwick, Cole, Rithner, Crans, and Levinger, 2012) was found in the middle of the AOT/isooctane water pool as anticipated with their high charges. In the case of the V-dipic complexes ($[\text{VO}_2\text{dipic}]^-$, $[\text{VOdipic}(\text{H}_2\text{O})_2]$ and $[\text{V}(\text{dipic})_2]^-$), the metal ion oxidation state and complex charge as well as the size of the complex determined the specific location of

the compound (Sostarecz, Gaidamauskas, Distin, Bonetti, Levinger, and Crans, 2014). However, when the charges of the interface changed then the location of these systems changed. Specifically, the decavanadate (Samart, Saeger, Haller, Aureliano, and Crans, 2014) and the HPTS (Sedgwick, Cole, Rithner, Crans, and Levinger, 2012) molecules moved from the middle of the water pool to the interface of the RMs water pool.

The antimalarial drug proguanil is on the market and the related derivatives PBG and metformin are anti-diabetic agents. These three compounds all are biguanides. The model studies presented here provide information documenting the ease by which these compounds can associate with and penetrate the membrane-like interface, which may be important for some of the biological responses. There is no doubt that the antimalarial drugs act in part by modifying the properties of the host membrane and therefore the findings that are reported here suggest that these compounds may be able to traverse the membrane much more readily than previously anticipated. It is known that PBG induces a response by associating with the 5-hydroxytryptamine (5HT₃) receptor, however, in addition these studies could be interpreted as PBG and proguanil may traverse membranes readily. The ability of this PBG to span the membrane interface is likely to be important to the metabolism. Perhaps such properties indicate a secondary effect of these compounds as protonophores, a mode of action already known for atovaquone which collapses of the mitochondrial membrane potential.

4.1 References

- Biot, C., Nosten, F., Fraisse, L., Ter-Minassian, D., Khalife, J., and Dive, D. (2011). The antimalarial ferroquine: from bench to clinic. **Parasite**. 18: 207-214.
- Chen, J. P., Vanpraag, H. M., van Praag, H. M., and Gardner, E. L. (1991). Activation of 5-HT₃ receptor by 1-phenylbiguanide increases dopamine release in the rat nucleus accumbens. **Brain Research**. 543: 354-357.
- Crans, D. C., Rithner, C. D., Baruah, B., Gourley, B. L., and Levinger, N. E. (2006). Molecular probe location in reverse micelles determined by NMR dipolar interactions. **Journal of the American Chemical Society**. 128: 4437-4445.
- Crans, D. C., Schoeberl, S., Gaidamauskas, E., Baruah, B., and Roess, D. A. (2011). Antidiabetic vanadium compound and membrane interfaces: interface-facilitated metal complex hydrolysis. **Journal of Biological Inorganic Chemistry**. 16: 961-972.
- Crans, D. C., Trujillo, A. M., Bonetti, S., Rithner, C. D., Baruah, B., and Levinger, N. E. (2008). Penetration of Negatively Charged Lipid Interfaces by the Doubly Deprotonated Dipicolinate. **The Journal of Organic Chemistry**. 73: 9633-9640.
- Dalpiazz, A., Ferrtti, V., Gilli, P., and Bertolasi, V. (1996). X-ray of 1-phenyl biguanide. **Acta Crystallographica Section B**. 52: 509-518.
- Krugliak, M., Deharo, E., Shalmiev, G., Sauvain, M., Moretti, C., and Ginsburg, H. (1995). Antimalarial effects of C18 fatty-acids on plasmodium-falciparum in culture and on plasmodium-vinckei-petteri and plasmodium-yoelii-nigeriensis in vivo. **Experimental Parasitology**. 81: 97-105.

- Loedige, M., Lewis, M. D., Paulsen, E. S., Esch, H. L., Pradel, G., Lehmann, L., Brun, R., Bringmann, G., and Mueller, A. K. (2013). A primaquine-chloroquine hybrid with dual activity against Plasmodium liver and blood stages. **International Journal of Medical Microbiology**. 303: 539-547.
- Maitra, A. (1984). Determination of Size Parameters of Water-Aerosol OT-Oil Reverse Micelles from Their Nuclear Magnetic Resonance Data. **The Journal of Physical Chemistry**. 88: 5122-5125.
- Plowe, C. V., Djimde, A., Bouare, M., Doumbo, O., and Wellems, T. E. (1995). Pyrimethamine and proguanil resistance-conferring mutations in plasmodium-falciparum dihydrofolate-reductase-polymerase chain-reaction methodes for surveillance in africa. **The American Journal of Tropical Medicine and Hygiene**. 52: 565-568.
- Salas, P. F., Herrmann, C., Cawthray, J. F., Nimphius, C., Kenkel, A., Chen, J., de Kock, C., Smith, P. J., Patrick, B. O., Adam, M. J., and Orvig, C. (2013). Structural Characteristics of Chloroquine-Bridged Ferrocenophane Analogues of Ferroquine May Obviate Malaria Drug-Resistance Mechanisms. **Journal of Medicinal Chemistry**. 56: 1596-1613.
- Samart, N., Saeger, J., Haller, K. J., Aureliano, M., and Crans, D. C. (2014). Interaction of decavanadate with interfaces and biological model membrane systems:characterization of soft oxometalate systems. **Journal of Molecular and Engineering Material**. 2: 140007.
- Sedgwick, M., Cole, R. L., Rithner, C. D., Crans, D. C., and Levinger, N. E. (2012). Correlating Proton Transfer Dynamics To Probe Location in Confined

- Environments. **Journal of the American Chemical Society**. 134: 11904-11907.
- Singh, K., Kaur, H., Smith, P., de Kock, C., Chibale, K., and Balzarini, J. (2014). Quinoline-Pyrimidine Hybrids: Synthesis, Antiplasmodial Activity, SAR, and Mode of Action Studies. **Journal of Medicinal Chemistry**. 57: 435-448.
- Sostarecz, A. G., Gaidamauskas, E., Distin, S., Bonetti, S. J., Lvinger, N. E., and Crans, D. C. (2014). Correlation of Insulin-Enhancing Properties of Vanadium-Dipicolinate Complexes in Model Membrane Systems: Phospholipid Langmuir Monolayers and AOT Reverse Micelles. **Chemistry-A European Journal**. 20: 5149-5159.
- Vermathen, M., Chodosh, A. B., Louie, E. A., and Simonis, U. (1999). Investigations of porphyrins and metalloporphyrins in model membranes. **Journal Inorganic Biochemistry**. 74: 328-328.
- Vermathen, M., Louie, E. A., Chodosh, A. B., Ried, S., and Simonis, U. (2000). Interactions of water-insoluble tetraphenylporphyrins with micelles probed by UV-visible and NMR spectroscopy. **Langmuir**. 16: 210-221.
- Vermathen, M., Stiles, P., Bachofer, S. J., and Simonis, U. (2002). Investigations of monofluoro-substituted benzoates at the tetradecyltrimethylammonium micellar interface. **Langmuir**. 18: 1030-1042.
- Yang, L. Q., Crans, D. C., Miller, S. M., la Cour, A., Anderson, O. P., Kaszynski, P. M., Godzala, M. E., Austin, L. D., and Willsky, G. R. (2002). Cobalt(II) and cobalt(III) dipicolinate complexes: Solid state, solution, and in vivo insulin-like properties. **Inorganic Chemistry**. 41: 4859-4871.

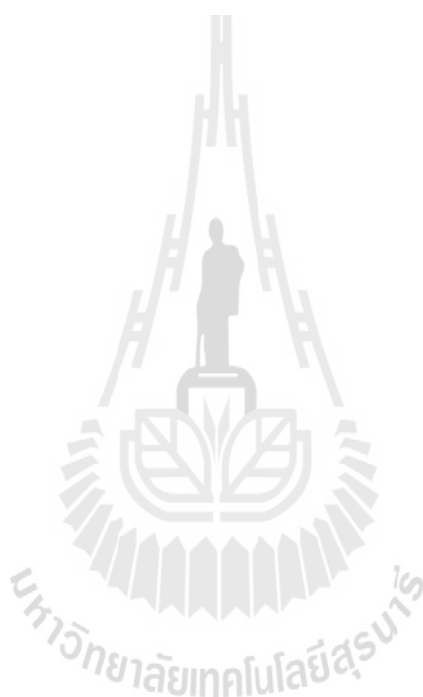
CHAPTER V

CONCLUSION

¹H NMR studies showed that the 1-phenylbiguanide (PBG) undergoes changes as it is placed in a RM environment. Since biguanides form strong hydrogen bonds in water, we investigated the effect of the biguanide on the water organization as the size of the RMs changes. Since the biguanide is near the interface and less bulk water is available as the size of the RM decreases, we observed the greatest change at the smaller w_0 sizes. The NOESY spectrum of PBG in AOT RM contains cross peaks between the PBG protons and AOT protons indicating that these protons are near each other, consistent with penetration of the hydrophobic part of the PBG into the interface. At the same time there is a cross peak between the biguanide NH moieties and the HOD signal placing the NH biguanide residues in the waterpool. Differential FTIR spectroscopy was used to demonstrate that the hydrogen-bonding properties in the waterpool changed in the presence of the biguanide. Since experiments carried out both in the inhomogeneous environment of AOT and CTAB RMs with similar results, suggesting that these findings are general and that PBG will reside at the interface and associate strongly both with the hydrophobic part of the interface and the waterpool at the same time.

In summary, the ability of PBG to serve as a bridge of interfaces was demonstrated and considering the relationship of this compound with the antimalarial drug, proguanil, this may be relevant for the action of this compound. Since PBG is

amphiphilic it will be soluble in water and more hydrophobic environments at the same time, which may be important for association with and how the compound can transverse across membranes.



APPENDICES



APPENDIX A

**INTERACTION OF BIGUANIDE COMPOUND WITH
MODEL MEMBRANE INTERFACE SYSTEM: PROBING
PROPERTIES OF ANTIMALARIA AND ANTIDIABETIC
COMPOUNDS**

This research is mainly of work. The work presented in this addition has appeared as the journal article, "Interaction of biguanide compound with model membrane interface system: probing properties of antimalaria and antidiabetic compounds" by Nuttaporn Samart, Cheryle N. Beuning, Kenneth J. Haller, Chris D. Rithner, and Debbie C. Crans, prepared for submission to *Langmuir*, (2014). Miss Beuning and Dr. Rithner performed the 2D NOESY NMR experiment of 1-phenylbiguanide that is mentioned. All the other work presented and data analysis were preformed by Nuttaporn Samart.

In addition to the work on phenylbiguanide this thesis also contains work carried out on the related metformin system, which has now been reported in *European Journal of Inorganic Chemistry* by Chatkon, Chatterjee, Sedgwick, Haller, and Crans, 2013 and *Inorganica Chemica Acta* by Chatkon, Barres, Samart, Boyle, Haller, and Crans, 2014. All studies carried for the Ph.D. Thesis has been focus on the interaction of biguanide drug with model membrane systems.

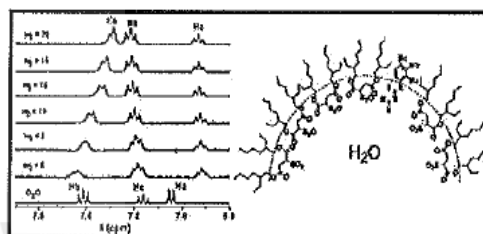
Interaction of a Biguanide Compound with Membrane Model Interface Systems: Probing the Properties of Antimalaria and Antidiabetic Compounds

Nuttaporn Samart,^{†,‡} Cheryle N. Beuning,[‡] Kenneth J. Haller,^{*,†} Chris D. Rithner,[‡] and Debbie C. Crans^{*,‡}

[†]School of Chemistry, Institute of Science, Suranaree University of Technology, Nakhon Ratchasima 30000 Thailand

[‡]Department of Chemistry, Colorado State University, Fort Collins, Colorado 80523-1872 United States

ABSTRACT: Since membrane penetration is important for drug efficacy, how antimalarial precursor material 1-phenylbiguanide (PBG) interacts with an interface was characterized using a reverse micelle (RM) model system. ¹H NMR studies show that PBG partitions across the membrane interface. Specifically, the ¹H NMR studies showed that the 1-phenylbiguanide compound in an aqueous environment changed when placed near an interface. PBG is known to affect hydrogen bonding in water, and as the size of the RMs changes, the water organization in the water pool is changed. The NOESY spectrum of PBG in AOT RM contains cross-peak signals between the PBG protons and AOT protons, which is consistent with the penetration of the PBG into the interface. At the same time, there is a cross peak between the biguanide moiety and the HOD signal. This shows that these NH protons are near the HOD protons, placing the biguanide functional group in the water pool. Preliminary differential FTIR spectroscopic studies confirmed this location. In summary, we found that PBG interacts with different regions of the interface, with the phenyl group penetrating the hydrophobic interface while the biguanide remains in the water pool.



INTRODUCTION

Drug uptake is critical for the mode of action but particularly important for diseases such as malaria in which cell membrane penetration is important for infection.^{1–8} Specifically, we are interested in how the properties of biguanides and associated drugs are affected near interfaces. One of the successful antimalaria drugs is proguanil (Figure 1).^{1,2,9} Proguanil is a biguanide and metabolizes to cycloguanil, which is a dihydrofolate reductase inhibitor.^{6,10–12} Another biguanide which is a common drug used for the treatment of diabetes is metformin.^{13–15} Metformin can dramatically impact the properties of other compounds and facilitate their solubility and is often coadministered with other drugs to help improve their uptake.^{13–16} No common mechanism of action for these biguanide drugs has been described.^{17,18} Although it is not known if the properties of the biguanide functionality are important to the mode of action, the possibility that metal complexation is involved has been proposed.¹⁸ The amphiphilic nature and special properties of these compounds encouraged us to investigate 1-phenylbiguanide (PBG), which is structurally related to both proguanil and metformin. In this article, we examine the interaction of 1-phenylbiguanide with surfactant interfaces in reverse micelles (RMs) using methods that would allow the identification of molecular interactions.

Malaria is an infectious disease caused by unicellular protozoan parasites of the genus *Plasmodium*. There are an estimated 200–300 million cases of the disease each year,

giving rise to an estimated 2 million deaths.^{7,19,20} Four species of plasmodia are infectious to humans: *Plasmodium falciparum*, *Plasmodium vivax*, *Plasmodium malariae*, and *Plasmodium ovale*. Most deaths worldwide result from *Plasmodium falciparum* infection. One of the most successful antimalaria drugs is chloroquine.^{1,2,9} Chloroquine is known to accumulate in the parasite's food vacuole and inhibit heme crystallization, which results in increased amounts of membrane-associated heme.^{1,2} Chloroquine therefore alters the membrane properties and upsets ion homeostasis. Recently, chloroquine was also found to associate with the membrane interface in model membrane systems.²¹ Unfortunately, chloroquine and proguanil treatment can both result in drug resistance. Proguanil in combination with Atovaquone is available under the trade name Malarone in many countries for the treatment of acute malaria caused by *Plasmodium falciparum*.^{10,22} Atovaquone is a ubiquinone antagonist that inhibits mitochondrial electron transport and collapses the mitochondrial membrane potential.²³ Although proguanil converted to cycloguanil is an inhibitor for dihydrofolate reductase, genetically altered human dihydrofolate reductase did not result in resistance to proguanil.²⁴

Proguanil is a biguanide and is structurally related to PBG and metformin as shown in Figure 1. The mode of action of

Received: April 26, 2014

Revised: June 12, 2014

Published: June 23, 2014

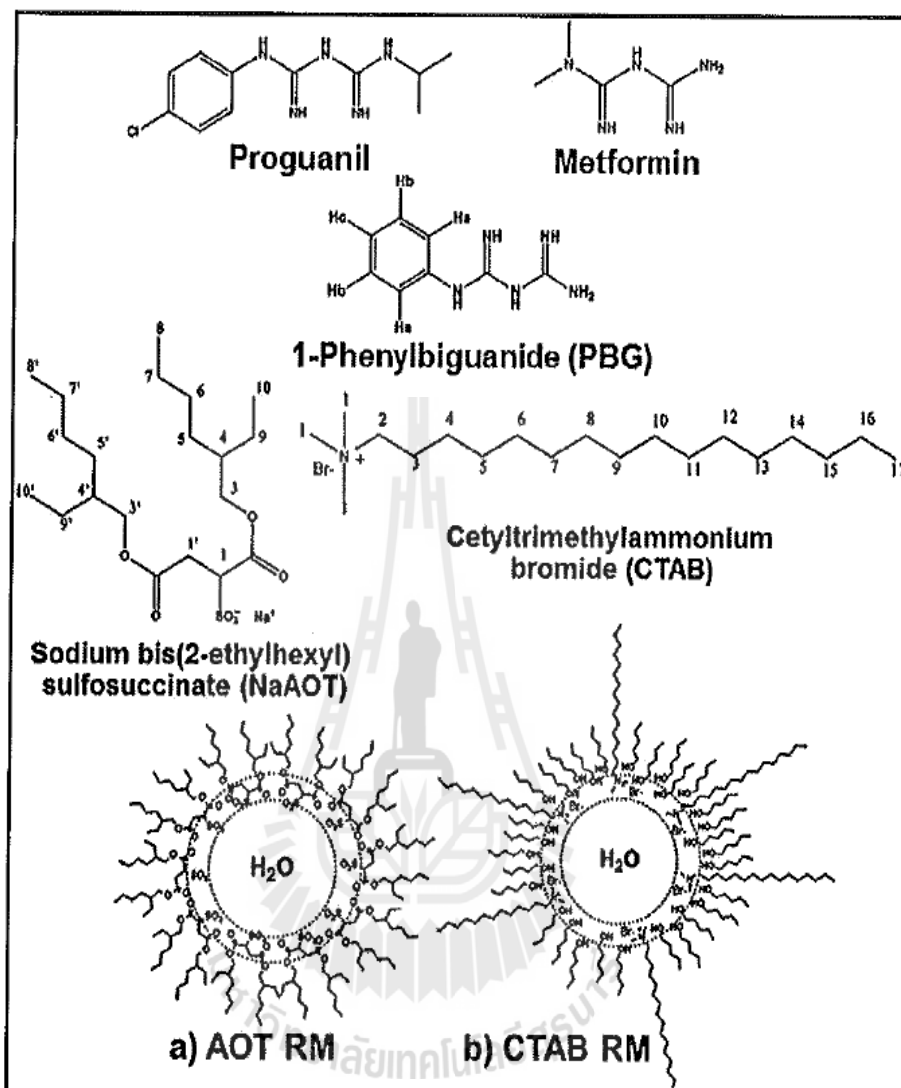


Figure 1. Schematic structures of proguanil, 1-phenylbiguanide (PBG), metformin, sodium bis(2-ethylhexyl) sulfosuccinate (AOT), cetyltrimethylammonium bromide (CTAB) and cartoon of AOT RM and CTAB with pentanol cosurfactant RM. In the AOT RM system, the sulfonate groups contains a negative charge, which is omitted in the schematic illustration.

metformin is poorly understood because several enzymes are inhibited by this compound^{13,14,18} and its physical properties could impact other compounds, membrane proteins, and membrane signaling. However, both proguanil and metformin are by simple transformation structurally related to PBG, which is investigated in this study. PBG has been reported to be a selective 5-hydroxytryptamine (5HT₃) receptor agonist.^{25,26} With the exception of the possibility that metal complexation is involved,¹⁸ no mechanistic connections involving the biguanide functionality have been reported between these drugs and their modes of action. However, the simple structural modification of metformin replacing the two methyl groups with a hydrogen and a phenyl group produced a compound able to engage in much more directed interface intercalation than reported for metformin.¹⁶

In ternary mixtures of polar, nonpolar, and amphiphilic molecules, self-assembly of the polar solvent to form nano-

droplets surrounded by an amphiphilic surfactant and the nonpolar organic solvent result in the formation of RMs (Figure 1).^{27–32} RMs have been used for many different applications including modeling biological reactions and serving as drug-delivery vessels. RMs can be prepared from various surfactants, giving rise to different types of interfaces classified by the charge of their polar headgroups.^{33–35} The four classes of surfactants are anionic, cationic, zwitterionic, and non-ionic.^{29,30} Figure 1 shows the structures for sodium bis(2-ethylhexyl) sulfosuccinate (aerosol OT or AOT) and cetyltrimethylammonium bromide (CTAB) that are commonly used surfactants to make RMs.^{36–38} A range of different organic solvents have been used for RM studies including cyclohexane, isooctane, benzene, chloroform, and others. Studies in our group have often used cyclohexane and "isooctane", although what has historically been named isooctane is in fact 2,2,4-trimethylpentane. Combining AOT in 2,2,4-trimethylpentane

with a little water results in an RM with a negative interface^{33,38–40} while combining organic solvent, CTAB, a short-chain alcohol, and water results in an RMs with a positive interface (Figure 1).^{38,41,42} The CTAB system is unlike the AOT reverse micelle system, as it requires the use of a cosurfactant.^{28,41}

Many of the known antimalarial drugs are hydrophobic basic amines, both features that are likely to be important to their mode of action. Here, we investigate how drugs containing the biguanide functionality associate with lipidlike interfaces. Such studies will allow us to evaluate whether membrane association or interactions could play a role in how these drugs work. To this end, we describe the investigation of PBG and its interaction with the aerosol-OT surfactant interface as well as the CTAB interface in RMs using ¹H NMR and 2D NOESY ¹H NMR spectroscopy.^{40,43,44}

EXPERIMENTAL SECTION

Materials. 1-Phenylbiguanide (PBG, Aldrich, 98.0%), activated charcoal (carbon 6–12 mesh, Fisher Scientific), sodium bis(2-ethylhexyl) sulfosuccinate (AOT, Sigma-Aldrich, 98.0%), deuterated dimethyl sulfoxide (*d*₆-DMSO), tetramethylsilane (TMS, Cambridge Isotope Laboratories), methanol (Sigma-Aldrich, 98.0%), 2,2,4-trimethylpentane (Sigma-Aldrich, 99.0%), deuterium oxide (D₂O, Aldrich, 99.9% deuterium), sodium deuteroxide (NaOD, Aldrich, 99% deuterium), deuterium chloride (DCl, Aldrich, 99% deuterium), cetyltrimethylammonium bromide (CTAB, Sigma-Aldrich, 99%), cyclohexane (Sigma-Aldrich, 99%), 1-pentanol (Sigma-Aldrich, 99%), and phosphorus pentoxide (Aldrich, 95%) were used as received. The purity of the solvents and materials was monitored using ¹H NMR spectroscopy.

Preparation of Samples for Analysis. Purification of NaAOT. NaAOT was purified by a slightly modified procedure.^{45,46} AOT (50.0 g) was dissolved in 250 mL of methanol and stirred overnight in the presence of 6–12 mesh activated charcoal (15.0 g). The suspension was filtered and then the methanol was removed by evaporation under high vacuum for at least 12 h. Purified AOT was dissolved in *d*₆-DMSO for ¹H NMR, and peak positions for the AOT protons were compared to those previously reported.^{45,46} The residual water content was found to be 0.3 water molecule per AOT molecule.^{45,46} When preparing reverse micelles, the ratios (*w*₀, the ratio of the amount of water to the amount of surfactant = [H₂O]/[AOT]) are calculated including the 0.3 water molecule already present in AOT.

Purification of CTAB. CTAB was purified by recrystallization from anhydrous ethanol, dried over phosphorus pentoxide for 48 h under reduced pressure, and stored over dried silica gel under vacuum.⁴²

Preparation of AOT/2,2,4-Trimethylpentane Stock Solution and Reverse Micelles. The 750 mM AOT/2,2,4-trimethylpentane stock solution was prepared by dissolving 8.34 g (18.8 mmol) of AOT in 25 mL of 2,2,4-trimethylpentane and vortex mixing until the solution cleared. Samples of various *w*₀ sizes were prepared using different amounts of AOT and D₂O. A range of RMs was prepared, with *w*₀ ranging from 6 to 20, by pipetting a specific volume of stock solution into aliquots of 750 mM AOT/2,2,4-trimethylpentane and vortex mixing until the solution was clear and suitable for ¹H, 2D NMR and FTIR analysis.

Preparation of Aqueous Stock Solutions of 1-Phenylbiguanide (PBG). The 100 mM PBG (0.886 g, 5.00 mmol) stock solution was prepared in deuterium oxide, D₂O (10 mL), in a volumetric flask. The solution was stirred until it was clear, and the pH of the suspension was adjusted using DCl and NaOD when needed. The pH of the solutions was measured at 25 °C on an Orion 720A+ pH meter, these readings were converted to pD by the formula pD = pH + 0.4,⁴⁷ and adjusted values are reported in this article.

Preparation of AOT/2,2,4-Trimethylpentane Reverse Micelles with 1-Phenylbiguanide (PBG) for 1D ¹H NMR Spectroscopic Studies. The solution containing 50 mM PBG was acidified using DCl and NaOD for pH values ranging from 1.21 to 12.3, where pD =

pH + 0.4 and were used to make AOT RMs. A range of RMs were prepared with *w*₀ ranging from 6 to 20 by pipetting a specific volume of stock solution into aliquots of 750 mM AOT/2,2,4-trimethylpentane. Upon mixing these solutions as prescribed, a cloudy solution resulted, which cleared after vigorous vortex mixing, and then the solutions were suitable for ¹H NMR analysis.

Preparation of the 2D ¹H NMR NOESY Sample in an AOT Reverse Micelle Solution with PBG. A *w*₀ = 10 sample of PBG in AOT/2,2,4-trimethylpentane was prepared with 100 mM PBG in D₂O solution with pD = 7.07 using NaOD and DCl to adjust the pH, where pD = pH + 0.4. The samples were slightly heated in a water bath up to 60 °C in order to dissolve precipitated PBG during the titration at this neutral pH. Purified AOT was used to make a 750 mM AOT solution in 2,2,4-trimethylpentane. Once the aqueous PBG and AOT in 2,2,4-trimethylpentane were mixed, the suspension was vortex mixed until the solution became transparent.

Preparation of the FTIR Sample in an AOT Reverse Micelle Solution with PBG. For IR spectroscopy experiments, two sets of aqueous solutions for each 10 and 100 mM PBG over a pH range of 6.59 to 7.07 were prepared. One set of solutions for each concentration was prepared by using 5% HOD in H₂O, and a second set of solutions for each concentration was prepared using only 100% H₂O. The pH was adjusted to be in this range by using DCl and NaOD for the sample containing D₂O and by using HCl and NaOH for the samples containing only H₂O. Purified AOT was used to make a 750 mM AOT solution in 2,2,4-trimethylpentane. The RM samples, having a *w*₀ of 10, were prepared by mixing the aqueous PBG with the AOT in 2,2,4-trimethylpentane and vortex mixed until the solution was transparent. This RM preparation was carried out for each 5% HOD and 100% H₂O solution for each concentration.

Preparation of CTAB Reverse Micelle Solution with 1-Phenylbiguanide (PBG). Each sample was prepared separately by combining purified solid CTAB, 1-pentanol, cyclohexane, and aqueous 50 mM PBG stock solution. CTAB and 1-pentanol concentrations in cyclohexane before the addition of the aqueous phase were 150 and 750 mM, respectively, and the molar ratios [H₂O]/[CTAB] (*w*₀) were equal to 8, 10, 16, 20, and 30 unless specified otherwise. All experiments were carried out using transparent and single-phase solution samples.⁴¹

Methods. 1D NMR Spectroscopy. The ¹H NMR spectra of RM solutions were recorded using an Agilent Inova spectrometer operating at 400 MHz at ambient temperature (25 ± 0.2 °C) in unlocked mode using routine parameters. Spectra were initially referenced against internal TMS (δ = 0.00 ppm) and then routinely against the 2,2,4-trimethylpentane resonance (δ = 0.904 ppm) for AOT RM as reported previously.^{16,40,44,48}

RM samples for NMR spectroscopy were prepared from 750 mM AOT stock solutions in 2,2,4-trimethylpentane and in 10, 50, and 100 mM PBG in D₂O at the desired pH values. The PBG stock solutions were adjusted to near the desired pH using DCl and NaOD before the final dilutions were made. The chemical shift was referenced against an external sample of 3-(trimethylsilyl)propanesulfonic acid (DSS). Data analysis was conducted using MestReC V4.5.9.1 NMR spectroscopic data processing software and ACD/NMR Processor Academic Edition for Windows.

2D NMR Spectroscopy. ¹H–¹H NOESY NMR experiments were performed on a 400 MHz Agilent Inova NMR spectrometer. The NOESY data were acquired with a 4500 Hz window for protons in *f*₂ and *f*₁. The NOESY mixing time was 200 ms, and 32 transients were acquired per increment. The total recycle time between transients was 1.85 s. The data set consisted of 1332 complex points in *f*₂ by 200 complex points in *f*₁ using States-TPPI. Cosine-squared weighting functions were matched to the time domain in both *f*₁ and *f*₂, and the time domains were zero filled prior to the Fourier transform. The final resolution was 2.2 Hz/pt in *f*₂ and 8.8 Hz/pt in *f*₁. Data processing was done using the Agilent VNMRJ-3.2D software.^{25,40,44}

RESULTS

NMR Spectra and Properties of 1-Phenylbiguanide (PBG). For the investigation of the interaction of biguanide compounds with model interfaces, first the spectroscopic properties of the different protonation states need to be determined in aqueous solution as the reference system at hand.

The ^1H NMR signals for PBG in aqueous solution are dependent on the pH of the solution as shown in Figure 2. The diprotonated, monoprotated, and neutral forms of PBG can be readily distinguished based on the location of the ^1H NMR signals. The signals for the deprotonated form are 0.05 to 0.15 ppm downfield from the monoprotated form that exists in

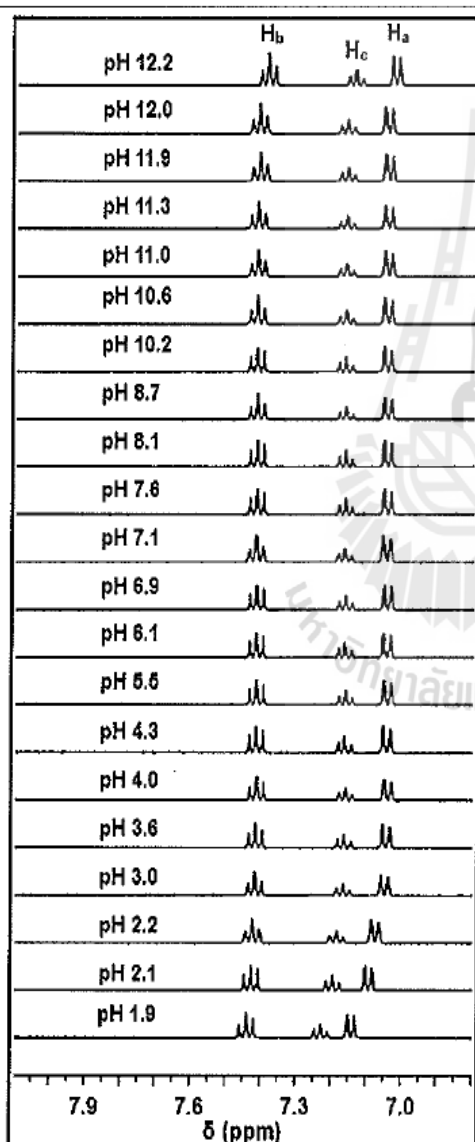


Figure 2. Partial ^1H NMR spectra were recorded in D_2O for 100 mM PBG in aqueous solution at pH values of between 1.0 and 12.3 measured at 400 MHz. Samples were referenced against a solution of DSS using an external lock. protons H_a , H_b , and H_c are labeled in the PBG drawing in Figure 1

solutions at pH 2 through 11. At basic pH, the shifts continue to move upfield as is generally observed upon deprotonation.⁴¹ These observations are in agreement with the reported pK_a values for this complex of 2.13 and 10.76.⁴⁹

1-Phenylbiguanide (PBG) in AOT/2,2,4-Trimethylpentane RMs: ^1H NMR Spectroscopic Studies. The interaction of PBG with the anionic surfactant layer in AOT RMs was studied using ^1H NMR spectroscopy. In Figure 3, the ^1H NMR spectra are shown for a 50 mM PBG aqueous stock solution containing the doubly protonated form of the PBG (at pH 1.0) in 750 mM AOT/2,2,4-trimethylpentane at w_0 ratios from 6 to 16. The ^1H NMR chemical shifts for the aqueous solution of the H_a proton is at 7.415 ppm (ortho position, a doublet signal), that for the H_b proton is at 7.576 ppm (the meta position, the larger triplet signal), and that for the H_c protons is at 7.498 ppm (the para position, the small triplet signal). When comparing the spectra of the RM systems with the spectra of the aqueous stock solution (Figure 2), an upfield shift is observed for all three protons. The H_b and H_c protons are most shifted by addition to the RMs. Both protons shift by 0.2 to 0.3 ppm upfield. A smaller downfield shift is observed for H_a . Overall, these spectra show a change in the order of the signals where H_a is the most upfield proton in aqueous solution but the most downfield proton in the RM system. The observed shifts therefore do not correspond to the deprotonation of the diprotonated species because none of the RM proton signals approach the spectra observed in aqueous solution at any pH value. The observed shifting is consistent with an environmental change upon placement of PBG into the RMs and a modest but observable change as the w_0 decreases. The increased line broadening as the w_0 size decreases indicates that the relaxation time of the proton is decreasing. This decrease is consistent with the decreasing mobility of the molecule as the size of the system is decreasing.

In Figure 4, the ^1H NMR spectra are shown for a 50 mM PBG aqueous stock solution containing deprotonated PBG (at pH 12.3) added to 750 mM AOT/2,2,4-trimethylpentane in w_0 from 6 to 20. The ^1H NMR chemical shift for the aqueous solution of the H_a proton is at 7.023 ppm (doublet), that for the H_b proton is at 7.385 ppm (triplet), and that for H_c protons is at 7.136 ppm (triplet), see Figure 2. When comparing the spectra of the RM systems with that of an aqueous stock solution, an upfield shift is observed for two of the protons and one proton shifts downfield, although the amount by which each peak shifted varied. The H_a protons are most shifted by addition to the RMs (by 0.4 ppm). These spectra show a change in the order of the signals; that is, H_a is the most upfield proton in aqueous solution but the most downfield proton in the RM system. The observed shifts therefore do not correspond to a simple change in protonation state. The largest shifts are observed in the small w_0 values; however, none of the RM proton spectra approach the spectra observed in aqueous solution at any pH value. This is consistent with a definite environmental change upon placement in the RMs and significant as found for the w_0 decrease.

Comparing the spectral series at low (Figure 3) and high pH (Figure 4), we observe shifting as the w_0 size change varies significantly. Perhaps most important is the fact that all three protons shifted downfield as the w_0 size decreased at low pH, whereas at higher pH only two out of the three protons shifted downfield and the third proton, H_a , shifted upfield. Such patterns, of some protons shifting one way and the other protons shifting in a different direction, have been attributed to

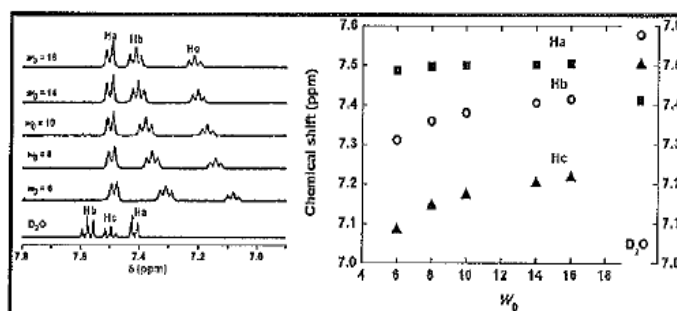


Figure 3. (Left) Partial ^1H NMR spectra of 100 mM PBG at pH 1.0 in 750 mM AOT/2,2,4-trimethylpentane RMs recorded at 400 MHz and referenced against the 2,2,4-trimethylpentane resonance at 0.904 ppm. (Right) Graph of the specific chemical shift of PBG protons, H_a (■), H_b (○), and H_c (▲), as a function of w_0 size. Protons H_a , H_b , and H_c are labeled in the PBG drawing in Figure 1.

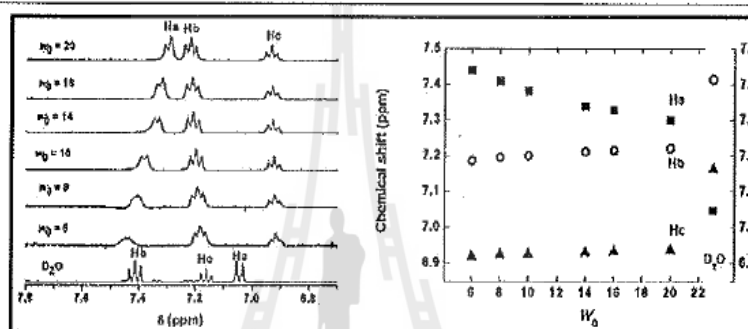


Figure 4. (Left) Partial ^1H NMR spectra of 50 mM PBG at pH 12.3 in 750 mM AOT/2,2,4-trimethylpentane RMs recorded at 400 MHz and referenced against the 2,2,4-trimethylpentane resonance at 0.904 ppm. (Right) Plot of the apparent specific chemical shifts of PBG, H_a (■), H_b (○), and H_c (▲), as a function of w_0 . Protons H_a , H_b , and H_c are labeled in the PBG drawing in Figure 1.

the specific location at the interface in the literature.^{25,40,43,44,50} The different multidirectional shifting patterns ruled out the possibility that the same protonation stages of the PBG are involved in these spectra, supporting the variation in the environmental change that is consistent with changing the location of the compound depending on the protonation state.

1-Phenylbiguanide (PBG) in an AOT RM 2D NOESY Study. To further characterize the interactions of PBG with AOT/2,2,4-trimethylpentane in this model membrane system, we employed 2D NMR NOESY to investigate the location of the drug in the RM system.^{25,40,44} Specifically, we characterized the interaction of the solution of 100 mM PBG at neutral pH ($\text{pD} = 7.07$) in 750 mM AOT using 2D ^1H NOESY. Since the spectra shown in Figure 5 are for studies carried out on samples prepared from a solution of PBG at neutral pH, the H_a signal was found to be different from those shown at $w_0 = 10$ at high or acidic pH. This effect will be investigated at a later time, but suffice it to say that for the series at basic pH, corresponding line broadening was observed at the lower w_0 values.

As shown in Figure 5, the partial 2D spectrum in the F2 frame is a close-up of phenyl protons H_a (2H, 7.57 ppm), H_b (2H, 7.32 ppm), and H_c (1H, 7.06 ppm) along with a broad H peak, which is the N–H signal (6.82 ppm) in PBG. The F1 frame is the full spectrum including an HOD peak (1H, 4.60 ppm), a broad and large peak of 2,2,4-trimethylpentane at 1.01 ppm, and especially the side-arm-chain methylene protons of AOT, which show an overlapping signal in AOT (4H, 1.41 ppm, 9,9' as labeled in Figure 1). The diagonal (solid line) is present to emphasize the two different scales of the sides on the 2D spectrum. As expected, there are intense cross peaks between H_a and H_b as well as between H_b and H_c from PBG,

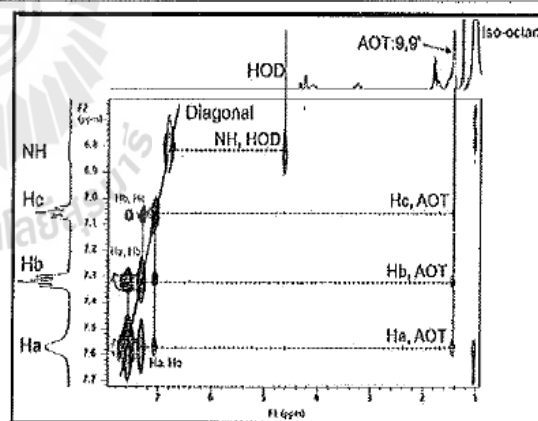


Figure 5. Partial ^1H NMR NOESY spectrum of 100 mM PBG at pD ($= \text{pH} + 0.4$) 7.07 in 750 mM AOT. The spectrum was recorded at 400 MHz using the parameters detailed in the Experimental Section. The F2 or y axis is enlarged for the phenyl and nitrogen protons in PBG, and the F1 or x axis is the full spectrum. The diagonal is the solid line, and prominent cross peaks are shown as dotted lines along with their respective hydrogen interactions.

and these signals demonstrate that the protons are near each other. A weaker cross peak between H_a and H_c was also observed. The cross peak between H_a and H_c is weak in comparison to the cross peak for H_a and H_b , indicating that these protons are not as close.

The intense cross peaks of H_a and H_b as well as those of H_b and H_c show that these protons are close together, which is

expected. Phenyl protons H_a , H_b , and H_c all have weak cross peaks with the 9,9'-methylene protons of AOT. Prominent cross peaks between the PBG and signals in AOT are indicated by dashed lines. The H_b and H_a protons can interact with the 9,9'-methylene protons in the backbone of the AOT tails; this peak is at approximately 1.41 ppm on AOT. As shown in Figure 5, the weak cross peak with the 9,9'-methylene AOT protons with H_a and H_b indicates the positioning of the molecule in the interface; H_c will interact less with these methylene protons. The lack of a cross peak of H_a , H_b , and H_c with the HOD signal at approximately 4.60 ppm shows that the phenyl group is less likely to interact with the water pool. Presumably, the phenyl group protons are mainly interacting with the AOT methylene protons since there is a defined cross peak with AOT. Thus, this portion of the PBG is nestled high in the interface of the RMs.

Finally, an intense cross peak to the NH signal was observed and traced to HOD. As seen in Figure 1, PBG has multiple NH groups and their signal is very broad, which is an indication that the relaxation times (t_1 and t_2) are very short and different from those of the phenyl protons. However, in the 2D spectrum we see a very intense NH signal along the diagonal and an intense cross peak with HOD indicating a close association between the NH protons and the HOD protons in the water pool. Although it is possible that some water molecules could penetrate the interface, the interaction observed between the NH and HOD protons is very strong, suggesting that this interaction of HOD and NH protons is very strong as expected if these groups are in or very near the water pool. The lack of an NH cross peak with any AOT protons also suggested that this part of the PBG is nestled inside the water pool.

Since the 2D NOESY studies suggested that part of the PBG molecule resides in the water pool, we carried out preliminary differential FTIR studies confirming that PBG affects the H bonding in the water pool of the RMs.³⁵ These studies characterized AOT/2,2,4-trimethylpentane RMs by comparing spectra in the absence and presence of 5% HOD. Differential FTIR spectra were recorded for RM samples with 100% H_2O and RMs containing 5% HOD at pH ~ 7.0 and 10 and 100 mM PBG in AOT RMs with $w_0 = 10$. These spectra were then subtracted to produce the resulting spectrum of OD stretching. Preliminary differential FTIR spectra confirmed the conclusion obtained by NMR spectroscopy studies that part of the PBG resides in the AOT RM water pool, as expected for an amphiphilic molecule.

In conclusion, PBG interacts both with the hydrophobic and hydrophilic parts of the interface as well as HOD in the water pool. This study shows an example of a probe that extends into both the interface and the water pool.

NMR spectroscopy results show that the chemical shift for the phenyl protons in PBG changes, which is consistent with penetration into the interface. The NOESY experiments furthermore show that the NH groups on the biguanide interact, consistent with the PBG molecule residing at the interface and extending deep into the hydrophobic part as well as in the water pool at the same time. The preliminary IR spectroscopy results show that the biguanide group in PBG significantly affects the hydrogen bonding present among the water molecules in the water pool. These results are consistent with the model illustrated in Figure 6.

1-Phenylbiguanide (PBG) in CTAB/Pentanol/Cyclohexane RMs: 1H NMR Spectroscopic Studies. In the

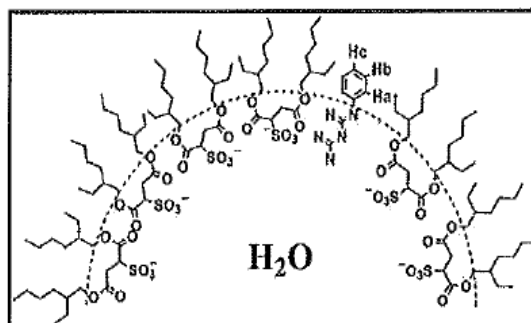


Figure 6. Cartoon illustrating the suggested location of 1-phenylbiguanide in the AOT reverse micelle.

following section, we determine the differences in cell loading if the charge on the RM interface changes. The interaction of PBG with the cationic surfactant layer in a CTAB RM was studied using 1H NMR spectroscopy. In Figure 7, the 1H NMR spectra are shown for a 50 mM PBG aqueous stock solution containing the doubly protonated form of the PBG (at pH 1) in 150 mM CTAB/750 mM pentanol in cyclohexane at w_0 ratios from 8 to 30. The 1H NMR chemical shift for the aqueous solution of the H_a proton (ortho to the biguanide group) is at 7.415 ppm (a doublet signal), that for the H_b proton (meta to the biguanide group) is at 7.576 ppm (the larger triplet signal), and that for the H_c protons (para to the biguanide group) is at 7.498 ppm (the small triplet signal). All three protons were observed to shift upfield when compared to the spectra of the RM systems in the aqueous stock solution (Figure 2). The H_a proton is most shifted by addition to the RM, and the proton shifted by 1.0–1.5 ppm upfield. No shifting was observed for H_b and H_c . A little observed shifting is consistent with an environmental change upon placement of PBG into the RMs and a modest but observable change as w_0 decreased.

The spectra in Figure 8 shows the shifts that were observed in the region of the CTAB headgroup and chains. The left panel contains a probe and is to be compared to the panel on the right that was run with no probe in it. As observed, the CTAB protons do not shift as a function of w_0 size, which suggests that there is no change in the environment of the surfactant. However, as seen from the comparison of the two panels, there is a small but distinct upfield shift in the water signal. This suggests that the H bonding and properties of the water pool are changing in the presence of the probe. These results show that the observations made for the AOT/2,2,4-trimethylpentane system and the location of the probe at the interface are also observed when the charges on the interface change. This is particularly interesting because the charge on PBG is positive and so is the interface. These results suggest that the location of the PBG is not only determined by Coulombic forces but that hydrophobic forces are likely to have an important influence with regard to the probe location.

DISCUSSION

Malaria and other infectious diseases represent a major health problem for impacted areas, and since people frequently travel, it can impact other areas of the world as well. The quest for the development of new treatments and drugs remains a high priority because of the problems associated with resistance development. Many approaches^{12,51,52} and new drugs^{53–54} are in various stages of development to combat malarial infections.

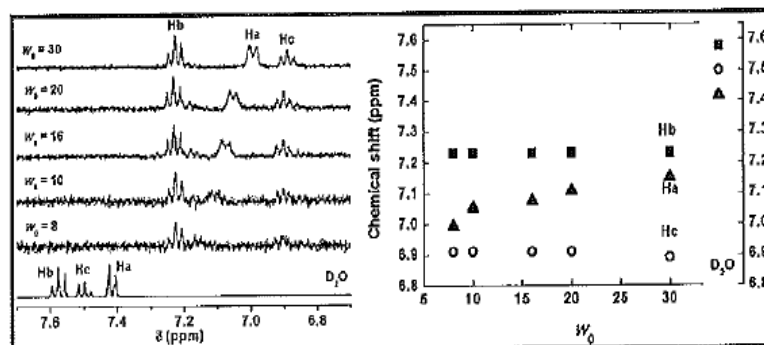


Figure 7. (Left) Partial ^1H NMR spectra of 50 mM PBG at pH 1 in 150 mM CTAB/750 mM pentanol in cyclohexane RMs recorded at 400 MHz and referenced against the cyclohexane resonance at 1.430 ppm. (Right) Graph of the specific chemical shift of PBG protons, H_a (▲), H_b (■), and H_c (○), as a function of w_0 size.

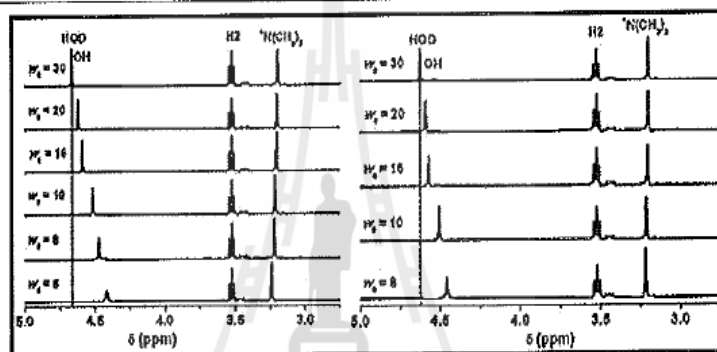


Figure 8. (Left) Partial ^1H NMR spectra of 50 mM PBG at pH 1 in 150 mM CTAB/750 mM pentanol in cyclohexane RMs recorded at 400 MHz and referenced against the cyclohexane resonance at 1.430 ppm. (Right) Plot of the AOT/cyclohexane RMs in the absence of the PBG probe.

The studies presented here investigate the interaction of PBG by model membrane interfaces using NMR spectroscopy. By choosing a simple model system for these studies, we determined molecular details of the solute interaction with the interface. In these studies, we used the AOT/2,2,4-trimethylpentane system as the model interface because this system is found to be an effective model system providing data that are in line with corresponding biological studies.⁴⁸ ^1H NMR studies are informative because they provide molecular information describing the environment of each H atom, which will identify the molecular positioning very precisely. Studies with more complex systems require the use of spectroscopic probes that provide changes in signals that report on environmental changes without molecular detail whereas NMR spectroscopy is a powerful method for defining molecular probe positioning.^{25,40,44} The chemical shift changes are consistent with the PBG being located at the membrane interface and the fact that it partially penetrates the interface. This interpretation was supported by FTIR and 2D NOESY experiments which each confirm the location of the PBG with the water pool and the hydrophobic interface. That is, the phenyl ring interacted with the AOT in the interface of the RMs and biguanide NH groups interacted with the water molecules in the water pool. We illustrate the location of PBG in Figure 6.

Using 1D NMR studies (i.e., chemical shift changes), we found that the environment changed upon placement of the PBG in the RM environment. Since ^1H NMR gives information with regard to all of the different signals in the NMR spectrum of the complex, the shifting of the signals is a measure of how

the environment is changing for the molecule. However, the interpretation of the shifting is nontrivial because both upfield and downfield shifting can be due to the penetration of PBG into the interface.^{43,48,55,56} For example, previously downfield shifting has been associated with $[\text{VO}_2\text{dipic}]^-$ penetration of the interface,⁴⁸ and similarly, upfield shifting has been associated with the penetration of fluorobenzoates into the interface.⁴³ We attribute these factors to the nature of the effects on shifting being a complex matter involving environmental hydrophobicity, charge, solubility, and in general a complementary interaction between the probe and interface. Additional information is therefore desirable, and we have been obtaining such information using 2D NMR and FTIR experiments.

The changes observed upon placement into the RM could potentially be attributed to changes in the pH of the solution. The ^1H NMR spectrum of PBG is reported for the pH and protonation state of the probe in addition to placement and environmental changes (Figures 2–4). The changes in the proton chemical shift of PBG by ^1H NMR spectroscopy were considered, and spectra were run at different pH values (Figure 2). Since greater shifts are found for H_a at high pH when placed into the RMs (Figure 4), this would suggest that the H_a proton is found to move from H_2O to the hydrophobic environment, possibly by rotation around the N–Ph bond, and thus experiences the most dramatic environmental change of the three protons. H_a is near the charged biguanide group, and as the molecule penetrates the hydrophobic interface, H_a will feel this difference in environment more than H_b and H_c that are not penetrated as far into the interface. At low pH, the

Table 1. Content of AOT/2,2,4-Trimethylpentane RMs Investigated as Determined by w_0 and Size

w_0	$n(\text{agg})$	$N(\text{probes})$	$N(\text{AOT})$	$N(\text{RMs})$	probes/RMs	size (radius)
6	50	4.52×10^{18}	4.18×10^{20}	8.35×10^{18}	0.54	28 Å
8	72	5.88×10^{18}	4.07×10^{20}	5.66×10^{18}	1.0	32 Å
10	98	7.17×10^{18}	3.98×10^{20}	4.06×10^{18}	1.8	34 Å
16	215	1.07×10^{19}	3.71×10^{20}	1.73×10^{18}	6.2	42 Å
20	302	1.28×10^{19}	3.55×10^{20}	1.18×10^{18}	11	44 Å
$[\text{H}_2\text{O}]/[\text{AOT}]$	"				$N(\text{probe})/N(\text{RMs})$	"

^aReference 30.

biguanide residue is doubly protonated and all three phenyl protons will feel the effect of the protonation when the probe is moved from an aqueous to a hydrophobic environment. In contrast, at high pH only H_a will be affected by this environmental change because it is closer to the polar interface. These observations are in line with what has been observed in the past.^{25,44,50}

The spectrum in Figure 5 shows a 2D NOESY experiment where PBG is interacting with the surfactant AOT. The diagonal signals demonstrate interactions between the AOT protons with the PBG protons. In addition, H_b , H_c , and H_d on the phenyl group are associating with the CH_2 groups (specifically 9,9' of AOT) high up in the hydrophobic part of the interface. This interaction is likely to be sensitive to the specific conditions of the system. The spectrum also showed the interaction of NH protons of PBG with HOD protons in the water pool.

We carried out the studies using 0.10 M PBG, and as w_0 increased and the number of water molecules increased in each RM, the number of probes in each RM increased as well. In Table 1 we show how the number of probes increases as w_0 increases and the water pool increases. The NOESY experiments were carried out with 1.8 PBG in each reverse micelle ($w_0 = 10$), documenting the fact that the interface can accommodate two such molecules per RM. In the systems that were investigated, about two layers of water molecules were solvating the RM.³⁰ The increasing number of probes as the w_0 increases may be important for the specific distribution of the probes and particularly for the smaller w_0 sizes that are barely large enough to hold the PBG⁵⁷ within the boundaries of the water pool. It is therefore to be expected that the interface may saturate as observed for other systems (unpublished data) and thus force some of the probes into the water pool.

The studies with CTAB/1-pentanol demonstrate that the biguanide favored bridging the membrane and having parts in the water pool and parts up high in the hydrophobic interfacial environment. Although other compounds could exhibit similar properties, we have not previously observed a molecule with such a clear-cut 2D NOESY spectrum bridging compartments. With the dipic ligand,⁴⁰ we found that the probe could move but preferred to reside high up in the interface; however, some cross peaks indicated that the ligand moved and that the compound could also sometimes be found near the polar headgroups of the interface. For $[\text{Co}(\text{dipic})]^{2-}$,⁵⁸ the ascorbic acid, $\text{Cr}(\text{pic})_3$ and BMOV ⁵⁹ all were found near the interface. In contrast, decavanadate⁵⁹ and HTPS⁴⁴ were found in the middle of the AOT/2,2,4-trimethylpentane water pool as anticipated by their high charges. In the case of the V-dipic complexes ($[\text{VO}_2\text{dipic}]^-$, $[\text{VOdipic}(\text{H}_2\text{O})_2]$, and $[\text{V}(\text{dipic})_2]^-$), the metal ion oxidation state and complex charge as well as the size of the complex determined the specific location of the compound.⁶⁰ However, when the charges on the interface

changed then the location of these systems changed. Specifically, the decavanadate⁵⁹ and HTPS⁴⁴ molecules moved from the middle of the water pool to the interface of the RM water pool.

Antimalarial drug proguanil is on the market, and related derivatives PBG and metformin are antidiabetic agents. These three compounds all are biguanides. The model studies presented here provide information documenting the ease by which these compounds can associate with and penetrate the membranelike interface, which may be important for some of the biological responses. There is no doubt that the antimalarial drugs act in part by modifying the properties of the host membrane; therefore, the findings that are reported here suggest that these compounds may be able to traverse the membrane much more readily than previously anticipated. It is known that PBG induces a response by associating with the 5-hydroxytryptamine (5HT3) receptor; however, these studies could also be interpreted as PBG and proguanil possessing the ability to traverse membranes readily. The ability of this PBG to span the membrane interface is likely to be important to the metabolism. Perhaps such properties indicate a secondary effect of these compounds as protonophores, a mode of action already known for atovaquone, which collapses the mitochondrial membrane potential.

CONCLUSIONS

¹H NMR studies showed that 1-phenylbiguanide (PBG) underwent changes as it was placed in an RM environment. Since biguanides form strong hydrogen bonds in water, we investigated the effect of biguanide on the water organization as the size of the RM changed. Since biguanide is near the interface and less bulk water is available as the size of the RM decreases, we observed the greatest change for the smaller w_0 sizes. The 2D NOESY spectrum of PBG in AOT RM contains cross-peak signals between the PBG protons and AOT protons, indicating that these protons are near each other, consistent with penetration of the hydrophobic part of the PBG into the interface. At the same time, there is a cross peak between the biguanide NH moieties and the HOD signal, placing the NH biguanide residues in the water pool. Differential FTIR spectroscopy was used to demonstrate that the hydrogen-bonding properties in the water pool changed in the presence of the biguanide. The experiments carried out in the inhomogeneous environment of AOT and CTAB RMs with similar results suggested that these findings are general and that PBG will reside at the interface and associate strongly with both the hydrophobic part of the interface and the water pool at the same time.

In summary, the ability of PBG to serve as a bridge for interfaces was demonstrated, and considering the relationship of this compound with antimalarial drug proguanil, this may be relevant to the action of this compound. Since PBG is

amphiphilic, it will be soluble in water and more hydrophobic environments at the same time, which may be important for association with and how the compound can traverse the membrane.

AUTHOR INFORMATION

Notes

The authors declare no competing financial interest.

ACKNOWLEDGMENTS

N.S. and K.J.H. thank the Commission on Higher Education, Thailand, for financial support for study and overseas travel support allowing research work at CSU. D.C.C. thanks the National Science Foundation (NSF) and Colorado State University for funding. We thank Mrs. Mary Fisher for carrying out the preliminary FTIR studies.

ABBREVIATIONS

AOT, sodium bis(2-ethylhexyl) sulfosuccinate; CTAB, cetyltrimethylammonium bromide; NOSEY, nuclear Overhauser effect spectroscopy; PBG, 1-phenylbiguanide; RMs, reverse micelles; BMOV, bis(maltolato)oxovanadium(IV); HPTS, 8-hydroxypyrene-1,3,6-trisulfonate

REFERENCES

- (1) de Souza Santos, M.; de Moraes Del Lama, M. P. F.; Siuti Ito, A.; Zumstein Georgetto Naal, R. M. Binding of chloroquine to ionic micelles: Effect of pH and micellar surface charge. *J. Lumin.* 2014, *147*, 49–58.
- (2) Ginsburg, H.; Famin, O.; Zhang, J. M.; Krugliak, M. Inhibition of glutathione-dependent degradation of heme by chloroquine and amodiaquine as a possible basis for their antimalarial mode of action. *Biochem. Pharmacol.* 1998, *56*, 1305–1313.
- (3) Hindley, S.; Ward, S. A.; Storr, R. C.; Searle, N. L.; Bray, P. G.; Park, B. K.; Davies, J.; O'Neill, P. M. Mechanism-based design of parasite-targeted artemisinin derivatives: Synthesis and antimalarial activity of new diamine containing analogues. *J. Med. Chem.* 2002, *45*, 1052–1063.
- (4) Mather, M. W.; Darrrouzet, E.; Valkova-Vaichanova, M.; Cooley, J. W.; McIntosh, M. T.; Daldal, F.; Vaidya, A. B. Uncovering the molecular mode of action of the antimalarial drug atovaquone using a bacterial system. *J. Biol. Chem.* 2005, *280*, 27458–27465.
- (5) Moura, P. A.; Dame, J. B.; Fidock, D. A. Role of Plasmodium falciparum Digestive Vacuole Plasmepsins in the Specificity and Antimalarial Mode of Action of Cysteine and Aspartic Protease Inhibitors. *Antimicrob. Agents Chemother.* 2009, *53*, 4968–4978.
- (6) Pudney, M.; Gutteridge, W.; Zeman, A.; Dickins, M.; Woolley, J. L. Atovaquone and proguanil hydrochloride: A review of nonclinical studies. *J. Travel Med.* 1999, *6*, S8–S12.
- (7) Griffith, K. S.; Lewis, L. S.; Mali, S.; Parise, M. B. Treatment of malaria in the United States - A systematic review. *J. Am. Med. Assoc.* 2007, *297*, 2264–2277.
- (8) Singh, K.; Kaur, H.; Smith, P.; de Kock, C.; Chibale, K.; Balzarini, J. Quinoline-Pyrimidine Hybrids: Synthesis, Antiplasmodial Activity, SAR, and Mode of Action Studies. *J. Med. Chem.* 2014, *57*, 435–448.
- (9) Radloff, P. D.; Philipps, J.; Nkeyi, M.; Hutchinson, D.; Kremsner, P. G. Atovaquone and proguanil for Plasmodium falciparum malaria. *Lancet* 1996, *347*, 1511–1514.
- (10) Ryley, J. P. The mode of action of proguanil and related antimalarial drugs. *Br. J. Pharmacol. Chemother.* 1953, *8*, 424–430.
- (11) Fidock, D. A.; Nomura, T.; Welles, T. E. Cycloguanil and its parent compound proguanil demonstrate distinct activities against Plasmodium falciparum malaria parasites transformed with human dihydrofolate reductase. *Mol. Pharmacol.* 1998, *54*, 1140–1147.
- (12) Plowe, C. V.; Djimde, A.; Bouare, M.; Doumbo, O.; Welles, T. E. Pyrimethamine and proguanil resistance-conferring mutations in Plasmodium falciparum dihydrofolate-reductase-polymerase chain-reaction methods for surveillance in Africa. *Am. J. Trop. Med. Hyg.* 1995, *52*, 565–568.
- (13) Graham, G. G.; Punt, J.; Arora, M.; Day, R. O.; Doogue, M. P.; Duong, J. K.; Furlong, T. J.; Greenfield, J. R.; Greenup, L. C.; Kirkpatrick, C. M.; Ray, J. E.; Timmins, P.; Williams, K. M. Clinical Pharmacokinetics of Metformin. *Clin. Pharmacokinet.* 2011, *50*, 81–98.
- (14) Scarpello, J. H. B.; Howlett, H. C. S. Metformin therapy and clinical uses. *Diab. Vasc. Dis. Res.* 2008, *5*, 157–167.
- (15) Tajima, A.; Hirata, T.; Taniguchi, K.; Kondo, Y.; Kato, S.; Saito-Hori, M.; Ishimoto, T.; Yamamoto, K. Combination of TS-021 with metformin improves hyperglycemia and synergistically increases pancreatic β -cell mass in a mouse model of type 2 diabetes. *Life Sci.* 2011, *89*, 662–670.
- (16) Chatkon, A.; Chatterjee, P. B.; Sedgwick, M. A.; Haller, K. J.; Crans, D. C. The antidiabetic compound formed from metformin and decavanadate complex: Counterion affects interaction with interfaces. *Eur. J. Inorg. Chem.* 2013, 1859–1868.
- (17) Wallace, E.; Ong, C. M. Y.; Heard, C. M. Delivery of atovaquone and proguanil across sublingual membranes, in vitro. *Pharm. Dev. Technol.* 2012, *17*, 770–776.
- (18) Sweeney, D.; Rayner, M. L.; Lockwood, T. D. Antidiabetic and antimalarial biguanide drugs are metal-interactive antiproteolytic agents. *Biochem. Pharmacol.* 2003, *66*, 663–677.
- (19) Olliaro, P. Mode of action and mechanisms of resistance for antimalarial drugs. *Pharmacol. Ther.* 2001, 207–219.
- (20) Cordel, H.; Cailhol, J.; Matheron, S.; Bloch, M.; Godineau, N.; Consigny, P.-H.; Gros, H.; Campa, P.; Bouree, P.; Fain, O.; Ralaimazava, P.; Bouchaud, O. Atovaquone-proguanil in the treatment of imported uncomplicated Plasmodium falciparum malaria: a prospective observational study of 553 cases. *Malaria J.* 2013, *12*.
- (21) Kirk, K. Membrane Transport in the Malaria-Infected Erythrocyte. *Physiol. Rev.* 2001, *81*, 495–537.
- (22) Looareesuwan, S.; Chulay, J. D.; Canfield, C. J.; Hutchinson, D. B. A.; Malarone Clinical Trials Study, G. Malarone (R) (atovaquone and proguanil hydrochloride): A review of its clinical development for treatment of malaria. *Am. J. Trop. Med. Hyg.* 1999, *60*, 533–541.
- (23) Srivastava, I. K.; Vaidya, A. B. A mechanism for the synergistic antimalarial action of atovaquone and proguanil. *Antimicrob. Agents Chemother.* 1999, *43*, 1334–1339.
- (24) Fidock, D. A.; Welles, T. E. Transformation with human dihydrofolate reductase renders malaria parasites insensitive to WR99210 but does not affect the intrinsic activity of proguanil. *Proc. Natl. Acad. Sci. U.S.A.* 1997, *94*, 10931–10936.
- (25) Chen, J. P.; Vanpraag, H. M.; van Praag, H. M.; Gardner, E. L. Activation of 5-HT₃ receptor by 1-phenylbiguanide increases dopamine release in the rat nucleus accumbens. *Brain Res.* 1991, *543*, 354–357.
- (26) Dukat, M.; Abdel-Rahman, A. A.; Ismaiel, A. M.; Ingher, S.; Teitler, M.; Gyermek, L.; Glennon, R. A. Structure–Activity Relationships for the Binding of Arylpiperazines and Arylbiguanides at 5-HT₃ Serotonin Receptors. *J. Med. Chem.* 1996, *39*, 4017–4026.
- (27) Lawrence, M. J.; Rees, G. D. Microemulsion-based media as novel drug delivery systems. *Adv. Drug Delivery Rev.* 2000, *45*, 89–121.
- (28) Palazzo, G.; Lopez, F.; Giustini, M.; Colafemmina, G.; Ceglie, A. Role of the cosurfactant in the CTAB/water/n-pentanol/n-hexane water-in-oil microemulsion. I. Pentanol effect on the microstructure. *J. Phys. Chem. B* 2003, *107*, 1924–1931.
- (29) De, T.; Maitra, A. Solution behavior of Aerosol OT in non-polar solvents. *Adv. Colloid Interface Sci.* 1995, *59*, 95–193.
- (30) Maitra, A. Determination of Size Parameters of Water-Aerosol OT-Oil Reverse Micelles from Their Nuclear Magnetic Resonance Data. *J. Phys. Chem.* 1984, *88*, S122–S125.
- (31) Eastoe, J.; Robinson, B. H.; Steytler, D. C.; Thornleeson, D. Structural Studies of Microemulsions Stabilized by Aerosol-OT. *Adv. Colloid Interface Sci.* 1991, *36*, 1–31.
- (32) Correa, N. M.; Biasutti, M. A.; Silber, J. J. Micropolarity of reverse micelles of aerosol-OT in n-hexane. *J. Colloid Interface Sci.* 1995, *172*, 71–76.

- (33) Zingaretti, L.; Correa, N. M.; Boscatto, L.; Chiocchiera, S. M.; Durantini, E. N.; Bertolotti, S. G.; Rivarola, C. R.; Silber, J. J. Distribution of amines in water/AOT/n-hexane reverse micelles: influence of the amine chemical structure. *J. Colloid Interface Sci.* **2005**, *286*, 245–252.
- (34) Correa, N. M.; Durantini, E. N.; Silber, J. J. Binding of nitrodiphenylamines to reverse micelles of AOT in n-hexane and carbon tetrachloride: Solvent and substituent effects. *J. Colloid Interface Sci.* **1998**, *208*, 96–103.
- (35) Moilanen, D. E.; Levinger, N. E.; Spry, D. B.; Fayer, M. D. Confinement or the nature of the interface? Dynamics of nanoscopic water. *J. Am. Chem. Soc.* **2007**, *129*, 14311–14318.
- (36) Baruah, B.; Roden, J. M.; Sedgwick, M.; Correa, N. M.; Crans, D. C.; Levinger, N. E. When Is Water Not Water? Exploring Water Confined in Large Reverse Micelles Using a Highly Charged Inorganic Molecular Probe. *J. Am. Chem. Soc.* **2006**, *128*, 12758–12765.
- (37) Lang, J.; Jada, A.; Malliaris, A. Structure and dynamics of water-in-oil droplets stabilized by sodium bis(2-ethylhexyl)sulfosuccinate. *J. Phys. Chem.* **1988**, *92*, 1946–1953.
- (38) Zulauf, M.; Blicke, H. F. Inverted micelles and microemulsions in the ternary system water/aerosol-OT/2,2,4,4-tetramethylpentane as studied by photon correlation spectroscopy. *J. Phys. Chem.* **1979**, *83*, 480–486.
- (39) Crans, D. C.; Trujillo, A. M.; Phatazayn, P.; Cohen, M. How environment affects drug activity: Localization, compartmentalization and reactions of a vanadium insulin-enhancing compound, dipicolinatooxovanadium(V). *Coord. Chem. Rev.* **2011**.
- (40) Crans, D. C.; Trujillo, A. M.; Bonetti, S.; Rithner, C. D.; Baruah, B.; Levinger, N. E. Penetration of Negatively Charged Lipid Interfaces by the Doubly Deprotonated Dipicolinate. *J. Org. Chem.* **2008**, *73*, 9633–9640.
- (41) Gaidamauskas, E.; Cleaver, D. P.; Chatterjee, P. B.; Crans, D. C. Effect of Micellar and Reverse Micellar Interface on Solute Location: 2,6-Pyridinedicarboxylate in CTAB Micelles and CTAB and AOT Reverse Micelles. *Langmuir* **2010**, *26*, 13153–13161.
- (42) Giustini, M.; Palazzo, G.; Colafemmina, G.; Della Monica, M.; Giomini, M.; Ceglie, A. Microstructure and Dynamics of the Water-in-Oil CTAB/n-Pentanol/n-Hexane/Water Microemulsion: A Spectroscopic and Conductivity Study. *J. Phys. Chem.* **1996**, *100*, 3190–3198.
- (43) Vermathen, M.; Stiles, P.; Bachofer, S. J.; Simonis, U. Investigations of monofluoro-substituted benzoates at the tetradecyltrimethylammonium micellar interface. *Langmuir* **2002**, *18*, 1030–1042.
- (44) Sedgwick, M.; Cole, R. L.; Rithner, C. D.; Crans, D. C.; Levinger, N. E. Correlating Proton Transfer Dynamics To Probe Location in Confined Environments. *J. Am. Chem. Soc.* **2012**, *134*, 11904–11907.
- (45) Eastoe, J.; Robinson, B. H.; Heenan, R. K. Water-in-oil microemulsions formed by ammonium and tetrapropylammonium salts of Aerosol OT. *Langmuir* **1993**, *9*, 2820–2824.
- (46) Stahl, M. L.; Baruah, B.; James, D. M.; Johnson, M. D.; Levinger, N. E.; Crans, D. C. ¹H NMR Studies of Aerosol-OT Reverse Micelles with Alkali and Magnesium Counterions: Preparation and Analysis of MAOTs. *Langmuir* **2008**, *24*, 6027–6035.
- (47) Glasoe, P.; Long, F. A. Use of glass electrodes to measure acidities in deuterium oxide. *J. Phys. Chem.* **1960**, *64*, 188–190.
- (48) Crans, D. C.; Rithner, C. D.; Baruah, B.; Gourley, B. L.; Levinger, N. E. Molecular probe location in reverse micelles determined by NMR dipolar interactions. *J. Am. Chem. Soc.* **2006**, *128*, 4437–4445.
- (49) Woo, L. C. Y.; Yuen, V. G.; Thompson, K. H.; McNeill, J. H.; Orvig, C. Vanadyl-biurea complexes as potential synergistic insulin mimics. *J. Inorg. Biochem.* **1999**, *76*, 251–257.
- (50) Crans, D. C.; Schoeberl, S.; Gaidamauskas, E.; Baruah, B.; Roess, D. A. Antidiabetic vanadium compound and membrane interfaces: interface-facilitated metal complex hydrolysis. *J. Biol. Inorg. Chem.* **2011**, *16*, 961–972.
- (51) Biot, C.; Nosten, F.; Fraisse, L.; Ter-Minassian, D.; Khalife, J.; Dive, D. The antimalarial ferroquine: From bench to clinic. *Parasite* **2011**, *18*, 207–214.
- (52) Krugliak, M.; Deharo, E.; Shalmiev, G.; Sauvain, M.; Moretti, C.; Ginsburg, H. Antimalarial effects of C18 fatty-acids on plasmodium-falciparum in culture and on plasmodium-vinckeii-petteri and plasmodium-yoellii-nigeriensis in vivo. *Exp. Parasitol.* **1995**, *81*, 97–105.
- (53) Loedige, M.; Lewis, M. D.; Paulsen, E. S.; Esch, H. L.; Pradel, G.; Lehmann, L.; Brun, R.; Bringmann, G.; Mueller, A.-K. A primaquine-chloroquine hybrid with dual activity against Plasmodium liver and blood stages. *Int. J. Med. Microbiol.* **2013**, *303*, 539–547.
- (54) Salas, P. F.; Herrmann, C.; Cawthray, J. F.; Nimphius, C.; Kenkel, A.; Chen, J.; de Kock, C.; Smith, P. J.; Patrick, B. O.; Adams, M. J.; Orvig, C. Structural Characteristics of Chloroquine-Bridged Ferrocenophane Analogues of Ferroquine May Obviate Malaria Drug-Resistance Mechanisms. *J. Med. Chem.* **2013**, *56*, 1596–1613.
- (55) Vermathen, M.; Chodos, A. B.; Louie, E. A.; Simonis, U. Investigations of porphyrins and metalloporphyrins in model membranes. *J. Inorg. Biochem.* **1999**, *74*, 328–328.
- (56) Vermathen, M.; Louie, E. A.; Chodos, A. B.; Ried, S.; Simonis, U. Interactions of water-insoluble tetraphenylporphyrins with micelles probed by UV-visible and NMR spectroscopy. *Langmuir* **2000**, *16*, 210–221.
- (57) Dalpiaz, A.; Ferruti, V.; Gilli, P.; Bertolasi, V. Stereochemistry of serotonin receptor ligands from crystallographic data. Crystal structures of NAN-190.HBr, 1-phenylbiguanide, MDL 72222 and mianserin.HCl and selectivity criteria towards 5-HT₁, 5-HT₂ and 5-HT₃ receptor subtypes. *Acta Cryst. Sec. Struct. Sci.* **1996**, *52*, 509–518.
- (58) Yang, L. Q.; Crans, D. C.; Miller, S. M.; la Cour, A.; Anderson, O. P.; Kaszynski, P. M.; Godzala, M. E.; Austin, L. D.; Willsky, G. R. Cobalt(II) and cobalt(III) dipicolinate complexes: Solid state, solution, and in vivo insulin-like properties. *Inorg. Chem.* **2002**, *41*, 4859–4871.
- (59) Samart, N.; Saeger, J.; Haller, K. J.; Aureliano, M.; Crans, D. C. Interaction of decavanadate with interfaces and biological model membrane systems: Characterization of soft oxometalate systems. *J. Mol. Eng. Mater.* **2014**, *1*, 2014.
- (60) Sostarecz, A. G.; Gaidamauskas, E.; Distin, S.; Bonetti, S. J.; Levinger, N. E.; Crans, D. C. Correlation of Insulin-Enhancing Properties of Vanadium-Dipicolinate Complexes in Model Membrane Systems: Phospholipid Langmuir Monolayers and AOT Reverse Micelles. *Chem.—Eur. J.* **2014**, *20*, 5149–5159.

APPENDIX B

INTERACTION OF DECAVANADATE WITH

INTERFACES AND BIOLOGICAL MODEL MEMBRANE

SYSTEMS: CHARACTERIZATION OF SOFT

OXOMETALATE SYSTEMS

My contribution to this work which was to assist in the preparation of the review. The manuscript by Samart, Saeger, Haller, Aureliano, and Crans. "Interaction of decavanadate with interfaces and biological model membrane systems: characterization of soft oxometalate systems" reported in *Journal of Molecular and Engineering Materials*, 2014. This including completing experiments by Ms. Jessica Saeger on the interaction of decavanadate with positively charged interfaces. In addition, studies with metformin in CTAB-pentanol RMs. These studies where the missing studies allowing comparison of decavanadate and metformin in all types of RMs, which was needed to establish the effects of decavanadate on interfaces.

INTERACTION OF DECAVANADATE WITH INTERFACES AND BIOLOGICAL MODEL MEMBRANE SYSTEMS: CHARACTERIZATION OF SOFT OXOMETALATE SYSTEMS

NUTTAPORN SMART^{*,†,§}, JESSICA SAEGER^{†,¶}, KENNETH J. HALLER^{*,||},
 MANUEL AURELIANO^{†,**} and DEBBIE C. CRANS^{†,††}

^{*}*School of Chemistry, Institute of Science
 Suranaree University of Technology
 Nakhon Ratchasima 30000, Thailand*

[†]*Department of Chemistry, Colorado State University
 Fort Collins, CO 80523-1872, USA*

[‡]*CCMar and DCBB, FCT Algarve University
 Faro 8005-139, Portugal*

[§]*nuttapornsmart@gmail.com*

[¶]*jbsaeger@gmail.com*

^{||}*ken.haller@gmail.com*

^{**}*maalves@ualg.pt*

^{††}*crans@lamar.colostate.edu*

Received 4 December 2013

Accepted 8 April 2014

Published 23 May 2014

Decavanadate is a polyoxometalate consisting of 10 octahedral vanadium centers, which has been found to exert biological effects and has been observed *in vivo*. Biological activity implies that a material is taken up into a cell or that the material interacts with membrane receptors. Because of the large size and the high molecular charge, it is nontrivial to anticipate how such a large anion interacts with membranes and whether it will be taken up by cells. Therefore, it becomes important to investigate how the anion interacts with membranes and membrane model systems. Since ion pairing is important for the interaction of this large complex with any membrane interface system, we investigate both the nature of Coulombic and neutral noncovalent interactions with membrane model interface systems and cellular systems. Specifically, we used microemulsions as model systems, and in the specific phase diagram regime where reverse micelles form. We find that, there is a large difference in the interaction with different interfaces, and that charge can have an important role. The negatively charged interface repels the anion, whereas a positive interface attracts the anion. However, the interface with neutral surfactant head groups also is found to repel the decavanadate. This result demonstrates that the discrete charge Coulombic interactions are not the only forces in effect, and that the interactions are at least to a first approximation dictated by the interface charge and not by the counterions in the system.

[§]This work was carried out as an exchange student at Department of Chemistry, Colorado State University, Fort Collins, CO 80523-1872, USA.

Alternative forces include van der Waals attraction, pH of the water pool, and field and surface effects. Because biological membranes have differently charged ligands, it is not clear which interface systems provide the best analogy with cell surfaces. However, surface charge may affect the compounds and facilitate the interactions that could be important. For example, a positively charged surface could potentially facilitate hydrolysis and sequential abstraction of one or two vanadium atoms at a time from decavanadate. Recently, decavanadate was used as a structural model for the V_2O_5 material. Negatively charged interfaces have also been found to accelerate compound hydrolysis or in other ways alter reactions in compounds near the interface. Lipid-like interfaces potentially contribute to processing of coordination compounds. Decavanadate has been found to interact with proteins and insulin enhancing effects have been reported. Interactions with coordination compounds and the mechanisms of interactions should continue to be investigated because such systems may reveal the mode of interaction of these compounds.

Keywords: Decavanadate; interface; membrane interaction; polyoxometalate; microemulsion; reverse micelle; soft oxometalates.

1. Introduction

Polyoxometalates have been reported to induce desirable properties in biological systems despite the high charge, the large dimensions of these complex anions, and difficulties with cellular uptake.¹⁻¹¹ Specifically, polyoxotungstates and polyoxovanadates have been used for treatment of diseases such as cancer, diabetes and HIV.^{2-4,6,12-37} Several forms of decavanadate (abbreviated V_{10}) and a range of Keggin anions were found to normalize elevated glucose levels in animal model systems (Fig. 1).^{16,35-37} Several more complex polyoxometalates such as HPA-23 (family of antimonate-tungstate polyoxometalate, specifically the sodium hexaocta-coxaononaantimonateheicosatungstate with the anion formula of $[NaO_{86}Sb_9W_{21}]^{18-}$) were used for treatment of AIDS, and other polyoxometalates were found to be effective against cancer^{2,7} and diabetes.^{20,38,39} Additionally, these systems have been found to interact with proteins,¹ and receptors in cell membranes.^{1,40,41} For example, V_{10} is an inhibitor

for ribonuclease,¹ cAMP kinase,⁴² Ca^{2+} ATPase^{43,44} and alkaline phosphatase⁴⁵ as has been demonstrated by monitoring their enzyme activities in the presence and absence of V_{10} . When the oxometalates are used as drugs, how they interact with the interface becomes important in getting the compounds into the cell.⁴⁰⁻⁴⁸ Regardless of the disease in question, polyoxometalates either act at the membrane through receptor binding, or somehow are transported through the cell membrane.^{2,7} In this paper, we examine the available literature to evaluate the association of multicharged potential drugs with membrane interfaces using the polyoxometalate, decavanadate, as the model solute and compare association with a series of model membrane systems and biological systems in general.

A range of model interface systems exist, including colloid systems such as vesicles, micelles, reverse micelles (RMs), and other more complex systems,^{17,49-61} which can aid understanding of the interaction of solutes with interfaces. Which type of system forms, depends on the specific nature of the

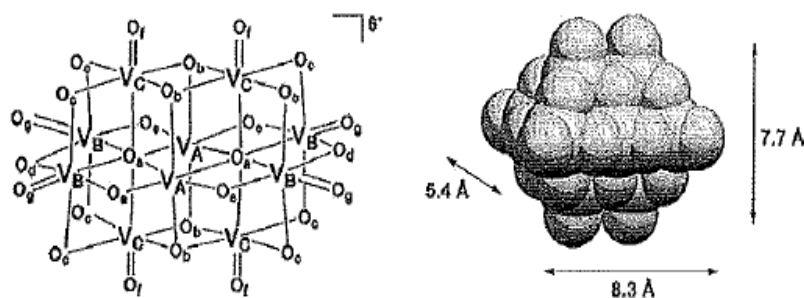


Fig. 1. Structures of decavanadate (V_{10}) shown in a stick model (left) and in a space filling model (right).

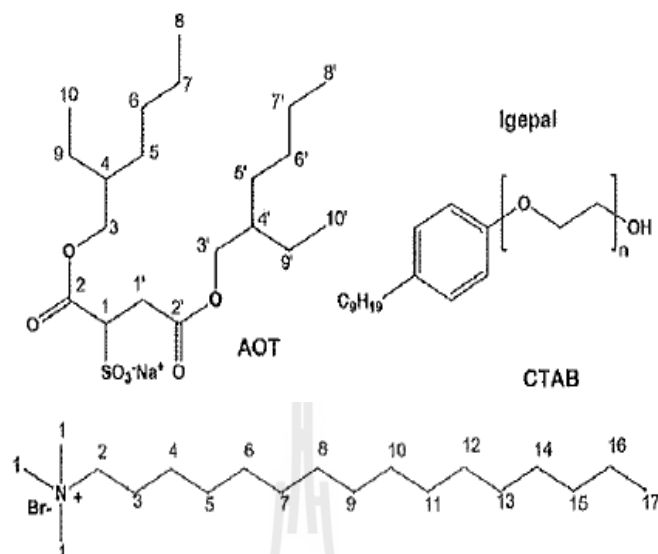


Fig. 2. Examples of typical anionic, cationic, and nonionic surfactant entities used in making RM for the studies described in this paper. The AOT anion, the CTAB cation, and the Igepal nonionic molecule are shown, where n is 5 for Igepal 520.

surfactant, organic solvent, and water as well as the component composition governed by the phase diagram of the system.^{51,62,63} Examples of common negatively charged surfactants are AOT (sodium bis(2-ethylhexyl)sulfosuccinate, see Fig. 2) and DSS (sodium dodecylsulfonate).^{17,57-59} An example of a positively charged surfactant is cetyltrimethylammonium bromide (CTAB, see Fig. 2),⁵² and examples of nonionic surfactants are Triton-X-100, Brij, and Igepal 520 or Igepal 610/430 nonylphenyl ethoxylates — the varying polyethylene oxide (PEO) part is specified in the Igepal number (see Fig. 2).^{53,61,64} The simplest system that has been frequently used to probe interactions at membrane interfaces is the RM system, also referred to as the water-in-oil phase. The RMs form in regions of the phase diagram where the water content is low and the organic solvent, also referred to as the oil, and a surfactant make up the major fraction of the sample. Depending on the nature of the surfactant and whether a cosurfactant is needed, the RM systems can be ternary or quaternary containing water droplets surrounded by a suitable surfactant that can self-assemble and form a polar-hydrophobic interface and transparent solutions. When working with these systems, it is important to recognize that they are dynamic systems and thus the potential for results reflecting different parts of the system exist and often several methods of study are needed to characterize the system.^{51,62,63,65}

Although examples in biology exist where counterions are important to the action of the compounds,^{1,6-8,16,35,37,41,66-69} we have recently documented that the interaction of V₁₀ with simple interface model systems is also dramatically dependent on counterions. The replacement of the Na⁺ ion with metformium counter ion, HMet⁺, doubled the V₁₀ solubility in heterogeneous RM system.¹ This finding led us to conduct a systematic comparison of the available studies⁷⁰⁻⁷⁵ probing the interaction of V₁₀ with different types of interfaces described in this paper. In the previous studies, we identified the subtle differences induced by counterions, and how the interaction with the interface would change as the charges change. These variations in properties suggest that some differences exist in the organization of the decavanadate within the RM. This is an example of the phenomenon where weak noncovalent supramolecular forces are key to aggregated solution structures containing the oxometalates, which have recently been referred to as "soft oxometalates".^{76,77} The objective of this paper is to evaluate the available data and the concept that RM systems containing decavanadate represent an example of a "soft oxovanadate" system.^{76,77}

Counterions are generally not considered to impact drug absorption,^{28,78} however, for polyanionic systems such as decavanadates, and other polyoxometalate systems, counterions are found to make

N. Samart et al.

a large difference.^{16,35,37} For example, the antidiabetic properties of V_{10} , when accompanied by polyammonium ions are reported to be particularly favorable.^{16,35,37} The counterion is believed to be important for the mode of action of these compounds.³⁷ Because of the high charge of the polyoxovanadates, the counterion effect is larger than with most coordination complexes, and thus these systems are ideal for investigation of the interactions with interfaces. How these drugs interact with different interfaces is important for understanding how the drug interacts in the biological system.

In this paper, we review the available information on the interaction of V_{10} with membrane interfaces.^{1,58,68,69} Additionally, we complement the reported work with new studies, which characterize how counterions affect how the oxometalate interacts with a positively charged interface.

2. Decavanadate, a Stable Polyoxovanadate

Decavanadate (V_{10}) is a polyoxometalate that forms in aqueous solutions of vanadium (V) from metavanadate or orthovanadate salts or from vanadium oxides.^{1,75} V_{10} is a compact anion containing 10 V atoms and 28 O atoms in the formula of $V_{10}O_{28}^{6-}$ in the deprotonated state (Fig. 1).⁷⁵ The V-atoms are placed in VO_6 -octahedra connected either through vertices, edges or faces of the octahedron. Eight of the 28 oxygen atoms are the V=O

functionality and the rest are either doubly or triply bridging or two of the oxygen atoms are surrounded by six vanadium atoms. The dimensions of the anion are $5 \times 7.7 \times 8.3 \text{ \AA}$, that is the shape of an elongated barrel, and has been described in more than 100 different structures reported.^{71,73-75,79,80}

It is recognized that both the counterions and the protonation state of the anion are important for the specific structures that form. When deprotonated, the overall charge of 6^- is delocalized over the entire anion. Although the deprotonated V_{10} anion ($V_{10}O_{28}^{6-}$) is most common,^{58,70,73,81,82} protonated states have been reported including diprotonated ($H_2V_{10}O_{28}^{4-}$),⁸²⁻⁸⁴ triprotonated ($H_3V_{10}O_{28}^{3-}$),⁸⁵⁻⁸⁷ and tetraprotonated V_{10} ($H_4V_{10}O_{28}^{2-}$).^{87,88} For example, for the Na^+ salt of the deprotonated V_{10} ($V_{10}O_{28}^{6-}$), the V_{10} units interact through NaO_6 octahedra forming a two-dimensional sheet, which is extended in the third dimension by H-bonding between the V_{10} anion and the edge-shared Na_2O_{10} (with numbers subscripted) double octahedron. The crystal structure of a material that contains both the deprotonated anion ($V_{10}O_{28}^{6-}$) and the diprotonated ($H_2V_{10}O_{28}^{4-}$) anion⁸³ is shown in Fig. 3. A polymeric chain forms through interaction between the two anions facilitated by a pyrrolidinium cation as well as a H-bond interaction between the deprotonated and protonated V_{10} anions.

The structures formed in the solid state are not only governed by protonation of the most basic sites, but also by the stability obtained by formation

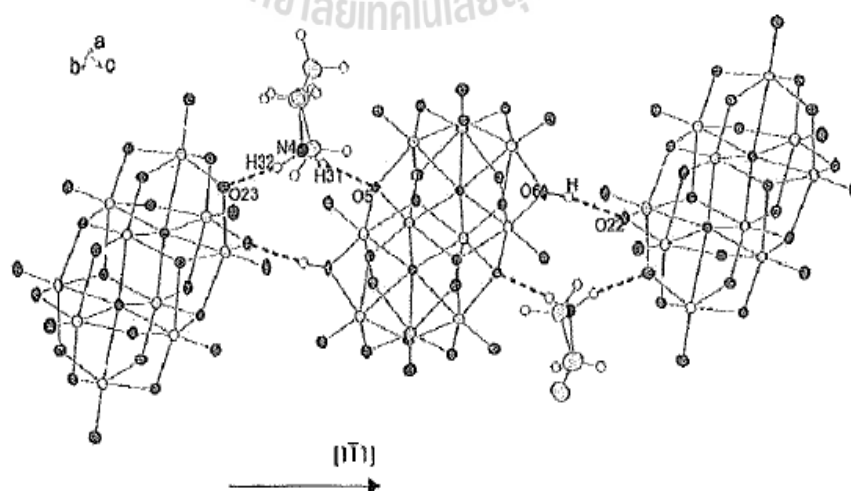


Fig. 3. The intermolecular interactions between V_{10} ($V_{10}O_{28}^{6-}$) and H_2V_{10} ($H_2V_{10}O_{28}^{4-}$) facilitated by a pyrrolidinium cation to form polymeric chains (see Ref. 83). Adapted with permission from Ref. 83.

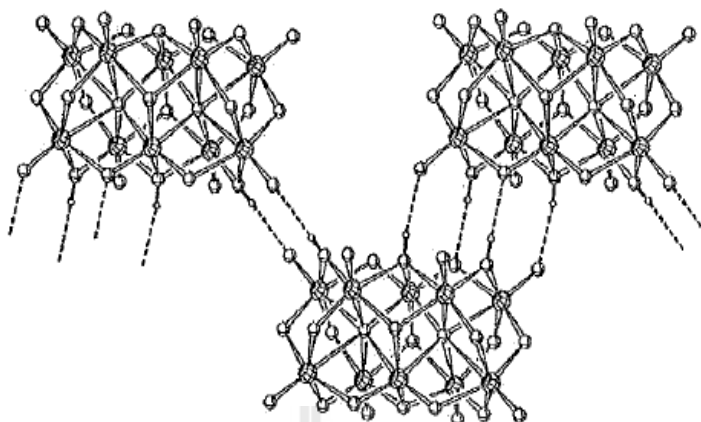
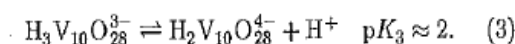
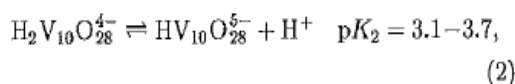
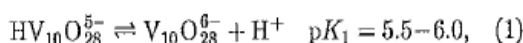


Fig. 4. Part of the material containing triprotonated V_{10} ($H_3V_{10}O_{28}^{3-}$) highlighting the H-bonding that exists between V_{10} anions (see Ref. 85). Adapted with permission from Ref. 85.

of the supramolecular network. Figure 4 shows the structure of a triprotonated V_{10} , ($H_3V_{10}O_{28}^{3-}$).⁸⁵ In this structure, the benzyltrimethylammonium counterion facilitates the crystallization of a material which supports six H-bonds to two other V_{10} anions in a (4 + 2) fashion. The fact that the H-bonds are on the same side of the oxometalate, allows formation of a variety of supramolecular networks. For example, in the case of the benzyltrimethylammonium counterion, the H-bonding between V_{10} anions creates a zigzag pattern.⁸⁵ In the case of the very hydrophobic counterion, tetraalkylphosphonium cation, if the six H-bonds remain on the same side, discrete dimers are formed surrounded by a ring of hydrophobic counterions.⁸⁶ Although protonation states are most commonly used to modify interactions, corresponding effects can be observed if a counterion replaces the proton as illustrated with the dimeric unit which was the basis for formation of the 3D-metal-organic network created from V_{10} , Zn^{2+} , imidazole, triazole, and dimethylammonium ion.⁸⁹

In solution, below pH 6.5, several protonated forms of V_{10} exist as defined by Eqs. (1)–(3).



The anion is thermodynamically stable at low pH but its stability decreases as the pH increases above neutral.⁷⁵ Despite the lower stability at neutral and

basic pH, the anion exists for significant amounts of time because the kinetics of hydrolysis is slow at neutral pH.^{1,70,90} Importantly, the V_{10} anion can exist for around 30 h at neutral pH values.^{1,70,90} The V_{10} anion in solution is readily described by ^{51}V NMR spectroscopy.⁹¹ The ^{51}V NMR nucleus is quadrupolar with a spin 7/2 and a large chemical shift window. As a result the ^{51}V NMR chemical shifts are very sensitive to their environment, and the protonation state of the V_{10} can be determined based on the chemical shifts of the anion, *vide infra*. ^{17}O NMR spectroscopy has also been used to characterize the different oxygen atoms in the anion,⁹²⁻⁹⁴ and have identified the triply bridging O-atoms to be most basic and the terminal O-atoms to be least basic.⁹⁴

Although the charge on V_{10} is delocalized, both solution and solid state studies show that there are certain regions of the surface that engage in H-bonding favoring a wide range of structural organization with this complex ion.^{70,71,85,87,89,92-96} A statistical analysis has shown that some trends in the supramolecular structure organization exist.⁷¹ Indeed, when a cation favors H-bonding with V_{10} it will tend to favor association around the barrel of the anion. For example, when two different cations can interact with different parts of the V_{10} surface several possible interactions could result however, the structure form optimizing the combination of counterion that forms strongest H-bonds and crystal packing. Our recent structure report shows the protonated guanylurea cations acting as tridentate ligands forming highly concerted and stronger H-bonds with the V_{10} , whereas $HMet^+$ interacts end

on at the head of the barrel at weaker H-bonding sites. Interestingly, this pattern was also observed in a crystal with cations forming only one H-bond each as we reported for the crystal structure containing two Gly-Gly and six NH_4^+ with V_{10} .⁹⁵ Although such preferences have mainly been reported in the solid state, presumably due to the ease of examination by single crystal X-ray crystallography, at least in part the structural preferences in supramolecular organization demonstrated in the solid state are likely to exist in solution as well. Indeed, a recent study shows variation in the organization of the V_{10} anion in the crystal lattice, depending on the solvent in the crystal. The variation is so subtle that cocrystallization of acetone with $\text{H}_3\text{V}_{10}\text{O}_{28}^{3-}$ leads to V_{10} dimers held together by H-bonding, whereas cocrystallization with dioxane, which competes better for the H-bonding, results in disruption of the dimeric motifs and a structure based on monomeric V_{10} units results.⁸⁷

3. Model Systems for Probing Membrane Interactions

An RM consists of surfactant molecules self-assembled to form a monolayer surrounding a nanosized water droplet with the hydrophilic head groups structurally organized facing the water pool and the hydrophobic tail groups facing outward into the nonpolar region and the surrounding organic solvent, see Fig. 5.⁵¹ When the surfactant is ionic, there is a charge compensation layer at the outer part of the water pool. The counterions in closest proximity with the charged head groups are generally viewed as being immobile and are sometimes called the Stern layer, and the remainder of the charge compensation layer provides the gradient of mobility to the solvated counterions in the water pool. Thus, the charge compensation layer partially neutralizes the charge of the surfactant at the micellar interface, while the remainder of the counterion charge distributes throughout the water pool.⁹⁷ Surfactant scientists have long known empirically that the charge compensation fraction is about 0.65 of the head group charge regardless of the system. A quantity that has recently been confirmed by successful application of thermodynamic modeling.⁹⁷⁻⁹⁹ The cartoon in Fig. 5(b) schematically illustrates the average sequestered water pool using shading to represent the increasing

immobilization of solution species (and in the case of ionic surfactants an approximation of the increasing charge of the charge compensation layer) on approach to the interface surface. Other notable features of the RM include the palisade region where the transition from polar to nonpolar environment occurs. This region is just outside of the interface and coincides with the closest approach of the surfactant tail groups due to the convex shape of the micelle.

AOT is a common surfactant used very successfully in previous studies from our group and others^{17,58,100-103} in forming the RMs. Part of the popularity of the AOT system is the fact that the AOT-RM systems are generally very reproducible, prepared from stock solutions, and the experiments conducted can readily be interpreted. Because of the simplicity of the system, we have been able to obtain detailed information with the decavanadate and other inorganic complexes that would not have been accessible through more complex model systems. The average size of the RMs is proportional to the ratio of the water concentration to the surfactant concentration, referred to as w_0 , equal to $[\text{H}_2\text{O}]/[\text{surfactant}]$. The specific size varies depending on the surfactant and the organic solvent. While the common organic solvents used in these studies are isooctane and cyclohexane, other solvents such as benzene, toluene, chloroform, and green options such as a range of oils have been reported. Usability of these systems is mainly limited by the region in the phase diagram in which transparent solutions form. Table 1 presents characteristic parameters for the AOT in isooctane nanosized RM particles assuming spherical shape which have been measured using dynamic light scattering (DLS).^{51,97} An AOT in cyclohexane RM system is slightly larger than the corresponding system formed in isooctane. The RM structures are described by a range of different physical parameters. Maitra previously characterized these systems by defining $\delta_{\text{observed}} = P_B \delta_B + P_F \delta_F$ representing the bound (B) and free (F) water molecules in addition to the number of water molecules in the system (n_w). The mean average aggregation number of the surfactant per droplet is defined as \bar{n} . The distances are determined as the core radius (r_w), the thickness of the surfactant layer (l_c) and the hydrodynamic radius (r_h). The calculated values for the polar head-group area are (f_{AOT}) and (d) is the thickness of the bound water layer.

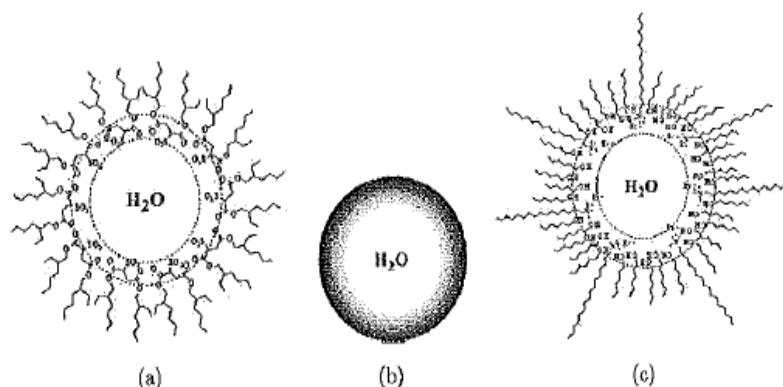


Fig. 5. Cartoon of an average sequestered water pool in a RM with surfactant around it. (a) Anionic AOT system, (b) schematic of the water pool with shading to indicate the charge compensation layer (see Ref. 97) and (c) cationic CTAB/1-pentanol system.

Finally, the packing factor of the AOT molecules in the microemulsion system is expressed as $(v/f_{AOT}l_c)$. For $w_0 < 10$, the packing factor shows that the AOT rotamers are gauche because the systems cannot accommodate all the AOT molecules at the interface. At higher w_0 values, the interface becomes more "soft", accommodating more trans rotamers and thus resulting in a wider layer.

CTAB (cetyltrimethylammonium bromide) is also a common surfactant used to form RMs,¹⁰⁴ and differs fundamentally with AOT in being a cationic rather than an anionic surfactant, and thus generates an interface with a positively charged monolayer surrounding the water pool. The

associated charge compensation layer is made up of a fraction of the negatively charged counter anions from the water pool. The CTAB system requires a cosurfactant, and is less convenient to work with because each solution must be individually prepared by mixing the components (organic solvent, cosurfactant, water or aqueous solution containing solute, and solid CTAB),¹⁰⁴ and also requires extensive sonication to achieve dissolution of the CTAB. Further, size determination using DLS is difficult because of the nature of the physical parameters in the measurement, but can be obtained if a high concentration of NaBr is added to the samples.⁶²

Table 1. Physical parameters for the AOT RM/isooctane (based on 0.1M AOT) system including sizes, proportion of bound water and calculated number of water molecules. Adapted from Ref. 51.

w_0	δ , ppm	n_w	P_D	\bar{n}^a	r_A^b , Å	r_w , Å	l_c , Å	d , Å	f_{AOT} , Å ²	$v/f_{AOT}l_c$
4	4.030	140	0.78	35	25	10	15	3.96	35.9	3.25
6	4.090	280	0.68	50	28	14	14	4.42	42.5	2.70
8	4.140	578	0.60	72	32	16	16	4.21	44.7	2.30
10	4.180	—	0.53	98	34	19	15	4.22	46.3	2.00
12	4.220	1553	0.47	129	37	22	15	4.10	47.1	1.84
14	4.250	—	0.42	176	40	26	14	4.32	48.4	1.63
16	4.275	—	0.37	215	42	29	13	4.14	49.3	1.51
18	4.300	—	0.33	257	43	32	11	4.00	50.0	1.38
20	4.320	6061	0.30	302	44	35	9	3.92	51.0	1.28
25	4.360	—	0.23	447	52	43	9	3.59	52.0	1.22
30	4.380	—	0.20	613	62	51	11	3.60	53.3	1.23
35	4.400	—	0.17	778	76	58	18	3.49	54.2	1.34
40	4.415	—	0.14	965	98	65	33	3.18	56.8	1.57
50	4.430	—	0.11	1380	118	79	39	3.00	56.8	1.57

^aH.-F. Eicke and J. Rehak, *J. Helv. Chim. Acta* **59**, 2883 (1976).

^bM. Zuluaf and H.-F. Eicke, *J. Phys. Chem.* **83**, 480 (1979).

Finally, nonionic surfactants can be used to form RMs with water droplets sequestered from the bulk medium by a neutral interface. One common class of nonionic RMs is made from Igepal CO surfactants,^{53–56} a class of surfactants containing an alkyl chain and a phenyl group as the hydrophobic part and a polyethyleneoxide (PEO) head group. The average length of the PEO chain varies. One study utilized the CO-520 surfactant (averaging 5 PEO units for each polar head group) and a 3:1 mixture of the CO-430 (averaging 4 PEO units per head group) and CO-610 (averaging 6 to 7 PEO units per head group) surfactants, abbreviated CO-610/430. The nonionic systems are more difficult to work with than the anionic AOT system, partially because they form transparent RMs in a smaller window of component composition. The average sizes of the RM structures for the nonionic surfactants are significantly larger than those prepared from AOT.⁶²

Combined, these diverse RM systems will allow us to characterize the interactions of decavanadate with several different systems and interfaces with different charges, providing information specifically focusing on the interactions between polyoxometalates and interfaces.

4. Decavanadate and Negatively-Charged Interfaces

4.1. Decavanadate in AOT RMs: Sodium salt

Based on simple Coulombic considerations, one would anticipate that the negatively charged V_{10} would be repelled by a negatively charged interface.^{17,57–59,105–109} The counterions to the surfactant might be critical to how the cations from the decavanadate salt interact with the interface and

may affect the details of how they interact with the interface in the water pool. The potential location of the counterions near the center of the water pool of the RMs, or in the interface layer where it provides direct charge compensation will impact not only the nature of the interface but also the properties of the solute. Studies have shown that the cationic counterion to AOT will be at the highest concentration between the water pool and the interface (the charge compensation layer).⁹⁷ In the following, we will review the work that has been carried out investigating the location of decavanadate in AOT/RM systems with their negatively charged interfaces.

The negatively charged interface model systems described here were prepared from NaAOT by first dissolving the NaAOT in isooctane, cyclohexane, or deuterated cyclohexane, then forming the RM solutions by adding the desired amount of aqueous oxometalate (suitably deuterated) solution to produce the target w_0 .^{17,57} The addition of V_{10} to AOT/isooctane RM solutions shifts the three ^{51}V NMR signals for the V_{10} anion compared to their shifts in aqueous solution. In addition the signals are broadened and an increase in their linewidths is observed upon placement in RMs. The greater the linewidth increase, the smaller the RM (Fig. 6).^{17,57} These changes are indicative of the changing aqueous environment in the RMs. The small chemical shift changes of the three signals in the ^{51}V NMR upon placement in a RM is consistent with the V_{10} being placed in the aqueous phase in the RM. As the size of the RM decreases, the signal linewidths continue to increase, indicative of the V_{10} anion beginning to feel the interface as the RM size decreases, and thus consistent with the V_{10} being located in the water pool.

When solutions of protonated V_{10} at acidic pH, and shown here specifically for pH 3.1 were added to AOT RM systems, the resulting ^{51}V NMR spectra

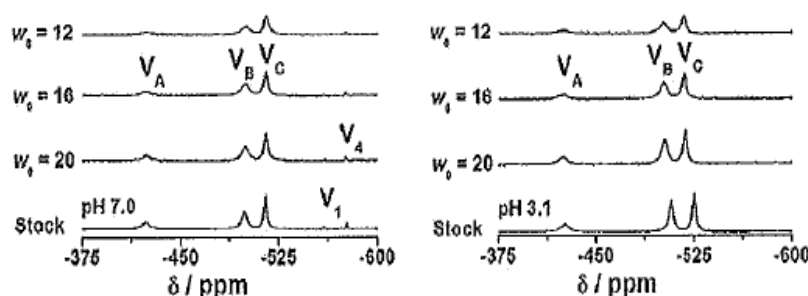


Fig. 6. The ^{51}V NMR spectra of solutions of V_{10} at pH 7.0 and pH 3.1 in AOT RM at various w_0 sizes (adapted from Ref. 17).

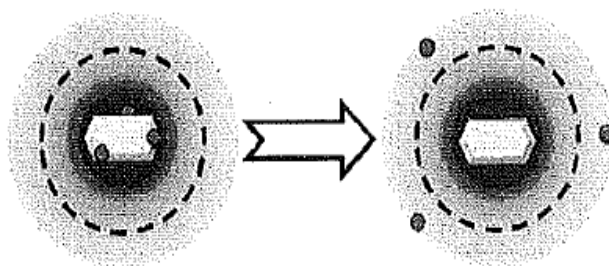


Fig. 7. (Color online) A cartoon illustrating the deprotonation of protonated V_{10} upon placement into RMs. The yellow V_{10} is associated with the red protons (adapted from Ref. 90).

showed shifted signals for V_{10} . The shifts are consistent with observation of deprotonated V_{10} as found at pH 5–6,^{17,57} i.e., the water pool near the V_{10} is near neutral pH. These observations were interpreted as the placement of the protonated V_{10} at pH 3 in the RM results in the deprotonation of V_{10} . Furthermore, we observe that the H^+ is being replaced by a hydrated Na^+ ion from the interface as illustrated in the schematic shown in Fig. 7. These results show that in the aqueous pool of an AOT RM the $H_2V_{10}O_{28}^{4-}$ ion deprotonates presumably as a consequence of a proton gradient that has been established in the RM system.

^{51}V NMR spectra were recorded of solutions of V_{10} at different pH values in aqueous solution and then added to AOT RM solutions.¹⁷ The effect of pH was found to vary depending on the w_0 size, and in Fig. 8 we show the chemical shifts plotted as a function of w_0 for all three signals in the V_{10} anion. We also show the chemical shifts of the aqueous system both at pH 7 and pH 3 for comparison at three different w_0 sizes. The solutions of V_{10} at neutral pH show a modest upfield shift in the chemical shift and a significant line broadening (changes in linewidth signal). In contrast the chemical shifts of the solutions of V_{10} at pH 3.1 show a downfield shift in the chemical shift accompanied by line broadening. These changes are consistent with the V_{10} being located in the water pool. This interpretation is supported by FTIR data and theoretical calculations.

4.2. Decavanadate in AOT RMs: Metformium salt

To investigate the possibility that the combination of two antidiabetic agents in one complex enhanced the antidiabetic effects, we prepared a complex between metformium¹¹⁰ and V_{10} .³⁷ The resulting

complex ($HMetV_{10}$) contains a replacement for the Na^+ counterion with both metformium and H^+ .⁵⁸ This compound was found to have insulin-enhancing properties.¹¹¹ The effect of counterions on the properties of V_{10} was investigated by exploring the

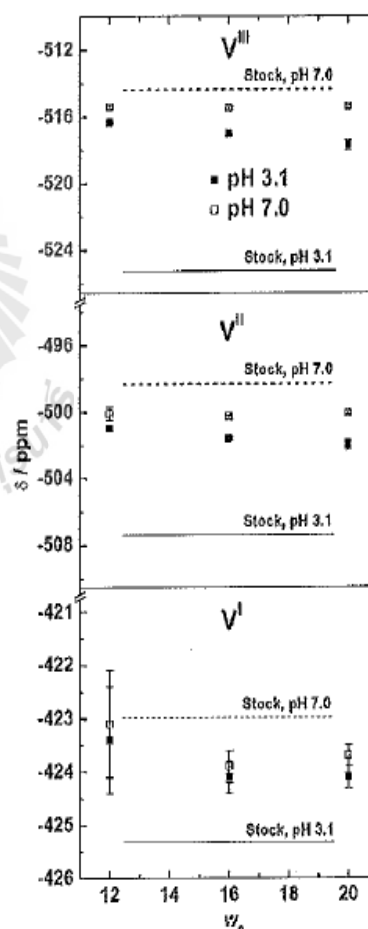


Fig. 8. The ^{51}V NMR chemical shifts of aqueous solutions of V_{10} and V_{10} placed in RMs at w_0 sizes of 12, 16 and 20 plotted as a function of pH. Error bars are SD and when not shown are covered by the symbol. Adapted with permission from Ref. 17.

interactions of this material with the interface. The metformium salt of V_{10} was found to be significantly different than the corresponding sodium salt in that it was not water soluble.⁵⁸ However, $HMetV_{10}$ is solubilized by the AOT/isooctane RM system. Therefore, the procedure for preparation of these samples required addition of solid compound to premade RMs. The presence of the metformium counterion doubles the solubility of the V_{10} even at less than 1% of the total cations present in the system.⁵⁸

To investigate the hydrogen bonding in the surroundings of the V_{10} anion in the AOT/isooctane RM system, differential FTIR spectra (see Fig. 9) were recorded using 5% HOD and subtracting the spectra of the corresponding sample in H_2O .⁵⁸ After normalization, these spectra allow subtraction of the parts associated with AOT and focus on the O–D stretching mode in HOD. Since the O–D stretching band is shifted away from the O–H stretching band, it is readily observed, and a sensitive probe to report on the hydrogen bonding in the water pool. The peak positions in the spectra show that the environment of V_{10} is the same whether $HMet^+$ is added to the system or only Na^+ is present as cations. However, a shoulder appears in the spectrum of the $HMetV_{10}$ system suggesting

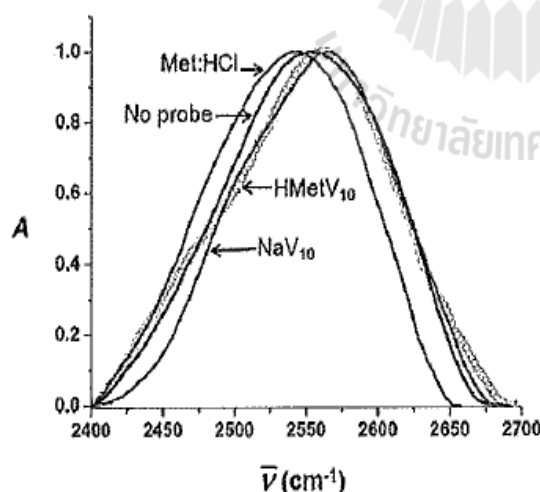


Fig. 9. Differential FTIR absorbances for the O–D stretch in AOT RMs containing aqueous solutions of Met/HCl, NaV_{10} and $HMetV_{10}$ (0.7 mM overall V_{10} concentration and 31.6 mM overall $HMet^+$ concentration, pH = 7.0). Each spectrum is obtained by subtraction of the normalized spectrum recorded in AOT/isooctane RM H_2O from that recorded in 5% HOD. Adapted with permission from Ref. 58.

that there may be a signal for RMs that contain no V_{10} but $HMet^+$ instead.⁵⁸

Because metformin is used in coadministration with many other drugs,¹¹⁰ and its presence is known to increase solubilization of other drugs,¹¹⁰ we were interested to learn more about the location and interaction of metformin with RMs. The +1 positive charge of metformin from pH 3–10 makes this compound a likely candidate for association with the negatively charged interface of AOT. 1H NMR studies showed little to no change in the chemical shift of the CH_3 group on metformin upon placement in the RM.⁵⁸ Unfortunately, the NH_2 -protons exchanged readily upon dissolution into D_2O and therefore no other 1H NMR signals were available for investigation. ^{13}C NMR spectroscopy was also used here to monitor this system, and found to be useful at higher concentrations in aqueous solution, but less so in the AOT RM environments.

4.3. Alternative related AOT/RM systems

A range of AOT RM systems have been investigated including counterions other than Na^+ , as well as with addition of other solutes and dyes.^{49,50,112} Specifically, other alkali, alkaline earth, or transition metal counterions have been used in place of Na^+ and the properties such as size of the water pools in the RM systems varies with each counterion.^{61,112–116} For example, in the case of K^+ , the range of the RM sizes decrease and RMs larger than w_0 of 8 cannot be made. A number of coordination complexes and simple ligands have been investigated in these systems by our group and by others. Although some of these systems might classify in analogous fashion as “soft oxometalate materials”,¹¹⁷ similar analysis was not attempted with these systems because less is generally known about them, precluding the comparison carried out in this paper.

5. Decavanadate and Neutral Interfaces

While the RM neutral interfaces do not contain discrete negative charges on the interfacial surface, the surfactant molecules are polar and thus create a system governed by dipole and polar effects. While individually one residue may have less pronounced effect compared to pure ionic systems, each unit will contain several PEO units, thus increasing the

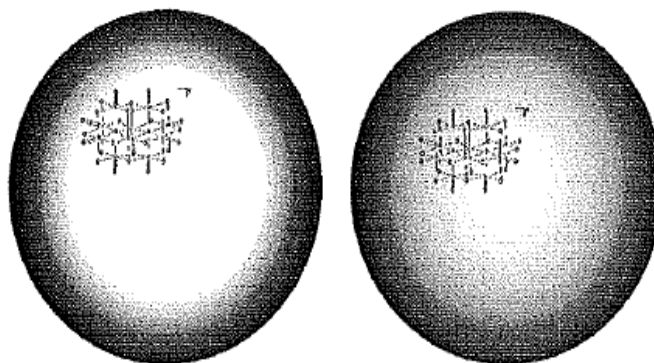


Fig. 10. Cartoons illustrating the relative nature of the water pools in Igepal CO-520 and in Igepal CO-610/430. The shaded regions represent the PEO head group and charge compensation layer encroachment on the water pool (Igepal head and tail groups not drawn for clarity). Adapted with permission from Ref. 53.

overall effect of each surfactant molecule. A non-ionic surfactant such as Igepal contains several O atoms in the PEO units, and thus will have residual/local negative surface charge (δ^-), which will repel the O-atom containing surface of V_{10} . Undoubtedly, the high charge on V_{10} is likely to be better solvated in the aqueous pool rather than at the interface leading to a system similar to that observed with negatively charged interfaces. We will review the available literature on the Igepal CO surfactant RM systems⁵⁴⁻⁵⁶ containing V_{10} .⁵³ The water layer adjacent to the interface⁹⁸ will include positively charged ions that are likely to attract the V_{10} and can place it near the charge compensation layer, and we present experimental results to support this prediction.

Studies were carried out using Igepal CO nonionic surfactants to create RMs with neutral interface that result from self-assembly by orientation of the dipoles of the surfactant molecules. These studies are important because they allow investigation of interactions with interfaces that, while containing a large number of dipolar sites, do not contain discrete charges. The RMs were prepared by dissolving either Igepal CO-520 or Igepal CO-610/430 surfactant in cyclohexane as the organic solvent, then adding water containing V_{10} in the amount needed to make the desired water pool/RM size. The V_{10} was prepared in two ways from $NaVO_3$ and from $NaOH$ and V_2O_5 .⁵³ The latter allowed for preparation of solutions containing varying exact Na^+ to V-atom ratios, whereas the former gives solutions with one Na^+ ion to V-atom ratio. ⁵¹V NMR spectra were recorded for different w_0 sizes of RMs containing V_{10} at different pH values. The diameters of the RMs and

of the water pools of these systems vary depending on water and surfactant concentration, but are in a similar range as those determined for AOT RMs (2–25 nm).¹¹⁸⁻¹²⁰ At low water concentration, the RMs are of similar size and the solution contains free surfactant which in the presence of water will form new RMs.¹¹⁸ However, as recently described, the water dynamics are similar at neutral and ionic interfaces.¹¹⁹ The spectra recorded from the Igepal CO-520 system showed a slight shifting consistent with placement of the V_{10} in the water pool. The line broadening observed is consistent with the water in the water pool restricting the motion. CO-610 has head groups that are on average about 1.5 PEO units longer than CO-520, and as anticipated for the presence of the longer head groups, studies with the Igepal CO-610/430 system showed a water pool with even less mobility than that in the CO-520 system. These studies suggest that there is a significant difference in the nature of the water pools as shown schematically in Fig. 10 (Igepal head and tail groups not drawn for clarity).

6. Decavanadate and Positively-Charged Interfaces

Studies using a cationic surfactant to prepare RMs were conducted and are described here¹²¹ to complement the studies reviewed above. Although several positively charged suitable surfactants exist (such as DTAB ($C_{15}H_{34}BrN$; dodecyltrimethylammonium) which does not require a cosurfactant,¹⁰⁹) we have used CTAB for studies probing the locations and changes in properties of antidiabetic

N. Samart et al.

agents and other solutes. CTAB has been reported to be more basic at the RM interface with isooctane as its organic solvent and 1-hexanol as cosurfactant in the system.^{104,122–124} Further, even though the solid CTAB can require extensive sonication to achieve complete dissolution and production of clear solutions,^{121,123} the utility and common use of CTAB (with a cosurfactant) in biology and in industry justify the choice of CTAB for investigations into this system. In the following, we will describe experiments (carried out in 1:5 CTAB/1-pentanol in cyclohexane) designed to investigate the interaction of the positively charged CTAB interface with V_{10} with both Na^+ (17, 57) and metformium,^{58,59} as counterions.

6.1. Decavanadate (V_{10}) in CTAB RMs

Examination of the CTAB/cyclohexane RM samples containing V_{10} was done to complete the investigation of these systems in preparation of this paper. The ^{51}V NMR spectra obtained are shown in Fig. 11. Since V_{10} associates with the positively charged interface and thus tumbles at the rate of the CTAB RM, the ^{51}V NMR signals from the aqueous solution should broaden considerably when placed in CTAB RMs. Broadening of the signals was observed with the Na^+ V_{10} salt as shown in Fig. 11. The

broadening effect was observed for both samples prepared from acid and neutral pH values (Fig. 11). That is V_{10} with different overall charges will associate with the interface. The signals are too broad to provide information of potential changes in the shifts as observed in negatively charged AOT/RM systems. However, the data clearly shows that the V_{10} nestle up against the positive interface in a manner not observed for negatively charged or neutral interfaces.

6.2. Metformin in CTAB RMs

Because of our interests in drug uptake and how the counterion effects interactions with interfaces, we investigated how the metformium ions affect V_{10} systems that contain a positive charge in this work. In this system, the same charge is found for the interface and the metformium ion. In the CTAB RMs containing metformin (in the absence of V_{10}), three signals are observed in the ^1H NMR spectra of HMet^+ at $\delta = 2.93$ (CH_3), 6.78 (NH_2), and 7.21 ppm (NH_2^+) as anticipated based on literature values.⁵⁰ The pH dependent shifts of $\delta = 3.05$ ppm at pH 1, 2.92 ppm at pH 7, and 2.77 ppm at pH 14, are consistent with protonation of HMet^+ at low pH and deprotonation of HMet^+ at neutral and higher pH (pKa values are 2.8 and 11.5).¹²⁵ In D_2O and

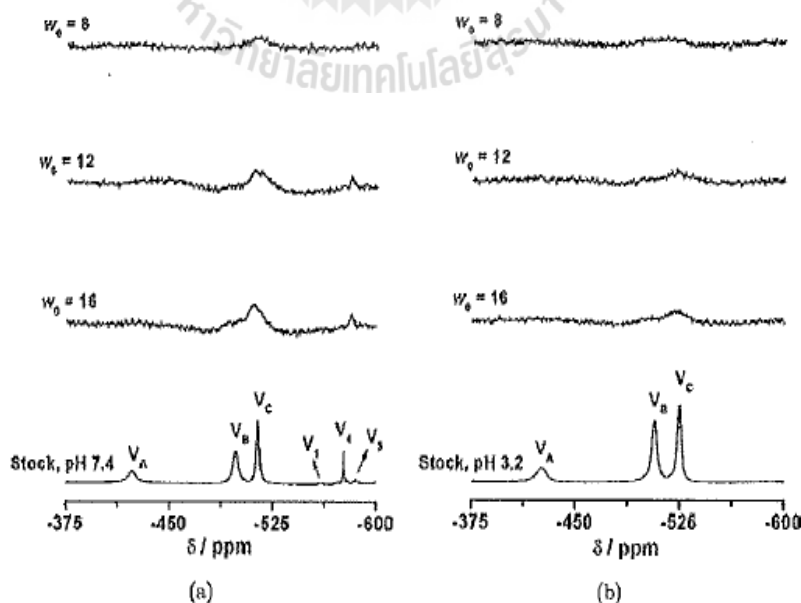


Fig. 11. ^{51}V NMR spectra of solutions of V_{10} at (a) pH 7.4 and (b) pH 3.2 in CTAB RM at various w_0 sizes.

d_4 -MeOH, the NH protons also exchange, and only one HMet⁺ peak of the CH₃ group is observed at $\delta = 2.91$ (D₂O) or 3.03 ppm (d_4 -MeOH).¹²⁶

In Figs. 12(a)–12(d), partial ¹H NMR spectra are shown for 1 M metformin hydrochloride in 0.2 M CTAB and 1.0 M 1-pentanol solutions at pH 5.9 for RM sizes $w_0 = 6, 8, 10, 12$ and 20 highlighting the H₂O and OH-pent [Fig. 12(a)], the NH₂ protons [Fig. 12(b)] and the CH₃ protons [Figs. 12(c) and 12(d)] are shown. The downfield shifting of the H₂O (HOD) signal as the w_0 size increases [Fig. 12(a)] attests to the changes in environment in the nano-sized water droplet. The observed upfield shift of the terminal NH₂ groups [Fig. 12(b)] is consistent with changing hydrogen bonding of these groups as the

w_0 size changes. The upfield shift of the CH₃ protons on HMet⁺ is consistent with partial penetration of the dimethyl amine part of HMet⁺ into the interface [Figs. 12(c) and 12(d)]. Spectra were recorded at high and low metformium concentrations, and both spectra are shown for the region containing the metformium CH₃-groups [Figs. 12(c) and 12(d)]. Combined, these spectra show that the change in water pool size affects the chemical shift of the CH₃ group, the NH₂ groups/the =NH₂⁺ group on HMet⁺ and the HOD signal differently. These observations lead to the proposal that the HMet⁺ is located at the interface with possible penetration of the CH₃ proton region into the CTAB RM interface as the size changes, Fig. 13.

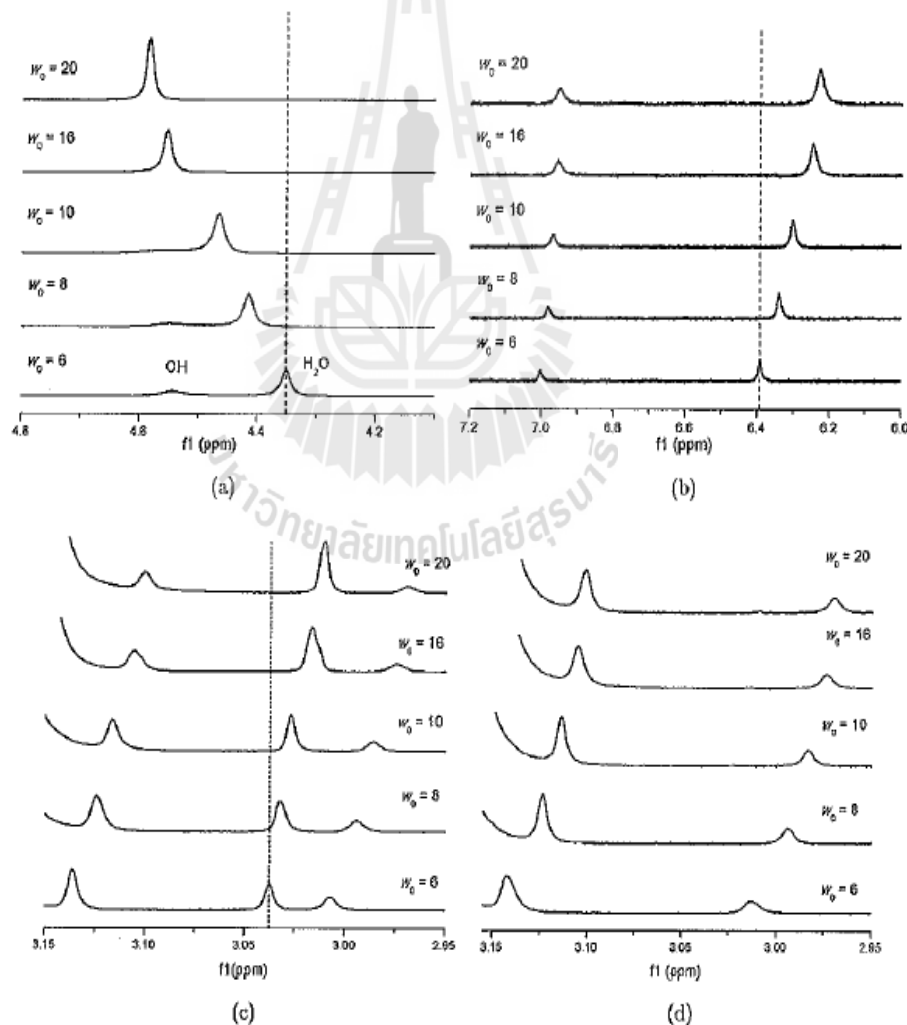


Fig. 12. ¹H NMR spectra of HMet⁺ in RMs prepared in cyclohexane/0.2 M CTAB/1.0 M 1-pentanol for $w_0 = 6, 8, 10, 12$ and 20. (a) NH₂ region of 0.1 M HMet⁺, (b) OH (1-pentanol) and H₂O region of 0.1 M HMet⁺, (c) CH₃ region of 0.1 M HMet⁺ and (d) CH₃ region of 0.001 M HMet⁺. Spectra were recorded at 25°C, chemical shifts are referenced against the cyclohexane resonance at 1.44 ppm.

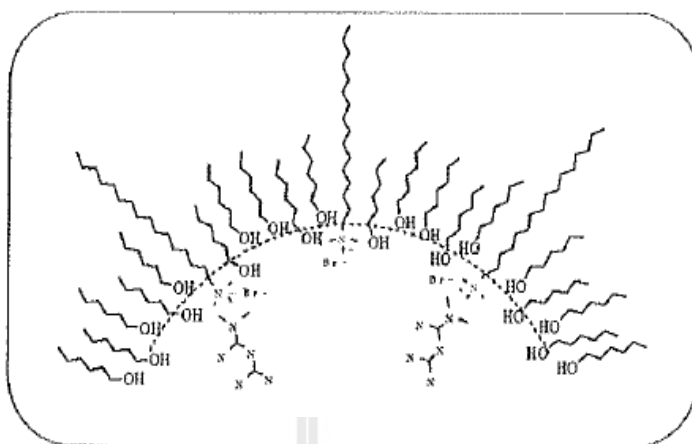


Fig. 13. Cartoon suggesting an orientation for metformin. Several possible locations of metformin in the CTAB RM exist and we illustrate one where the metforminium ion interacts with the interface.

The partial ^1H NMR spectra of the HOD and the OH-pent region show two different signals indicative of some level of structure of the system and slow exchange. The broad lines coalesce as the w_0 size increases to $w_0 = 20$. We and others have previously reported a change in dynamics in these CTAB-RM systems as evidenced by changes in signal broadening (linewidth increase) and merging signals.¹²⁷⁻¹²⁹ Because HMet^+ is known to form strong H-bonds, and because of the shifts mentioned above, the observation that H^+ exchange rate increases as the RM size increases is consistent with less structure as the w_0 size increases.

Since the HMet^+ cation shift is affected by increasing size of the water pool, we also carried out these studies at lower concentration. However, at lower concentrations, the signal intensity of the NH_2 and $=\text{NH}_2$ groups and the methyl peaks falls below the observation threshold and only the AOT signals remain in the ^1H NMR spectrum of HMet^+ at the concentration of 0.001 M HMet^+ in CTAB RM (Fig. 12). These spectra confirm the expectation that the N-H signals for the HMet^+ are no longer observable as well, and also define the changes in the CTAB signals as the water pool increases and the solute presence observed at the higher concentrations shown in Fig. 12. In Fig. 13, we illustrate the possible location of the metforminium/metformin consistent with the data provided.

These studies are important for two reasons. First, they provide a counter example to the studies carried out with a negatively charged V_{10} in a system with a negatively charged interface. Second,

metforminium as a counterion to V_{10} was found to increase solubility significantly, and more information is desirable to understand these processes.

7. Decavanadate Effects in Cells: Does it Act at Membrane Proteins or/and at Subcellular Targets?

Oxometalates such as V_{10} and other systems have been reported to exert antidiabetic, antibacterial, antiprotozoal, antiviral and anticancer activities.^{6,8,130} Specifically, V_{10} may act as an insulin-enhancing agent by lowering glycemia^{35,37} and increasing insulin receptor localization in membrane microdomains.¹³¹ In fact, vanadium treatments of diabetics have been known for more than 100 years.²⁶ On the other hand, it was suggested that, at least in part, the anticancer activity of vanadate as well as V_{10} and derivatives might be due to action through oxidative stress processes.^{26,35,132,133} Upon *in vivo* administration of V_{10} in an animal model system in fish, changes in antioxidant enzyme and reactive oxygen species levels were observed.^{134,135} Recently, it was suggested that V_{10} structurally resembles vanadium pentoxide, V_2O_5 .¹³⁶ Because of this structural analogy and because vanadium oxides are believed to impact human health,¹³⁶ the biological effects of V_{10} are of interest. Also, because V_{10} has been observed to form in yeast treated with vanadate and vanadyl sulfate, the interest in the biological effect of V_{10} is not limited to its effects as a drug, but also as a metabolite.¹³⁷⁻¹³⁹

V_{10} can exert its effects through interaction with intracellular targets or by interaction with membrane proteins such as receptors, ion pumps, ion channels, or exchangers.^{46,48,140-153} By changing ion homeostasis, V_{10} may affect several cellular processes with well-known physiological implications in several organs and tissues, for example in muscular dysfunction. The maintenance of Na^+ , K^+ and Ca^{2+} ion homeostasis has been correlated with physiological well-being in humans. Alternatively, V_{10} may exert its action after getting into the cell, for instance through anion channels,^{46,48} to modulate transient receptor protein channels¹⁴² and to interact specifically with the K^+ channel and other cation channels.^{45,153} It is likely that either V_{10} mode of action, i.e., targeting membrane proteins or transportation, takes place in biological systems (Fig. 14). In this section, we analyze both possibilities and discuss the putative effects of V_{10} on biological processes and how they are inhibited by V_{10} , the membrane E1E2-ATPases, such as Na^+ , K^+ -ATPase, and Ca^{2+} -ATPase are well known V_{10} targets.^{1,43,44,48,140,143,145,146}

Not only are the E1E2 ATPases membrane targets for V_{10} , but also ion channels and signal transduction receptors bind V_{10} . In fact V_{10} has been found to be a nucleotide P2X receptor antagonist,⁸⁰ to modulate transient receptor protein channels⁸⁷

and to interact specifically with the K^+ channel and other cation channels.^{45,88,89,153} However, for the Ca^{2+} -ATPase, the V_{10} binding site has been described to be at the cytoplasmic side, i.e., in a pocket formed by three protein domains,¹⁴⁰ suggesting that V_{10} must cross the membrane before targeting these E1E2-ATPases. Recently, it was proposed that the V_{10} interaction with the ion pumps might also occur from the extracellular side, as reported with several anti-ulcer, and cardiotoxic drugs that impact these proteins.⁴⁸ By targeting these ion pumps from inside or from extracellular space, V_{10} will induce changes in ion homeostasis, for instance, in Ca^{2+} homeostasis with well-known consequences and resulting cell death.

How V_{10} would enter cells is a nontrivial question because of its large size and large charge. Other anions such as vanadate, arsenate, or sulfate, enter through well-known anion channels or the nonspecific ion channel.¹⁴⁷⁻¹⁵⁰ However, these ions have much smaller size and significantly lower overall charge. Recently, it has been suggested that reactions at the interface could change the properties of the vanadium compound, and in the case of V_{10} such reactions could involve dissociation of one or two vanadium atoms at a time.^{20,137} Modification of V_{10} has been reported and covalent binding of appendages can take place,⁷⁵ which would make transportation of the V_{10} in parts much easier. Little experimental information is available on this topic.

Once inside the cell and at the cytoplasm, V_{10} has been proposed to target mitochondria. In mitochondria, V_{10} closes the porin channel by interfering with the purine-nucleotide binding sites¹⁵¹ and it induces membrane depolarization.¹⁵² It was also found that vanadium levels in heart or liver mitochondria are increased upon *in vivo* exposure to V_{10} .^{134,136} This cross-talk between mitochondria and V_{10} is supported by *in vitro* studies.^{152,153} Specifically, V_{10} causes mitochondrial depolarization (IC_{50} 40 nM) and oxygen consumption (IC_{50} 99 nM) which induces reduction of cytochrome b (Complex III).^{152,153} Therefore, V_{10} effects in biological systems are, at least in part, due to interactions with membrane proteins such as receptors, ion pumps, and ion channels within cytoplasmic or mitochondrial membranes.

There are many potential intracellular targets for vanadium compounds.^{27,75,154,155} Perhaps the most well recognized mode of action is the inhibition

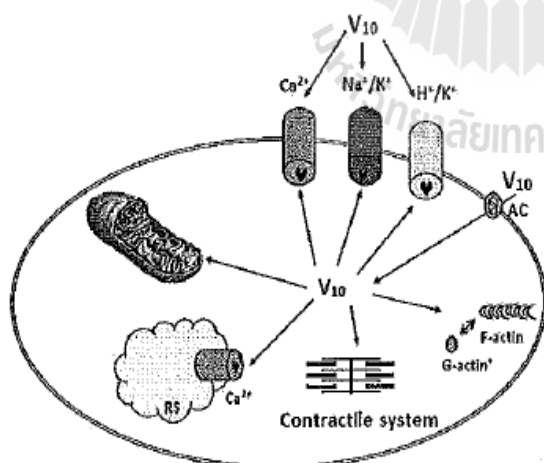


Fig. 14. Scheme of proposed V_{10} cellular targets. V_{10} uptake through anionic channels (AC). V_{10} might interact with membrane proteins from both inside and outside the cell. V_{10} may target subcellular organelles, such as mitochondria and sarcoplasmic reticulum (SR) pumps, affecting their function. V_{10} also targets the contractile system and its regulation, as well as G-actin, thus preventing its polymerization to F-actin. Adapted with permission from Ref. 48.

N. Samart et al.

of protein tyrosine phosphatases and other phosphatases,^{22,40,45,154-162} which thus activates protein kinases and enhances the effects promoted by insulin. However, V_{10} is a large anion and the reports of interaction with protein tyrosine phosphatase generally involve monomeric vanadate^{22,40,46,154-158,161} or simple mononuclear vanadium compounds.^{45,157,161} Although recently a report suggested that V_{10} also inhibited phosphatases, these effects could be attributed to delivery of monomeric vanadate to the active sites of the phosphatases.⁴⁵

Some POMs have been found to interact weakly and nonspecifically with DNA. Therefore, their effects can be distinguished from the antitumor mechanism of a mononuclear metal complex such as cisplatin and other organometallic compounds.¹⁶³ More recently, it was suggested that the antitumor activity of certain POMs depends not only on their affinity for DNA, but also strongly on their penetration ability to the cell membrane.¹⁶⁴ The toxicity of the POMs were reduced when liposome-encapsulated POMs were employed against HL-60 tumors *in vivo*.¹⁶⁵ POMs were also described as potent and selective inhibitors of alkaline phosphatases with profound anticancer and amoebicidal activities.¹⁵⁷ Regarding V_{10} , relevant intracellular targets also include myosin-actin interactions and actin polymerization,^{1,166} processes well known to be responsible for the contractile muscle contraction system and cytoskeleton structures, respectively. Note that, the disruption of the actin cytoskeleton was recently linked to alterations of the cytosolic calcium concentration¹⁶⁷ and therefore to cell death. Therefore, changes in the cytoskeleton dynamics, for instance, G-actin and F-actin equilibrium, is probably an early event induced by V_{10} in cells with severe implications to cell viability and proliferation. In this case, the mode of action for V_{10} after crossing the membrane could involve two pathways: by direct interaction with actin,⁹⁸ or indirectly by inducing the increase of reactive oxygen^{46,135,152} and nitrogen species known to affect the actin cytoskeleton.¹⁶⁷

8. Comparing the Interactions of Decavanadate with the Different Interfaces

The polyoxometalate, V_{10} , has been observed in yeast.¹³⁹ The uptake mechanism was not demonstrated and the authors concluded that the V_{10}

forms from the simple salts.^{139,168} Therefore, evidence exists that V_{10} can form under physiological conditions. In this paper, we compile the reported experimental data on the interaction of a representative polyoxometalate, V_{10} , with interfaces. In light of the effects of V_{10} on interfacial systems and with several proteins and channels associated with the membrane,^{1,43-45,48,140,141,145,146} and the possibility that V_{10} binds at the cytoplasmic side of the membrane,¹⁴⁰ the potential role for some involvement of the membrane in the action of V_{10} seems likely. The objective of the work was to gather experimental data and to provide answers to questions about where the oxometalate is located in a simple model system. Such studies provide some information, assisting and facilitating interpretation of the studies in biological systems. The location of the polyoxometalate and how the compound acts in biological systems is important. However, membranes are heterogeneous and nontrivial to investigate and therefore fundamental information is needed in model systems where interpretations can be made.¹⁶⁹

Although Coulombic forces often take center stage, at least conceptually,⁵¹ we have shown in the studies with Igepal surfactants, that the interface affinity for protons does not require the negatively charged surface.⁵³ Therefore, both the negatively charged and neutral interfaces show similar behavior placing the negatively charged V_{10} in the water pool. Both of these interfaces are able to affect the protonation state of the probe in the water pool establishing a proton gradient beginning at neutral pH in the center of the water pool.⁵³ These studies show that both these systems are suitable models for investigation of membrane-like interfaces and potential effects on drugs. Indeed, the studies described here suggest that some higher order exists as was described in cases of other "soft"^{76,77} supramolecular interactions in systems ranging from 10–500 nm in diameter showing soft-matter properties. Indeed, evidence is obtained on systems such as the V_{10} in the presence of metformium counterions in which three different functionalities in the molecule shift different amounts in the ¹H NMR spectrum. These shifts suggest varying locations and are consistent with the changes as the RM form and bind. Combined, these studies demonstrate that the subtle effects of the counterions impact the systems drastically and that such counterions will have an important role in any soft supramolecular structure generated.

9. Summary

In cells, the membrane is comprised of a complex mixture of differing lipids, proteins, and other metabolites such as cholesterol. Differing model membrane systems will mimic one of these types of membrane systems, however, their differences apart from Coulombic effects are not well understood. In this paper, we summarize the results available on the membrane interactions with a charged drug such as decavanadate (V_{10}). Interactions are often believed to be governed by Coulombic forces and hydrophobic forces as described when Lepinski summarized the empirical rules of drug uptake.⁷⁸ Since membranes contain lipids that can be neutral, positively, or negatively charged depending on the nature of each lipid, they exhibit properties that can be investigated using simple model systems. V_{10} is repelled by the interface in negatively charged and neutral nanosized water droplets, whereas a positively charged interface will attract the anion. Because it is not clear which of these interfaces best describe the membrane interface, we examined the behavior of all these systems when a charged probe is added.

In addition to the interactions with the lipid interface directly, V_{10} can interact with receptors, channels and membrane proteins. It has been demonstrated that V_{10} effects in biological systems are, at least in part, due to interactions with membrane proteins such as receptors, ion pumps, and ion channels within cytoplasmic or mitochondrial membranes. To understand such systems, information on this mode of action and that of passive interaction with the lipid interface are needed. As we show in this paper, lipid-like interfaces are not likely to be passive bystanders, but are actively involved in modifying the properties of drugs, both at the interfacial layer and the near solution properties of the double layer. Such effects are especially pronounced with large highly charged oxometalate species such as V_{10} and therefore the topic of this paper. The mode of action of vanadium compounds at the membrane continues to be complex, but it is premature to rule out either passive or active interactions at the interface with both protein and lipid substructures ("raft") within the membrane.

10. Experimental Method

Materials: CTAB (99%, Aldrich), cyclohexane (HPLC grade, Fisher), 1-pentanol ($\geq 99.5\%$, Aldrich), ethanol (95%, Fisher), NaAOT (98%,

Sigma-Aldrich), isooctane (99%, Sigma-Aldrich), deuterated dimethylsulfoxide (99%, d_6 -DMSO), metformin hydrochloride (Met/HCl, Sigma-Aldrich) were used as purchased. Deionized water was used for all RM systems.

Method: The ^1H NMR and ^{13}C NMR spectra of RM solutions were recorded using a Varian Inova spectrometer operating at 400 MHz at ambient temperature ($25 \pm 0.2^\circ\text{C}$) in the unlocked mode. Spectra were initially referenced against internal TMS ($\delta = 0.00$ ppm) and then routinely against the cyclohexane resonance ($\delta = 1.443$ ppm) for CTAB RM and isooctane resonance ($\delta = 0.904$ ppm) for AOT RM. Data analysis was conducted using MestReC V.4.5.9.1 NMR spectroscopic data processing software and ACD/NMR Processor Academic Edition for Windows.⁵⁸

Metformin solutions: Stock solution of 1.00 M metformin hydrochloride (1.656 g) was added into deionized water (10 mL), and the suspension was adjusted to the desired pH using HCl and NaOH.

Preparation of NaAOT: NaAOT was purified by dissolution in methanol, adding activated charcoal (6–12 mesh) into the solution and stirring overnight. The suspension was filtered, and methanol was removed by evaporation under vacuum for at least 12 h. Typical yields range from 99% and up.^{17,100} Clear stock solution of 0.75 M AOT was prepared by dissolving 8.335 g of AOT in isooctane (25 mL), and vortically mixing for about 30 min until a clear solution was obtained.

RM solutions with NaAOT: Each sample was prepared separately by combining 0.75 M purified AOT stock solution and aqueous 0.1 M metformin hydrochloride stock solution. The molar ratios $[\text{H}_2\text{O}]/[\text{CTAB}]$ (w_0) were equal to 6, 10 and 16, unless specified otherwise. All samples were transparent, single-phase solutions throughout the experiments.

Preparation of CTAB: CTAB was purified by recrystallization from anhydrous ethanol and dried over phosphorus pentoxide for 48 h under reduced pressure, and stored over dried silica gel under vacuum.¹²³

RM solutions with CTAB: Each sample was prepared separately by combining purified solid CTAB, 1-pentanol, cyclohexane, and solid metformin hydrochloride to make a stock solution of

N. Samart et al.

0.001 M or 0.10 M. CTAB and 1-pentanol concentrations in cyclohexane before the addition of aqueous phase were 0.20 M and 0.05 M, respectively, and the molar ratios $[H_2O]/[CTAB]$ (w_0) were equal to 6, 8, 10, 12 and 20, unless specified otherwise. All samples were transparent, single-phase solutions throughout the experiments.

Acknowledgments

DCC thanks the National Science Foundation (NSF) and Colorado State University, USA for funding. NS and KJH thank the Commission on Higher Education, Thailand for financial support for study and overseas travel support allowing research work at CSU. JS thanks the Beckman Foundation. We thank Dr. Christopher D. Rithner for assisting with the NMR experiments and plots.

References

- M. Aureliano and D. C. Crans, *J. Inorg. Biochem.* **103**, 536 (2009).
- B. Hasenknopf, *Front. Biosci.* **10**, 275 (2005).
- A. Müller, F. Peters, M. T. Pope and D. Gatteschi, *Chem. Rev.* **98**, 239 (1998).
- C. E. Müller, J. Iqbal, Y. Baqi, H. Zimmermann, A. Rollich and H. Stephan, *Bioorg. Med. Chem. Lett.* **16**, 5943 (2006).
- M. T. Pope and A. Müller, *Angew. Chem., Int. Ed. Engl.* **30**, 34 (1991).
- J. T. Rhule, C. L. Hill, D. A. Judd and R. F. Schinazi, *Chem. Rev.* **98**, 327 (1998).
- C. L. Hill, M. S. Weeks and R. F. Schinazi, *J. Med. Chem.* **33**, 2767 (1990).
- D. A. Judd, J. H. Nettles, N. Nevins, J. P. Snyder, D. C. Liotta, J. Tang, J. Ermolieff, R. F. Schinazi and C. L. Hill, *J. Am. Chem. Soc.* **123**, 886 (2001).
- G.-S. Kim, D. A. Judd, C. L. Hill and R. F. Schinazi, *J. Med. Chem.* **37**, 816 (1994).
- D. L. Long, E. Burkholder and L. Cronin, *Chem. Rev.* **36**, 105 (2007).
- E. Coronado and C. J. Gomez-Garcia, *Chem. Rev.* **98**, 273 (1998).
- C. Jasnin, J.-C. Chermann, G. Herve, A. Teze, P. Souchay, C. Boy-Loustau, N. Raynaud, F. Sinoussi and M. Raynaud, *J. Nat. Cancer Inst.* **53**, 469 (1974).
- L. Wang, B. Zhou and J. Liu, *Chin. Acad. Sci.* **25**, 1131 (2013).
- P. Sharma, D. Perez, A. Cabrera, N. Rosas and J. L. Arias, *Acta Pharmacol. Sin.* **29**, 881 (2008).
- T. Yamase, *J. Mater. Chem.* **15**, 4773 (2005).
- E. G. Vergara, E. S. Lara, A. P. Bonítez and A. Mendoza, Decavanadate salts of 4-Dimethylaminopyridine and metforminium dication as potential pro-drugs for the treatment of type II Diabetes, in *15th Int. Conf. Biological Inorganic Chemistry*, Vancouver, Canada, 2011.
- B. Baruah, J. M. Roden, M. Sedgwick, N. M. Correa, D. C. Crans and N. E. Levinger, *J. Am. Chem. Soc.* **128**, 12758 (2006).
- M. V. Mäkinen, R. Bamba, L. Ikujima, C. Wiettholt, C. T. Chen and S. D. Conzen, *J. Chem. Soc. Dalton Trans.* **42**, 11862 (2013).
- S. B. Etcheverry, D. C. Crans, A. D. Keramidias and A. M. Cortizo, *Arch. Biochem. Biophys.* **338**, 7 (1997).
- A. M. Metelo, R. Perez-Carro, M. M. Castro and P. L. Larrubia, *J. Inorg. Biochem.* **115**, 44 (2012).
- D. Rehder, J. C. Pessoa, C. Gerales, M. Castro, T. Kabanos, T. Kiss, B. Meier, G. Micera, L. Pettersson, M. Rangel, A. Salifoglou, I. Turel and D. R. Wang, *J. Biol. Inorg. Chem.* **7**, 384 (2002).
- A. Levina and P. A. Lay, *J. Chem. Soc. Dalton Trans.* **40**, 11675 (2011).
- H. Sakurai, K. Tsuchiya, M. Nukatsuka, J. Kawada, S. Ishikawa, H. Yoshida and M. Komatsu, *J. Clin. Biochem. Nutr.* **8**, 193 (1990).
- H. Sakurai, Structure-activity relationship and molecular action mechanism in the family of anti-diabetic bis(Picolinato)oxovanadium(IV) complexes, in *Vanadium: The Versatile Metal*, eds. K. Kustin, J. C. Pessoa and D. C. Crans, ACS Symposium Series, Vol. 974 (American Chemical Society, 2007), p. 110.
- J. H. McNeill, V. G. Yuen, H. R. Hoveyda and C. Orvig, *J. Med. Chem.* **35**, 1489 (1992).
- K. H. Thompson, J. Lichter, C. LeBel, M. C. Scaife, J. H. McNeill and C. Orvig, *J. Inorg. Biochem.* **103**, 554 (2009).
- K. H. Thompson and C. Orvig, *J. Inorg. Biochem.* **100**, 1925 (2006).
- D. C. Crans, A. Trujillo, P. Pharazyn and M. Cohen, *Coord. Chem. Rev.* **19–20**, 2178 (2011).
- P. Buglyo, D. C. Crans, E. M. Nagy, R. L. Lindo, L. Q. Yang, J. J. Smee, W. Z. Jin, L. H. Chi, M. E. Godzala and G. R. Willsky, *Inorg. Chem.* **44**, 5416 (2005).
- G. Willsky, P. Kaszynski, M. Godzala, P. Kostyniak and A. Goldfine, *Faseb J.* **14**, A1479 (2000).
- M. Li, W. J. Ding, J. J. Smee, B. Baruah, G. R. Willsky and D. C. Crans, *Biometals* **22**, 895 (2009).
- J. C. Pessoa and I. Tomaz, *Curr. Med. Chem.* **17**, 3701 (2010).
- Q. Wang, T. T. Liu, Y. Fu, K. Wang and X. G. Yang, *J. Biol. Inorg. Chem.* **15**, 1087 (2010).

34. M. J. Xie, X. D. Yang, W. P. Liu, S. P. Yan and Z. H. Meng, *J. Inorg. Biochem.* **104**, 851 (2010).
35. A. Zorzano, M. Palacin, L. Martí and S. García-Vicente, *J. Inorg. Biochem.* **103**, 559 (2009).
36. F. Yraola, S. Garcia-Vicente, L. Martí, F. Albericio, A. Zorzano and M. Royo, *Chem. Biol. Drug Des.* **69**, 423 (2007).
37. M. J. Pereira, E. Carvalho, J. W. Eriksson, D. C. Crans and M. Aureliano, *J. Inorg. Biochem.* **103**, 1687 (2009).
38. K. Nomiya, H. Torii, T. Hasegawa, Y. Nemoto, K. Nomura, K. Hashino, M. Uchida, Y. Kato, K. Shimizu and M. Oda, *J. Inorg. Biochem.* **86**, 657 (2001).
39. M. Passadouro, A. M. Metelo, A. S. Melão, J. R. Pedro, H. Paneca, E. Carvalho and M. M. C. A. Castro, *J. Inorg. Biochem.* **104**, 987 (2010).
40. Y. Shechter, J. P. Li, J. Meyerovitch, D. Gefel, R. Bruck, G. Elberg, D. S. Miller and A. Shisheva, *Mol. Cell. Biochem.* **153**, 39 (1995).
41. A. R. Saltiel and C. R. Kahn, *Nature* **414**, 799 (2001).
42. S. Pluskey, M. Mahroof-Tahir, D. C. Crans and D. S. Lawrence, *Biochem. J.* **321**, 333 (1997).
43. G. Fraqueza, C. A. Ohlin, W. H. Casey and M. Aureliano, *J. Inorg. Biochem.* **107**, 82 (2012).
44. G. Fraqueza, L. A. E. Batista de Carvalho, M. P. M. Marques, L. Maia, C. A. Ohlin, W. H. Casey and M. Aureliano, *J. Chem. Soc. Dalton Trans.* **41**, 12749 (2012).
45. C. C. McLauchlan, J. D. Hooker, M. A. Jones, Z. Dymon, E. A. Backhus, B. A. Greiner, N. A. Dornier, M. A. Youkhana and L. M. Manus, *J. Inorg. Biochem.* **104**, 274 (2010).
46. M. Aureliano and R. M. C. Gândara, *J. Inorg. Biochem.* **99**, 979 (2005).
47. M. Aureliano, *World J. Biol. Chem.* **2**, 215 (2011).
48. M. Aureliano, G. Fraqueza and C. A. Ohlin, *J. Chem. Soc. Dalton Trans.* **42**, 11770 (2013).
49. M. J. Lawrence and G. D. Rees, *Adv. Drug Delivery Rev.* **45**, 89 (2000).
50. T. De and A. Maitra, *Adv. Colloid Interface Sci.* **59**, 95 (1995).
51. A. Maitra, *J. Phys. Chem.* **88**, 5122 (1984).
52. M. C. Barbero, J. M. Valpuesta, E. Rial, J. I. G. Gurtubay, F. M. Goni and J. M. Macarulla, *Arch. Biochem. Biophys.* **228**, 560 (1984).
53. M. A. Sedgwick, D. C. Crans and N. E. Levinger, *Langmuir* **25**, 5496 (2009).
54. G. Fleischer, K. Grätz, J. Kärger, H. W. Meyer, K. Quitzsch, *J. Colloid Interface Sci.* **190**, 9 (1997).
55. K. Gratz, M. Helmstedt, H. W. Meyer and K. Quitzsch, *Colloid Polym. Sci.* **276**, 131 (1998).
56. D. E. Moilanen, N. E. Levinger, D. B. Spry and M. D. Fayer, *J. Am. Chem. Soc.* **129**, 14311 (2007).
57. B. Baruah, L. A. Swafford, D. C. Crans and N. E. Levinger, *J. Phys. Chem. B* **112**, 10158 (2008).
58. A. Chatkon, P. B. Chatterjee, M. A. Sedgwick, K. J. Haller and D. C. Crans, *Eur. J. Inorg. Chem.* **2013**, 1859 (2013).
59. A. Chatkon, Synthesis and structural study of materials combining metformin with other compounds used for diabetes therapy, Ph.D. Thesis, Suranaree University of Technology, Nakhon Ratchasima, Thailand, 2012.
60. N. M. Correa, M. A. Biasutti and J. J. Silber, *J. Colloid Interface Sci.* **172**, 71 (1995).
61. R. D. Falcone, N. M. Correa, M. A. Biasutti and J. J. Silber, *Langmuir* **16**, 3070 (2000).
62. M. D. Fayer and N. E. Levinger, *Ann. Rev. Anal. Chem.* **3**, 89 (2010).
63. N. M. Correa, E. N. Durantini and J. J. Silber, *J. Colloid Interface Sci.* **208**, 96 (1998).
64. D. R. Karsa and J. Houston, *Chemistry and Technology of Surfactants*, ed. R. J. Farn (Blackwell Publishing Ltd., Oxford, 2007), p. 1.
65. J. L. Gebicki, *Cent. Eur. J. Chem.* **2**, 371 (2004).
66. I. Goldwasser, D. Gefel, E. Gershonov, M. Fridkin and Y. Shechter, *J. Inorg. Biochem.* **80**, 21 (2000).
67. Y. Zhang, X.-D. Yang, K. Wang and D. C. Crans, *J. Inorg. Biochem.* **100**, 80 (2006).
68. X. Yang, K. Wang, J. Lu and D. C. Crans, *Coord. Chem. Rev.* **237**, 103 (2003).
69. X.-G. Yang, X.-D. Yang, L. Yuan, K. Wang and D. C. Crans, *Pharm. Res.* **21**, 1026 (2004).
70. H. T. Evans, *Inorg. Chem.* **5**, 967 (1966).
71. N. Bosnjakovic-Pavlovic, J. Prevost and A. Spasojevic-de Bire, *Cryst. Growth Des.* **11**, 3778 (2011).
72. D. C. Crans, *Comm. Inorg. Chem.* **16**, 35 (1994).
73. D. C. Crans and P. K. Shin, *J. Am. Chem. Soc.* **116**, 1305 (1994).
74. D. Rehder, *Bull. Mag. Reson.* **4**, 33 (1982).
75. D. C. Crans, J. Smee, E. Gaidamauskas and L. Yang, *Chem. Rev.* **104**, 849 (2004).
76. S. Roy, *Comments Inorg. Chem.* **32**, 113 (2011).
77. B. Roy, M. Arya, P. Thomas, J. Jurgschat, K. V. Rao, A. Banerjee, C. M. Reddy and S. Roy, *Langmuir* **29**, 14733 (2013).
78. C. A. Lipinski, F. Lombardo, B. W. Dominy and P. J. Feeney, *Adv. Drug Deliv. Rev.* **23**, 3 (1997).
79. I. Correia, F. Aveçilla, S. Marcao and J. C. Pessoa, *Inorg. Chim. Acta* **357**, 4476 (2004).
80. K. Bukietynska, K. Krot and P. Starynowicz, *Transit. Met. Chem.* **26**, 311 (2001).
81. M. M. Zhang and M. M. Chen, *Inorg. Chem. Comm.* **6**, 206 (2003).
82. W. T. Hou, J. Y. Guo, Z. X. Wang and Y. Xu, *J. Coord. Chem.* **66**, 2434 (2013).
83. L. Jouffret, M. Rivenet and F. Abraham, *Inorg. Chem. Comm.* **13**, 5 (2010).

N. Samart et al.

84. P. Roman, A. Aranzabe, A. Luque, J. M. Gutierrez-Zorrilla and M. Martínez-Ripoll, *J. Chem. Soc. Dalton Trans.*, Issue 13, 2225 (1995).
85. A. Dewan, D. K. Kakati and B. K. Das, *Indian J. Chem. A* 49, 39 (2010).
86. S. S. Mal, O. Troppner, I. Ivanovic-Burmazovic and P. Burger, *Eur. J. Inorg. Chem.*, Issue 10-11, 1960 (2013).
87. S. Nakamura and T. Ozeki, *J. Chem. Soc. Dalton Trans.*, Issue 44, 6135 (2008).
88. M. Biagioli, L. Strinna-Erre, G. Micera, A. Panzanelli and M. Zema, *Inorg. Chem. Comm.* 2, 214 (1999).
89. W. T. Xu, F. L. Jiang, Y. F. Zhou, K. C. Xiong, L. Chen, M. Yang, R. Feng and M. C. Hong, *J. Chem. Soc. Dalton Trans.* 41, 7737 (2012).
90. D. C. Crans and N. E. Levinger, *Acc. Chem. Res.* 45, 1637 (2012).
91. L. Pettersson, B. Hedman, I. Andersson and N. Ingri, *Chim. Scr.* 22, 254 (1983).
92. H. C. Lee and E. Oldfield, *J. Am. Chem. Soc.* 111, 1584 (1989).
93. W. G. Klemperer and W. Shum, *J. Am. Chem. Soc.* 99, 3544 (1977).
94. V. W. Day, W. G. Klemperer and D. J. Maltbie, *J. Am. Chem. Soc.* 109, 2991 (1987).
95. D. C. Crans, M. Mahroof-Tahir, O. P. Anderson and M. M. Miller, *Inorg. Chem.* 33, 5586 (1994).
96. A. Chatkon, B. Barres, N. Samart, S. Boyle, K. J. Haller and D. C. Crans, *Inorg. Chim. Acta* (2013), doi: 10.1016/j.ica.2013.12.031.
97. M. R. Harpham, B. M. Ladanyi and N. E. Levinger, *J. Phys. Chem.* 109, 16891 (2005).
98. A. Maneedaeng, K. J. Haller, B. P. Grady and A. E. Flood, *J. Colloid Interface Sci.* 356, 598 (2011).
99. A. Maneedaeng, A. E. Flood, K. J. Haller and B. P. Grady, *J. Surf. Deterg.* 15, 523 (2012).
100. B. Baruah, L. A. Swafford, D. C. Crans and N. E. Levinger, *J. Phys. Chem. B* 112, 10158 (2008).
101. D. C. Crans, B. Baruah, A. Ross and N. E. Levinger, *Coord. Chem. Rev.* 253, 2178 (2009).
102. E. Abuin, E. Lissi, R. Duarte, J. J. Silber and M. A. Biasutti, *Langmuir* 18, 8340 (2002).
103. M. A. Sedgwick, A. M. Trujillo, N. Hendricks, N. E. Levinger and D. C. Crans, *Langmuir* 27, 948 (2011).
104. E. Gaidamauskas, D. P. Cleaver, P. B. Chatterjee and D. C. Crans, *Langmuir* 26, 13153 (2010) and references therein.
105. J. J. Silber, A. Biasutti, E. Abuin and E. Lissi, *Adv. Colloid Interface Sci.* 82, 189 (1999).
106. J. J. Silber, R. D. Falcone, N. M. Correa, M. A. Biasutti, E. Abuin, E. Lissi and P. Campodonico, *Langmuir* 19, 2067 (2003).
107. L. Zingaretti, N. M. Correa, L. Boscatto, S. M. Chiacchiera, E. N. Durantini, S. G. Bertolotti, C. R. Rivarola and J. J. Silber, *J. Colloid Interface Sci.* 286, 245 (2005).
108. D. C. Crans, B. Baruah and N. E. Levinger, *Biomed. Pharmacother.* 60, 174 (2006).
109. F. Moyano, R. D. Falcone, J. C. Mejuto, J. J. Silber and N. M. Correa, *Chem. Eur. J.* 16, 8887 (2010).
110. J. H. B. Scarpello and H. C. S. Howlett, *Diab. Vasc. Dis. Res.* 5, 157 (2008).
111. I. Sánchez-Lombardo, E. Sánchez-Lara, A. Pérez-Benitez, Á. Mendoza, S. Bernès and E. González-Vergara *Eur. J. Inorg. Chem.* (2014), submitted.
112. M. L. Stahla, B. Baruah, D. M. James, M. D. Johnson, N. E. Levinger and D. C. Crans, *Langmuir* 24, 6027 (2008).
113. J. Eastoe, T. F. Towey, B. H. Robinson, J. Williams and R. K. Heenan, *J. Phys. Chem.* 97, 1459 (1993).
114. J. Eastoe, B. H. Robinson and R. K. Heenan, *Langmuir* 9, 2820 (1993).
115. J. Eastoe, G. Fragneto, B. H. Robinson, T. F. Towey, R. K. Heenan and F. J. Leng, *J. Chem. Soc. Faraday Trans.* 88, 461 (1992).
116. J. Eastoe, G. Fragneto, D. C. Steytler, B. H. Robinson and R. K. Heenan, *Physica B* 180, 555 (1992).
117. S. Roy, *Comments Inorg. Chem.* 32, 113 (2011).
118. J. L. Lemyre, S. Lamarre, A. Beaupre and A. M. Ritcey, *Langmuir* 26, 10524 (2010).
119. E. E. Fenn, D. B. Wong and M. D. Fayer, *Proc. Natl. Acad. Sci.* 106, 15243 (2009).
120. T. H. van der Loop, M. R. Panman, S. Lotze, J. Zhang, T. Vad, H. J. Bakker, W. F. C. Sager and S. Woutersen, *J. Chem. Phys.* 137, 044503 (2012).
121. N. Samart, A. M. Trujillo, K. J. Haller and D. C. Crans, Interaction of the antidiabetic drug metformin with model membrane systems, CTAB reverse micelles, in *15th Asian Chemical Congr.*, Singapore, 2013.
122. P. K. Das and A. Chaudhuri, *Langmuir* 15, 8771 (1999).
123. M. Giustini, G. Palazzo, G. Colafemmina, M. D. Monica, M. Giomini and A. Ceglie, *J. Phys. Chem.* 100, 3190 (1996).
124. G. Palazzo, F. Lopez, M. Giustini, G. Colafemmina and A. Ceglie, *J. Phys. Chem. B* 107, 1924 (2003).
125. Z. Szakacs, M. Kraszni and B. Noszal, *Anal. Bioanal. Chem.* 378, 1428 (2004).
126. H. H. Gadape and K. S. Parikh, *Eur. J. Chem.* 8, 767 (2011).
127. A. M. Trujillo, Simplified membrane-like systems describing the physical behaviors of cholesterol and

- anti-diabetic drugs, Ph.D. Thesis, Colorado State University (2013).
128. N. A. Halliday, A. C. Peet and M. M. Britton, *J. Phys. Chem. B* **114**, 13745 (2010).
 129. D. A. Binks, N. Spencer, J. Wilkie and M. M. Britton, *J. Phys. Chem. B* **114**, 12558 (2010).
 130. H. Stephan, M. Kubeil, F. Emmerling and C. E. Müller, *Eur. J. Inorg. Chem.* **2013**, 1585 (2013).
 131. P. W. Winter, A. Al-Qatati, A. L. Wolf-Ringwall, S. Schoeberl, P. B. Chatterjee, B. G. Barisas, B. A. Roess and D. C. Crans, *J. Chem. Soc. Dalton Trans.* **41**, 6419 (2012).
 132. T. Kiss, T. Jakusch, D. Hollender, Á. Dörnyei, É. A. Enyedy, J. C. Pessoa, H. Sakurai and A. Sanz-Medel, *Coord. Chem. Rev.* **252**, 1153 (2008).
 133. C. Sanchez-Gonzalez, C. Bermudez-Pena, C. E. Trenzado, H. Goenaga-Infante, M. Montes-Bayon, A. Sanz-Medel and J. Llopis, *Metallomics* **4**, 814 (2012).
 134. R. M. C. Gândara, S. S. Soares, H. Martins, C. Gutierrez-Merino and M. Aureliano, *J. Inorg. Biochem.* **99**, 1238 (2005).
 135. S. S. Soares, H. Martins, C. Gutierrez-Merino and M. Aureliano, *Comp. Biochem. Physiol. C, Pharmacol. Toxicol. Endocrinol.* **147**, 168 (2008).
 136. A. Al-Qatati, F. L. Fontes, B. G. Barisas, D. Zhang, D. A. Roess and D. C. Crans, *J. Chem. Soc. Dalton Trans.* **42**, 11912 (2013).
 137. G. R. Willsky, A. B. Goldfine and P. J. Kostyniak, *ACS Symp. Ser.* **711**, 278 (1998).
 138. G. R. Willsky, D. A. Preischel and B. C. McCabe, *Biophys. J.* **45**, A76 (1984).
 139. G. R. Willsky, D. A. White and B. C. McCabe, *J. Biol. Chem.* **259**, 3273 (1984).
 140. S. Hua, G. Inesi and C. Toyoshima, *J. Biol. Chem.* **275**, 30546 (2000).
 141. A. D. Michel, M. Xing, K. M. Thompson, C. A. Jones and P. P. A. Humphrey, *Eur. J. Pharmacol.* **534**, 19 (2006).
 142. B. Nilius, J. Prenen, A. Janssens, T. Voets and G. Droogmans, *J. Physiol.* **560**, 753 (2004).
 143. P. Proks, R. Ashfield and F. M. Ashcroft, *J. Biol. Chem.* **274**, 25393 (1999).
 144. L. Csanády and V. Adam-Vizi, *J. Gen. Physiol.* **123**, 743 (2004).
 145. M. Aureliano and V. M. C. Madeira, *Biochim. Biophys. Acta* **1221**, 259 (1994).
 146. D. Krstic, M. Colovic, N. Bosnjakovic-Pavlovic, A. Spasojevic-De Bire and V. Vasic, *Gen. Physiol. Biophys.* **28**, 302 (2009).
 147. M. Ishaque Khan, Q. Chen, D. P. Goshorn, H. Hope, S. Parkin and J. Zubieta, *J. Am. Chem. Soc.* **114**, 3341 (1992).
 148. G. R. Willsky, R. L. Bennett and M. H. Malamy, *J. Bacteriol.* **113**, 529 (1973).
 149. G. R. Willsky and M. H. Malamy, *J. Bacteriol.* **144**, 356 (1980).
 150. S. Silver, K. Budd, K. M. Leahy, W. V. Shaw, D. Hammond, R. P. Novick, G. R. Willsky and M. H. Malamy, *J. Bacteriol.* **146**, 983 (1981).
 151. M. Gutiérrez-Aguilar, V. Pérez-Vázquez, O. Bunoust, S. Manon, M. Rigoulet and S. Uribe, *Biochim. Biophys. Acta (BBA), Bioenerg.* **1767**, 1245 (2007).
 152. S. S. Soares, C. Gutiérrez-Merino and M. Aureliano, *J. Inorg. Biochem.* **101**, 789 (2007).
 153. M. Aureliano, *J. Chem. Soc. Dalton Trans.*, Issue 42, 9093 (2009).
 154. D. C. Crans, *J. Inorg. Biochem.* **80**, 123 (2000).
 155. K. H. Thompson and C. Orvig, *Met. Ions Biol. Syst.* **41**, 221 (2004).
 156. G. R. Willsky, L.-H. Chi, M. Godzala, P. J. Kostyniak, J. Smee, A. M. Trujill, J. A. Alfano, D. Ding, Z. Hu and D. C. Crans, *Coord. Chem. Rev.* **255**, 2258 (2011).
 157. R. Raza, A. Matin, S. Sarwar, M. Barsukova-Stuckart, M. Ibrahim, U. Kortz and J. Iqbal, *J. Chem. Soc. Dalton Trans.* **41**, 14329 (2012).
 158. X. L. Gao, L. P. Lu, M. L. Zhu, C. X. Yuan, J. F. Ma and X. Q. Fu, *Acta Chim. Sinica* **67**, 929 (2009).
 159. G. Huyer, S. Liu, J. Kelly, J. Moffat, P. Payette, B. Kennedy, G. Tsaprailis, M. J. Gresser and C. Ramachandran, *J. Bio. Chem.* **272**, 843 (1997).
 160. M. Zhang, M. Zhou, R. L. VanEtten and C. V. Stauffacher, *Biochemistry* **36**, 15 (1997).
 161. D. C. Crans, C. M. Simone, A. K. Saha and R. H. Glow, *Biochem. Biophys. Res. Commun.* **165**, 246 (1989).
 162. R. L. VanEtten, P. P. Waymack and D. M. Rehkop, *J. Am. Chem. Soc.* **96**, 6782 (1974).
 163. H. Fujita, T. Fujita, T. Sakurai, T. Yamase and Y. Seto, *Tohoku J. Exp. Med.* **168**, 421 (1992).
 164. S. Dianat, A. K. Bordbar, S. Tangestaninejad, B. Yadollahi, S. H. Zarkesh-Esfahani and P. Habibi, *J. Photochem. Photobiol. B, Biology* **124**, 27 (2013).
 165. X. Wang, F. Li, S. Liu and M. T. Pope, *J. Inorg. Biochem.* **99**, 452 (2005).
 166. S. Ramos, J. J. G. Moura and M. Aureliano, *Metallomics* **4**, 16 (2012).
 167. T. Tlago, D. Marques-da-Silva, A. K. Santhan-Arias, M. Aureliano and C. Gutierrez-Merino, *Cell Calcium* **49**, 174 (2011).
 168. D. C. Crans, B. Baruah and C. Ryan-Murphy, Interaction of decavanadate with model lipid interfaces, *Vanadium Biochemistry*, ed. M. Aureliano (2007), p. 1.
 169. D. E. Warschawski, A. A. Arnold, M. Beaugrand, A. Gravel, E. Chartrand and I. Marcotte, *Biochim. Biophys. Acta* **1808**, 1957 (2011).

APPENDIX C

GUANYLUREA METFORMIUM DOUBLE SALT OF DECAVANADATE, $(\text{HGU}^+)_4(\text{HMet}^+)_2(\text{V}_{10}\text{O}_{28}^{6-}) \cdot 2\text{H}_2\text{O}$

My contribution to this work was carried out to examine when guanyl urea form by hydrolysis of metformium. These studies were done while mentoring a CSU undergraduate student, Sarah Boyle and completing the studies by Ms. Alexa Barres, a summer intern of CSU. In addition, I assisted in the preparation of the manuscript.

The manuscript by Chatkon, Barres, Samart, Boyle, Haller, and Crans. "Guanylurea metformium double salt of decavanadate, $(\text{HGU}^+)_4(\text{HMet}^+)_2(\text{V}_{10}\text{O}_{28}^{6-}) \cdot 2\text{H}_2\text{O}$ " describes an unusual X-ray structure formed from metformin and decavanadate with two cation metformin and guanylurea. This compound was prepared characterized and X-ray structure was determined by Dr. Aungkana Chatkon.



Contents lists available at ScienceDirect

Inorganica Chimica Acta

journal homepage: www.elsevier.com/locate/ica

Guanylyurea metformium double salt of decavanadate, (HGU⁺)₄(HMet⁺)₂(V₁₀O₂₈⁶⁻)·2H₂O

Aungkana Chatkon^{a,b}, Alexa Barres^b, Nuttaporn Samart^{b,c}, Sarah E. Boyle^b, Kenneth J. Haller^{c,*},
Debbie C. Crans^{b,*}

^a Chemistry Program, Faculty of Science and Technology, Nakhon Ratchasima Rajabhat University, Nakhon Ratchasima 30000, Thailand

^b Department of Chemistry, Colorado State University, Fort Collins, CO 80523, USA

^c School of Chemistry, Institute of Science, Suranaree University of Technology, Nakhon Ratchasima 30000, Thailand

ARTICLE INFO

Article history:
Available online xxx

Keywords:
Decavanadate
Metformin
Guanylyurea
Mixed counterion complex
X-ray crystallography
Metformin hydrolysis

ABSTRACT

Metformin and vanadate were combined to form a double salt of decavanadate (V₁₀O₂₈⁶⁻) with two cations, namely metformium and a hydrolysis product of metformin, protonated guanylyurea (HGU⁺). The material was prepared by heating metformin and decavanadate in aqueous solution at pH 6.5 at 60 °C for 25 h. The title compound crystallizes in the triclinic space group P1̄, Z = 1. The structures of both cations and the decavanadate anion correspond to those reported previously. The V₁₀O₂₈⁶⁻ lies on an inversion center and charge is balanced by four HGU⁺ cations around the central axis and two HMet⁺ cations capping the ends of the V₁₀O₂₈⁶⁻ cylinder. These ions and two waters of solvation engage in an extensive multiple H-bonded network with the HGU⁺ bound at the strongest H-bond acceptor sites of the V₁₀O₂₈⁶⁻ and the HMet⁺ at lesser sites. The hydrolysis of metformin in the presence of a vanadium(V) (i.e. decavanadate, VO₂⁺ or H₂VO₄⁻) catalyst was confirmed in solution studies using ¹H, ¹³C, and ⁵¹V NMR spectroscopy. © 2014 Elsevier B.V. All rights reserved.

1. Introduction

Decavanadate (V₁₀O₂₈⁶⁻) is a polyoxometalate that has been extensively investigated, including from the point of view of anion structure, interactions with counterions and H-bonding [1–16]. Combination of oxovanadates with the biguanide metformin (Fig. 1) is particularly interesting because both vanadium [1,10–31] and metformin are antidiabetic agents [32–37]. Metformin hydrochloride is a preferred antidiabetic drug used in early stages of diabetes in combination with other drugs [38,39] and V₁₀O₂₈⁶⁻ has also been found to normalize elevated glucose levels [10,29–31]. Metformin can form compounds both as a multidentate ligand and as a counter ion in salts. Metformin has been reported to form a coordination complex with vanadyl, which has little solubility and exhibits limited if any improved antidiabetic effects upon administration in animals [40,41]. More recently we and others have investigated V₁₀O₂₈⁶⁻ salts, with protonated metformin (HMet⁺) as a counter ion [10,42]. The HMet⁺ salts were found to have significantly different properties than the Na⁺ salt

and we recently characterized how this material interacted with interfaces [42,43]. Here we describe the preparation and structural characterization of a double salt containing decavanadate and a mixture of metformium and protonated guanylyurea counterions.

The V₁₀ anion contains three types of vanadium atoms with different environments as reported previously [5,8,44–46] and shown in Fig. 1c. There are two V atoms in the center (V_A), each binding to six bridging O atoms, including both of the μ₆-O atoms of the cluster. There are four V atoms (V_B) completing a V₆O₁₂ equatorial plane, each binding one μ₆-O atom, four μ₂-O atoms, and a terminal O atom. Finally, there are four V atoms (V_C), each with five bridging O atoms and one terminal O atom, capping the equatorial plane of the oxometalate. At this time more than 100 different structures of decavanadate have been reported [8,44–48], varying in protonation state, counter ions, and the specific interactions and H-bonding network that the decavanadate is involved in. Although vanadium forms a number of oxovanadates in aqueous solution, at a pH of about 3–6 the V₁₀ species is the major species in solution [49,50]. Metformin has two types of protons that can be observed by ¹H NMR spectroscopy in organic solvents, but only the methyl protons are observable in D₂O. Two pK_a values for metformin (2.8 and 11.5) and guanylyurea (1.8 and 8.2) result mainly in the formation of the monoprotonated species from neutral to

* Corresponding authors. Tel.: +1 970 491 7635; fax: +1 970 491 1801 (D.C. Crans).
E-mail addresses: crans@lamar.colostate.edu, debbie.crans@colostate.edu (D.C. Crans).

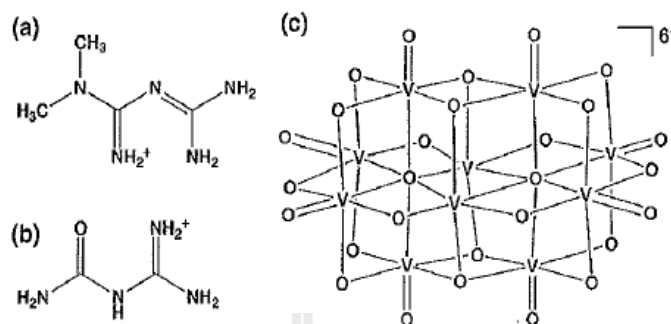


Fig. 1. Stereochemical diagrams of (a) metformium cation, (b) guanilyurea cation, and (c) decavanadate anion. The formulation of the protonated metformin and guanilyurea shown is that commonly used in the literature and not the formulation found in the structures described in this work (see below).

moderately low pH values although at low pH the diprotonated species can form [51].

In this work we characterize a crystalline material formed from decavanadate and metformin at pH 6.5. Since decavanadate forms a double salt with two equivalents of metformium cation and four equivalents of protonated guanilyurea cation as counter ions, the hydrolysis of metformin to guanilyurea in the presence of vanadium was explored. Using ^{13}C NMR spectroscopy, the decomposition of metformin was demonstrated confirming the possibility that decavanadate catalyzed the hydrolysis of metformin at near-neutral pH.

2. Experimental

2.1. Materials and methods

Metformin hydrochloride (1,1-dimethylbiguanide hydrochloride) was isolated from the diabetes drug tablet, Merck glucophage, 850 mg dosage, for the preparation of the crystal and was purchased from Pfaltz & Bauer for the solution studies. Vanadium oxide ($\text{V}_2\text{O}_5 \geq 98.0\%$) was obtained from Fluka. Deuterium oxide (99.9%) was obtained from Isotec and HCl (36.5–38%) from EMD. NMR analysis was done on a Varian Inova 400 FT-NMR spectrometer equipped with a ^1H – ^{13}C dual probe operating at 400.1 MHz for proton analysis and 100.6 MHz for carbon analysis. Infrared spectra were recorded in the mid-IR range 4000–400 cm^{-1} on a Perkin Elmer GX spectrophotometer with 4 cm^{-1} resolution using KBr pellets.

2.2. Synthesis of $(\text{HGU}^+)_4(\text{HMet}^+)_2(\text{V}_{10}\text{O}_{28}^{6-}) \cdot 2\text{H}_2\text{O}$ (1)

A solution of metformin hydrochloride (0.240 g, 1.45 mmol) in 8 mL of deionized water was added to a stirred aqueous suspension of V_2O_5 (0.220 g, 1.20 mmol) in 8 mL of deionized water. The pH was adjusted to 6.5 by 1.0 M NaOH and the orange solution was heated at 60 °C for 25 h at which point the mixture was filtered. The solution was kept at ambient temperature until light orange needle-like crystals formed in 5% yield based on vanadium (0.020 g, 0.012 mmol). (Heating for only 15 h resulted in a mixture of the orange needles and yellow-orange plates similar to those reported previously [42,43].) MW 1666.27; IR (KBr, cm^{-1}): 3556 (w), 3328 (w), 1715 (s), 1691 (m), 1584 (w), 1626 (m), 1583 (m), 1500 (w), 1457 (w), 1410 (w), 1330 (w), 1077 (w), 967 (s), 947 (m), 813 (s), 756 (m), 615 (b).

2.3. Solution preparation and NMR spectroscopy

A 0.400 M solution of metformin at pH 6.7 was prepared and used as stock solution for the hydrolysis studies from the solid

hydrochloride salt. When needed, solutions at lower pH were prepared. Decavanadate stock solution was prepared from V_2O_5 . Because the V_{10} is thermodynamically stable at acidic pH, 5 mM stock solutions were prepared at low pH (ranging from pH 3 to 5) by heating the suspension of V_2O_5 in D_2O in the presence of 2 equivalents (or 2.2 equivalents) of NaOH in order to dissolve the solid V_2O_5 . The suspension often took two days of stirring and heating to become transparent. The presence of decavanadate was verified using ^{51}V NMR spectroscopy (for example at pH 5.6 –421, –499, –515 ppm) and by the characteristic orange color. From these stock solutions three groups of decavanadate:metformin solutions were prepared; the high ratio of metformin to decavanadate containing a high concentration of metformin (180 mM) and 1.25 mM decavanadate (12.5 mM vanadium(V)), a solution with a lower ratio of metformin to decavanadate containing a lower concentration of metformin (60 mM) and higher concentration of decavanadate (3.75 mM; 37.5 mM vanadium(V)) and finally, conditions similar to those used during the crystallization procedure (see above). The pH of these solutions were adjusted ranging from pH 2 to 7 and those samples were subjected to various treatments, and analysis.

The hydrolysis reactions were routinely analyzed by both ^1H and ^{13}C NMR spectroscopy. The samples were referenced against an external sample of sodium 4,4-dimethyl-4-silapentane-1-sulfonate (DSS). The ^1H NMR spectra were recorded using routine parameters. However, the ^{13}C NMR spectra required some parameter optimization in part because of the ease of metformin hydrolysis and in part because of the difference in relaxation times between the quaternary C-atoms on the guanide part and CH_3 -dimethylamine atoms. Parameters used for monitoring the metformin hydrolysis reaction were: decoupled relaxation delay 60 s, acquisition time 3 s, pulse angle 60°, 256 scans, and window width of 25 157.2 Hz. Selected samples, particularly those with added decavanadate were also investigated using ^{51}V NMR spectroscopy and the parameters reported previously [43].

2.4. X-ray crystal structure determination of $(\text{HGU}^+)_4(\text{HMet}^+)_2(\text{V}_{10}\text{O}_{28}^{6-}) \cdot 2\text{H}_2\text{O}$ (1)

Intensity data measurements were carried out on a single rod-shaped section of a needle crystal of 1 at 100 K on a Bruker SMART APEX II CCD diffractometer with a graphite monochromatized Mo K α ($\lambda = 0.71073 \text{ \AA}$) X-ray radiation source. All nonhydrogen atoms were located by direct methods and all hydrogen atoms were located on a single successive Fourier difference electron density map using the SHELX program system [52]. The structure was refined against all data using the SHELXL software package [52]. In the final cycles of refinement atomic displacement motion was

Table 1
Crystal data and summary of refinement details for 1.

Empirical formula	C ₁₆ H ₅₆ N ₂₆ O ₃₄ V ₁₀
Formula weight (g mol ⁻¹)	1666.27
Crystal system	triclinic
Space group	P1
a (Å)	10.5330 (4)
b (Å)	10.9952 (3)
c (Å)	12.9375 (5)
α (°)	84.795 (2)
β (°)	67.139 (2)
γ (°)	87.114 (2)
V (Å ³)	1374.75 (8)
Z	1
D _{calc} (Mg m ⁻³)	2.013
Radiation type & wavelength (Å)	Mo Kα (λ = 0.71073)
Absorption coefficient, μ (mm ⁻¹)	1.73
T (K)	100 (2)
Crystal size (mm)	0.37 × 0.10 × 0.08
Color	orange
Shape	rod
Diffractometer	Bruker SMART APEX II
Absorption corrections	multiscan
Measured reflections	35 924
Independent data	9070
R _{int} > 2σ(F _o ²)	6798
R _{merge}	0.0322
2θ _{max}	63
h range	−15 to 15
k range	−14 to 16
l range	−18 to 19
Refinement on	F _o ²
R[F _o ² > 2σ(F _o ²)]	0.0308
wR(F _o ²)	0.0799
Goodness of fit (GOF) on I ²	1.014
Weights, w = 1/σ ² (F _o ²) + (0.0355(F _o ² + 2F _c ²)/3) ² + 0.4474((F _o ² + 2F _c ²)/3)	
Δρ _{max} , Δρ _{min} , Δρ _{est} error (e Å ⁻³)	0.39/−0.40/0.08
Structure refinement program	SHELXL97
Atomic scattering factors from	international tables

Computer programs: APEX2 Software [53], SAINT [54], SHELXS97 [52], SHELXL97 [52], ORTEP-III [55], and PUPLOT [56].

assumed to be anisotropic for the nonhydrogen atoms and isotropic for the hydrogen atoms. Positions of the hydrogen atoms bound to N or O atoms were refined with soft realistic distance restraints (22 restraints) and the methyl H atoms were refined as rigid (C₃) rotating groups each with tetrahedral angles and a variable C–H bond length. Details of the crystal data and a summary of refinement details for 1 is given in Table 1. Coordinates and atomic displacement parameters are available in a crystallographic data deposition at the Cambridge Crystallographic Data Center as CCDC 964622.

3. Results

3.1. Synthesis

The decavanadate crystals isolated from solutions prepared from V₂O₅ at pH 6.5 were lighter in color than the crystals formed at lower pH and characterized previously [42,43]. The product reported herein was isolated in 5% yield after 25 h of heating at 60 °C. Shorter heating time produced smaller orange needle crystals mixed with the yellow-orange plate crystals reported previously [42].

3.2. Crystal structure of (HGU⁺)₄(HMet⁺)₂(V₁₀O₂₈)·2H₂O (1)

An ORTEP perspective diagram illustrating the decavanadate anion and the crystallographically unique cations and water molecule is shown in Fig. 2. Fig. 2 also shows the H-bond interactions among

the components in the illustration as well as the atomic numbering scheme employed. The X-ray crystallographic structure determination unequivocally establishes the unit cell contents to be two metformium monocations, four protonated guanylurea cations, one unprotonated decavanadate hexaanion, and two water solvate molecules, i.e. (HGU⁺)₄(HMet⁺)₂(V₁₀O₂₈)·2H₂O.

The V₁₀O₂₈⁶⁻ anion can be viewed as a barrel-shaped molecule (Fig. 1). The four HGU⁺ cations have several N–H···O_{V10} H-bond interactions, primarily with μ₂-O and μ₃-O atoms (only one interaction for each HGU⁺ cation with a terminal O atom) about the barrel axis of the anion. The first HGU⁺ exhibits a strong N₁₄–H_{14b}···O₃₅ H-bond (2.759(2) Å), and bifurcated H-bonds at N₁₁ (N₁₁–H_{11b}···O₂₄, 3.144(2); N₁₁–H_{11b}···O₂₃₆, 3.012(2) Å) and N₁₃ (N₁₃–H₁₃···O₂₃₆, 3.093(2); N₁₃–H₁₃···O₃₅, 3.280(2) Å). The second unique HGU⁺ exhibits bifurcated H-bonds at N₂₂ and N₂₄ of N₂₂–H_{22a}···O₂, 3.058(2); N₂₂–H_{22a}···O₁₂₃, 2.810(2) and N₂₄–H_{24b}···O₂₄, 2.871(2); N₂₄–H_{24b}···O₁₄, 3.065(2) Å, and weaker trifurcated H-bonds at N₂₁ and N₂₃ (N–H···O range 3.069–3.265 Å). The HMet⁺ cation exhibits considerably fewer, and weaker (only terminal and μ₂-O atoms of the anion), supramolecular interactions, with the ends of the V₁₀O₂₈⁶⁻ barrel. The strongest H-bond interactions of HMet⁺ are at N₄, one of which is with a terminal O atom of the anion (N₄–H_{4a}···O₂, 2.844(2) Å) and the other with the O atom of the second HGU⁺ cation (N₄–H_{4b}···O₂₁, 2.846(2) Å). The opposite end of the HMet⁺ cation engages in two H-bonds (N₂–H_{2a}···O₄, 3.254(2) and N₂–H_{2b}···O₁₅, 2.926(2) Å) and one bifurcated H-bond at N₁ (N₁–H_{1b}···O₄₅, 3.062(2); N₁–H_{1b}···O₄, 3.331(2) Å). The waters of solvation fill small voids in the structure, exhibiting H-bond interactions at all four potential sites ranging from 2.803(3) to 3.282(3) Å. A packing diagram showing the extensive 3-D supramolecular interactions is given in Fig. 3.

3.3. Structure of the counterions HGU⁺ and HMet⁺

The structures of the counter ions in the salt are not well described by the abbreviations represented in the cartoon in Fig. 1. For the monocation HMet⁺ to have the indicated bond pattern and hydrogen atom sites, all biguanide carbon and nitrogen atoms would have to be sp² hybridized and the biguanide grouping would have to be totally planar. This is however not the case because the interplanar angle between the two guanidine moieties is nearly 60°. The indicated bond pattern in the monocation HGU⁺ would require sp³ hybridization, a lone pair on the central N atom linking the two guanidine moieties, and thus pyramidal geometry. This is not the case; the doubly determined interplanar angle is only about 10°, which as noted above, is consistent with literature, beginning with the first HGU⁺ structure [57]. The HGU⁺ monocation, thus, exhibits delocalization over the entire moiety. In summary, the mono cations in this structure are consistent with the structural literature, but do not contain the bond patterns and protonation sites illustrated in the simple ChemDraw renditions of Fig. 1: in contrast HMet⁺ contains distinct lone pair character at the N atom connecting the two guanidine units, while HGU⁺ is planar and completely delocalized.

3.4. Hydrolysis of metformin in aqueous solution in the presence and absence of decavanadate

Metformin is known to hydrolyse in aqueous solution to form guanylurea and a range of other products [58,59]. The nature of the hydrolysis products depends on pH, temperature, and potential catalysts and has been studied previously [58,59]. The goal with these studies is to investigate which of the known hydrolysis products form in the presence of decavanadate and thus, are competent to form under the conditions from which the crystal reported here-

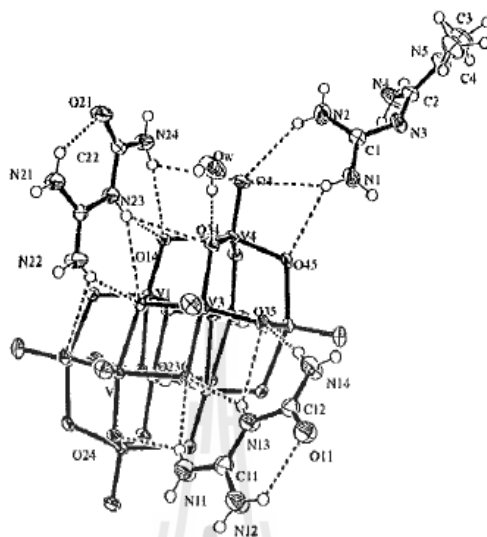


Fig. 2. Perspective view of one $V_{10}O_{28}^{6-}$ and the crystallographically unique counter ions and water molecule. The labeling scheme is indicated on the crystallographically unique atoms and hydrogen bonds are indicated by dashed lines (drawing by *osyr-III*; atomic displacement parameters indicated at the 50% probability level for the nonhydrogen atoms).

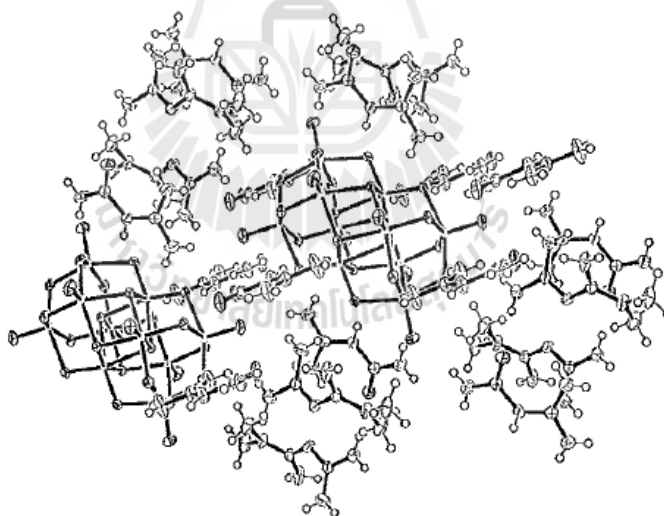


Fig. 3. Perspective diagram of a portion of the extended structure of 1 drawn with *osyr-III*. The decavanadate, metformium, and protonated guanylurea are shown in 3D, highlighting the steric relationship between the components in the crystal.

in formed. As a result we treated solutions of metformin with a range of conditions including the presence and absence of aqueous vanadium(V) (which depending on pH contained only decavanadate or a mixture of decavanadate and other vanadate oligomers [50]). Considering the speciation of metformin and guanylurea and the fact that limited information would be accessible by use of 1H NMR spectra in D_2O , ^{13}C NMR spectroscopy was used to monitor the decomposition of metformin. Unfortunately, the sensitivity of ^{13}C is low, so it was necessary to carry out these hydrolysis studies at higher concentrations. Furthermore, the relaxation time of

the ternary ^{13}C atoms in metformin and guanylurea are very long, so a relaxation delay of 60 s was needed to observe these signals as shown in Fig. 4a. However, using these parameters the dimethyl amine signals will have largely relaxed, and only a minor signal will be present. Therefore, the low intensity of the dimethyl amine signals can be attributed to both hydrolysis as well as the differences in relaxation parameters of the C-atoms. At neutral pH in aqueous solution the ^{13}C NMR spectrum of metformin shows 3 signals, 159 and 158 ppm for the two carbon imines, and 37 ppm for dimethyl amine (data not shown). Fig. 4 shows the signals

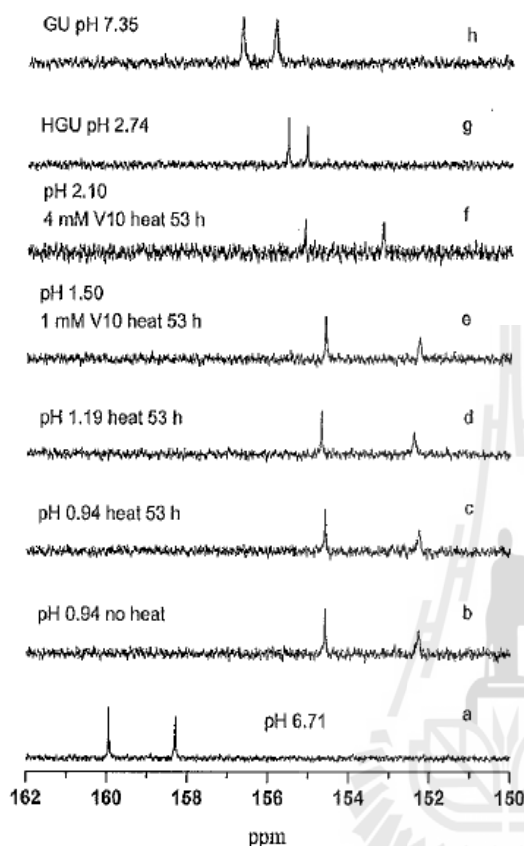


Fig. 4. ^{13}C NMR spectra of metformin solutions (a) 400 mM metformin in aqueous solution at neutral pH; (b) 240 mM metformin pH 0.94 no heat; (c) 240 mM metformin pH 0.94 25 h heat; (d) 240 mM metformin pH 1.19 53 h heat; (e) 180 mM metformin pH 1.50, 1.25 mM decavanadate (i.e. 12.5 mM vanadium(V)), 53 h heat; (f) 60 mM metformin pH 2.10, 3.75 mM decavanadate (i.e. 37.5 mM vanadium(V)), 53 h heat; (g) 200 mM guanylyurea (HGU) pH 2.74 and (h) 200 mM guanylyurea (GU) pH 7.35.

observed in the range of 150 to 162 ppm and the upfield shifts upon protonation of guanylyurea, which are different than the metformin signals.

In aqueous solution the ^1H NMR spectra of the dimethyl protons formed a triplet of peaks centralized at 2.8 ppm while the central nitrogen proton generated a peak at 6 ppm (data not shown) [59]. The terminal nitrogen protons showed very similar shifting to the central nitrogen protons at 6 and 7 ppm. In agreement with literature [58–61], no hydrolysis products were observed in solutions incubated at ambient temperature at neutral pH even after several weeks. Therefore, in order to observe hydrolysis metformin was subjected to treatment in acidic solution pH \sim 1 in a water bath at 55 °C for 24 h. This treatment led to formation of several hydrolysis products in agreement with literature reports [58–61]. The major observable degradation product peaks were upfield of the metformin signals at 152 and 154 ppm in the ^{13}C NMR spectrum consistent with guanylyurea in these solutions, see Fig. 4. Using the recording conditions favoring observation of the slowly relaxing ternary carbon atoms shows only a weak signal in the ^{13}C NMR spectrum for the dimethyl amine. However, when the relaxation time is decreased a larger signal upfield could be observed (data not shown). We conclude based on ^{13}C NMR studies

and confirmed by ^1H NMR studies that in addition to being difficult to observe the dimethyl amine may oxidize and/or evaporate as it forms resulting in limited accumulation of dimethyl amine in the solutions.

Finally, we used ^{13}C NMR spectroscopy to investigate if the decavanadate accelerated the decomposition of metformin. Fig. 4 shows the spectra of guanylyurea and metformin at neutral and at lower pH for reference, focusing on the signals of the guanyl part of the molecules. The addition of 1 mM decavanadate to an acidic solution of metformin resulted in decomposition of metformin as evidenced by the decreasing ^{13}C NMR signal heights of both the dimethyl amine and the guanyl C-atoms (Fig. 4). Increasing the amounts of decavanadate increased the decomposition and furthermore resulted in the hydrolysis of the guanylyurea as well. When monitoring the hydrolysis reactions at lower concentrations approximating the conditions of the crystallization using ^{13}C NMR spectroscopy, the signal to noise was too poor for observation. However, when examining these solutions using ^1H NMR spectra, the spectra show signals consistent with formation of guanylyurea and dimethylamine as shown above for studies at higher concentration (data not shown) [42,43].

Decavanadate is the thermodynamically stable form of vanadium(V) at acidic pH, however, depending on the concentrations of vanadium(V), the speciation will vary between several protonated decavanadates and monomeric vanadate [50]. Because the reactions are very slow at higher pH values, we carried out these studies near pH 2 to avoid the extensive heating treatments. Based on the reported speciation constants [50] a significant fraction of the vanadium(V) should be present in the form of decavanadate, however, some monomeric vanadate (V_1) may exist. Therefore the observed catalysis may in part be due to monomeric vanadate. The possibility that undissolved V_2O_5 was contributing as catalyst is less likely because the solutions are transparent. Under these acidic conditions interconversion between monomeric vanadate and decavanadate is fast, and it is not possible to completely attribute the observed effects to either monomeric vanadate or decavanadate. We recorded the ^{51}V NMR spectra of representative solutions of 180 mM metformin and 12.5 mM vanadium(V). The representative solution of decavanadate was mainly intact prior to heating with >95% of the V-atoms were in the form of V_{10} . Following the heating treatments the majority of the vanadium(V) was still in the form of decavanadate although some V_1 formed during the treatment (9% of the V-atoms were in the form of V_1).

The observed hydrolysis of metformin facilitated by the decavanadate solution is consistent with the hypothesis that the formation of guanylyurea took place during the heating of the metformin and decavanadate. Because of the rapid interconversion between vanadate monomer and decavanadate at low pH, we cannot attribute the effects to only one species, nor can we rule out the involvement of solely monoprotonated or deprotonated metformin. However, the hydrolysis experiments showed that once the guanylyurea forms, it is also susceptible to hydrolysis, and results in complete disappearance of the material.

During heating and/or the crystallization process, metformin hydrolyzes to form guanylyurea, but in the presence of decavanadate the formation of the mixed cation metformin guanylyurea decavanadate salt that we characterized in this manuscript can form. The reaction appears pH-dependent because the yellow-orange plate crystals are observed at lower pH values as well [43], whereas the orange rod crystals are observed only at pH 6.5. The more prevalent product reported previously [43] contains three hydronium ions per decavanadate, and thus is favored by lower pH even at the same time as HGU is formed, perhaps explaining why the protonated guanylyurea species reported herein is only observed at the highest pH value studied.

Table 2
Supramolecular H-bond interactions in the structure of 1.

D-H...A	D-H	H...A	D...A	Angle	Symmetry code
N1-H1a...O11	0.81	2.18	2.985(3)	163(2)	1 - x, 1 - y, 2 - z
N1-H1b...O45	0.81	2.43	3.062(2)	136(2)	
N1-H1b...O4	0.81	2.58	3.331(2)	154(2)	
N2-H2a...O4	0.81	2.50	3.254(2)	155(2)	
N2-H2b...O15	0.81	2.15	2.926(2)	160(3)	1 - x, 2 - y, 1 - z
N4-H4a...O2	0.82	2.06	2.844(2)	158(2)	1 + x, 1 + y, z
N4-H4b...O21	0.82	2.05	2.846(2)	163(2)	1 + x, 1 + y, z
N11-H11a...N24	0.81	2.61	3.248(3)	137(3)	x, -1 + y, z
N11-H11a...O236	0.81	2.64	3.282(3)	137(3)	x, -1 + y, z
N11-H11b...O236	0.81	2.26	3.012(2)	156(2)	
N11-H11b...O24	0.81	2.53	3.144(2)	134(2)	
N12-H12a...OW	0.81	2.02	2.803(3)	164(3)	x, -1 + y, z
N12-H12b...O11	0.81	2.09	2.675(2)	129(2)	
N12-H12b...N3	0.81	2.64	3.266(3)	136(2)	1 - x, 1 - y, 2 - z
N13-H13...O236	0.78	2.38	3.093(2)	153(2)	
N13-H13...O35	0.78	2.64	3.280(2)	140(2)	
N14-H14a...O5	0.81	2.20	2.984(2)	162(3)	x, y, 1 - z
N14-H14b...O35	0.81	1.96	2.759(2)	173(2)	
N21-H21a...O45	0.81	2.39	3.151(2)	158(2)	-1 + x, y, z
N21-H21a...O24	0.81	2.60	3.139(2)	126(2)	-x, 1 - y, 1 - z
N21-H21a...O25	0.81	2.44	3.059(2)	136(2)	-x, 1 - y, 1 - z
N21-H21b...O21	0.81	2.00	2.643(2)	136(2)	
N22-H22a...O123	0.81	2.03	2.810(2)	162(3)	
N22-H22a...O2	0.81	2.61	3.058(2)	117(2)	
N22-H22b...O25	0.81	2.02	2.762(2)	151(2)	-x, 1 - y, 1 - z
N23-H23...O123	0.79	2.52	3.199(2)	145(2)	
N23-H23...O14	0.79	2.56	3.252(2)	147(2)	
N23-H23...O34	0.79	2.64	3.265(2)	137(2)	
N24-H24a...O24	0.80	2.08	2.871(2)	168(2)	x, 1 + y, z
N24-H24b...O14	0.81	2.28	3.065(2)	162(2)	
OW-HWa...O34	0.75	2.03	2.774(2)	175(3)	
OW-HWb...O11	0.74	2.34	3.074(3)	172(3)	-x, 1 - y, 2 - z

4. Discussion

The X-ray structure of the title compound shows a range of different types of anion-cation interactions. Although HGU⁺ and HMet⁺ contain similar functionalities, their geometric configurations are not similar. The planarity in HGU⁺ and the lack of planarity in HMet⁺ as well as their different charge density translates into different degrees of complementarity to the surface of decavanadate. The bond lengths and angles observed for the [V₁₀O₂₈]⁶⁻ unit are within the ranges previously reported [1–16]. The biguanide portion of the metforminium cation is distinctly nonplanar with an angle of 57.26(9)° between the two guanidine planes, while the protonated guanylyurea cations (HGU⁺) are nearly planar (interplanar angle between the two guanidine residues within the two HGU⁺ cations of 11.12(15)° and 7.79(7)°, similar to the values found in several HGU⁺ cations, beginning with the first reported structure, (HGU⁺)(H₂PO₄⁻), from 1986 [57] due to the π -electron delocalization throughout the HGU⁺ cation. The planarity of the HGU⁺ cations is further reinforced by a strong intramolecular N-H...O hydrogen bond (N₁₂-H_{12b}...O₁₁, 2.675(2) Å; N₂₁-H_{21b}...O₂₁, 2.643(2) Å Table 2). As apparent from the X-ray structure shown in Fig. 2, three NH-groups in HGU⁺ are involved in H-bonding with decavanadate as a tridentate “ligand” and at sites on the V₁₀ surface that form the stronger H-bonds. In contrast HMet⁺ is only involved in H-bonding side-on capping the V₁₀ system. Thus the complementarity of HGU⁺ to V₁₀ is greater than that of HMet⁺. Furthermore, the overall strengths of the concerted interactions of HGU⁺ may be sufficient to make it a favored solution species, thereby driving the metformin to guanylyurea reaction. The yellow-orange plate-like species isolated at lower pH, (HMet⁺)₃(H₃O⁺)₃(V₁₀O₂₈)₃·3H₂O [43], is also obtained mixed with the current product from the reaction at pH 6.5. The latter product, containing three hydronium ions, is favored by lower pH, apparently precluding formation of the HGU⁺ product even as the acid

catalyzed hydrolysis of metformin to guanylyurea and the GU to HGU speciation would be favored.

Metformin forms a range of hydrolysis products depending on specific conditions. Metformin hydrolyzes at acidic pH but the hydrolysis products are undetected by NMR at pH 6.5. Decomposition at neutral pH requires the addition of heat, a catalyst, or both. New ¹³C NMR signals are observed in the region 150–160 ppm and are consistent with formation of guanylyurea upon the addition of acid, prolonged heating and in the presence of catalyst. Crystallization of another hydrolysis product has been demonstrated previously in the preparation of (Me₂NH₂)₆(V₁₀O₂₈)·H₂O by decomposition of guanine in the presence of vanadium in DMF [48]. In some of our spectra the accompanying product dimethyl amine was not observable at all. This is probably due to the parameters used for recording the spectra which favor slowly relaxing C-atoms and not the faster relaxing C-atoms of the dimethylamine fragment. The amounts of dimethylamine can also decrease by oxidation to carbon dioxide or evaporation from solution during the extensive period of heating. The presence of decavanadate in acidic solution and in the presence of heat, increases the degradation of both metformin and guanylyurea compared to samples containing no decavanadate (shown in Fig. 4). However, as we show using ⁵¹V NMR spectroscopy (data not shown), some decavanadate hydrolyzes to form V₁ under these conditions. Therefore, we cannot rule out the possibility that V₁ is also an active catalyst. In summary, our studies demonstrate that the presence of decavanadate or some aqueous form of vanadium(V) will catalyze the degradation of metformin over a 24 h period even at neutral pH.

The fact that metformin can form guanylyurea suggests that the observed guanylyurea came from metformin. The double salt reported forms, after an extended heating period which is demonstrated to favor hydrolysis of metformin to guanylyurea, from an extended room temperature crystallization during which metformin may continue to hydrolyze to form additional guanylyurea, while at the same time formation of the double salt characterized here removes HGU⁺ from the reaction further driving the metformin decomposition. It is interesting that at neutral pH conditions at which metformin and guanylyurea are most stable and should not hydrolyze, in fact we do observe hydrolysis of metformin to guanylyurea. Because the metformin and guanylyurea hydrolysis both increase in the presence of decavanadate, formation of guanylyurea may be balanced by the depletion of both metformin and guanylyurea by hydrolysis. Based on the X-ray structure, it appears that the protonated guanylyurea topology and charge distribution is very complementary to the strongest H-bonding sites on decavanadate, potentially leading to stable supramolecular precursors in solution as four guanylyurea cations cover the barrel surface of the decavanadate. Near neutral pH, low concentration of hydronium ions leaves the more plentiful metforminium cations to complete the charge balance while resorting to the weaker H-bonding sites capping the polyoxymetalate. Thus, although decavanadate is present in all samples, the speciation and associated interactions are likely to be important for the properties of the system and may be the reason why the crystal with both HMet⁺ and HGU⁺ is only observed at pH 6.5 and not at lower pH values [43].

Decavanadate has been reported to exhibit antidiabetic properties [1,29–31] in line with the larger number of coordination complexes [15,17–28] and the simple vanadate and vanadyl cation salts [20,21,24]. Different counterions have been tested including sodium [1,31], ammonium [29,30], and metformin [10]. As we showed recently [43], the presence of a small amount of metformin significantly changed the solubility of a metformin-decavanadate salt in a heterogeneous environment. This would suggest that the salt will also act differently in biological systems [22], and as a result, fundamental studies may be an important contributor in

consideration and evaluation of the effects of metal-based-drugs in treatment of diabetes and other diseases.

5. Conclusions

A solution of vanadate and metformin results in the precipitation, crystallization, and structural characterization of the mixed cation oxometalate salt $(\text{HMet}^+)_2(\text{HGU}^+)_4(\text{V}_{10}\text{O}_{26}) \cdot 2\text{H}_2\text{O}$. The structure consists of decavanadate flanked by four molecules of guanylurea tightly H-bonded to the anion capped off with two metformin molecules that are also H-bonded to the anion. The crystallographic determination of the counterions illustrates once again that the 'normal' protonation sites shown in localized bond drawings as in Fig. 1 are not accurate descriptions of the actual electron density distribution, instead HMet^+ contains distinct lone pair character at the N atom connecting the two guanidine units while the HGU^+ unit is planar and completely delocalized. Because four equivalents of guanylurea are found in the X-ray structure, and only metformin was added to the solution, the guanylurea must have formed from the metformin. Aqueous solution studies were carried out to demonstrate that metformin could hydrolyze in the presence of decavanadate or other aqueous forms of vanadate(V), even at neutral pH, and thus supporting the conclusion that the observed guanylurea arose from the hydrolysis of metformin. These results are consistent with the formation of the guanylurea during the synthesis and crystallization of the decavanadate–metformin–guanylurea-salt at neutral pH.

Acknowledgements

DCC thanks the National Science Foundation (NSF) and Colorado State University, USA for funding. AC, NS, and KJH thank the Commission on Higher Education, Thailand for financial support for study and overseas travel support allowing research work at CSU. AB thanks the University of Michigan–Flint for funding the HONORS thesis internship allowing her to visit CSU to carry out this research. We thank Drs. Christopher D. Rithner and Myles Sedgwick for assisting with the NMR experiments and plots.

Appendix A

CCDC 964622 contains the supplementary crystallographic data for compound 1. These data can be obtained free of charge from The Cambridge Crystallographic Data Centre via www.ccdc.cam.ac.uk/data_request/cif.

References

- [1] M. Aureliano, D.C. Crans, *J. Inorg. Biochem.* 103 (2009) 536.
- [2] A. Müller, F. Peters, M.T. Pope, D. Gatteschi, *Chem. Rev.* 98 (1998) 239.
- [3] M.T. Pope, A. Müller, *Angew. Chem., Int. Ed. Engl.* 30 (1991) 34.
- [4] B. Hasenknopf, *Front. Biosci.* 10 (2005) 275.
- [5] H.T. Evans, *Inorg. Chem.* 5 (1966) 967.
- [6] D.L. Long, E. Burkholder, I. Cronin, *Chem. Rev.* 36 (2007) 105.
- [7] E. Coronado, C.J. Gomez-Garcia, *Chem. Rev.* 98 (1998) 273.
- [8] N. Bosnjakovic-Pavlovic, J. Prevost, A. Spasojevic-de Bire, *Cryst. Growth Des.* 11 (2011) 3778.
- [9] D.C. Crans, M. Mahroof-Tahir, O.P. Anderson, M.M. Miller, *Inorg. Chem.* 33 (1994) 5586.
- [10] E.G. Vergara, E.S. Lara, A.P. Benítez, A. Mendoza, Decavanadate salts of 4-dimethylaminopyridine and metforminium dication as potential pro-drugs for the treatment of type II diabetes, in: 15th International Conference on Biological Inorganic Chemistry, Vancouver, Canada, 2011.
- [11] B. Baruah, J.M. Roden, M. Sedgwick, N.M. Correa, D.C. Crans, N.E. Levinger, *J. Am. Chem. Soc.* 128 (2006) 12753.
- [12] M.V. Mäkinen, R. Bamba, L. Ikejima, C. Wietholt, C.T. Chen, S.D. Conzen, *Dalton Trans.* 42 (2013) (1867) 11862.
- [13] S.B. Etcheverry, D.C. Crans, A.D. Keramidis, A.M. Cortizo, *Arch. Biochem. Biophys.* 338 (1997) 7.
- [14] A.M. Melo, R. Perez-Carro, M.M. Castro, P.L. Larrubia, *J. Inorg. Biochem.* 115 (2012) 44.
- [15] D. Rehder, J.C. Pessoa, C. Geraldes, M. Castro, T. Kabanos, T. Kiss, B. Meier, G. Micera, L. Pettersson, M. Rangel, A. Salifoglou, I. Turel, D.R. Wang, *J. Biol. Inorg. Chem.* 7 (2002) 384.
- [16] A. Levina, P.A. Lay, *Dalton Trans.* 40 (2011) 11675.
- [17] H. Sakurai, K. Tsuchiya, M. Nukatsuka, J. Kawada, S. Ishikawa, H. Yoshida, M. Komatsu, *J. Clin. Biochem. Nutr.* 8 (1990) 193.
- [18] H. Sakurai, Structure–activity relationship and molecular action mechanism in the family of antidiabetic bis(picolinato)oxovanadium(IV) complexes, in: K. Rustin, J.C. Pessoa, D.C. Crans (Eds.), *Vanadium: The Versatile Metal*. ACS Symposium Series, vol. 974, American Chemical Society, Washington, DC, 2007, pp. 110–210.
- [19] J.H. McNeill, V.G. Yuen, H.R. Hoveyda, C. Orvig, *J. Med. Chem.* 35 (1992) 1489.
- [20] K.H. Thompson, J. Lichtner, C. LeBel, M.C. Scailie, J.H. McNeill, C. Orvig, *J. Inorg. Biochem.* 103 (2009) 554.
- [21] K.H. Thompson, C. Orvig, *J. Inorg. Biochem.* 100 (2006) 1925.
- [22] D.C. Crans, A. Trujillo, P. Pharaayn, M. Cohen, *Coord. Chem. Rev.* 266 (2011) 2178.
- [23] P. Buglyo, D.C. Crans, E.M. Nagy, R.L. Lindo, L.Q. Yang, J.J. Smece, W.Z. Jin, L.H. Chi, M.E. Godzala, G.R. Willsky, *Inorg. Chem.* 44 (2005) 5416.
- [24] G. Willsky, P. Kaszynski, M. Godzala, P. Kostyniak, A. Goldfine, *FASEB J.* 14 (2000) A1479.
- [25] M. Li, W.J. Ding, J.J. Smece, B. Baruah, G.R. Willsky, D.C. Crans, *Biomaterials* 22 (2009) 895.
- [26] J.C. Pessoa, I. Tomaz, *Curr. Med. Chem.* 17 (2010) 3701.
- [27] M.J. Xie, X.D. Yang, W.P. Liu, S.P. Yan, Z.H. Meng, *J. Inorg. Biochem.* 104 (2010) 851.
- [28] Q. Wang, T.T. Liu, Y. Fu, K. Wang, X.G. Yang, *J. Biol. Inorg. Chem.* 15 (2010) 1087.
- [29] A. Zorzano, M. Palacin, I. Martí, S. García-Vicente, *J. Inorg. Biochem.* 103 (2009) 559.
- [30] F. Yraola, S. Garcia-Vicente, I. Martí, F. Albericio, A. Zorzano, M. Royo, *Chem. Biol. Drug Des.* 69 (2007) 423.
- [31] M.J. Pereira, E. Carvalho, J.W. Eriksson, D.C. Crans, M. Aureliano, *J. Inorg. Biochem.* 103 (2009) 1687.
- [32] M. Harilharan, S.S. Rajan, R. Srinivasan, *Acta Crystallogr., Sect. C* 45 (1989) 911.
- [33] S.L. Childs, L.J. Chyall, J.T. Dunlap, D.A. Coates, B.C. Stahly, G.P. Stahly, *Cryst. Growth Des.* 4 (2004) 441.
- [34] L.P. Lu, H.M. Zhang, S.S. Feng, M.L. Zhu, *Acta Crystallogr., Sect. C* 60 (2004) 0740.
- [35] M.L. Zhu, L.P. Lu, P. Yang, *Acta Crystallogr., Sect. E* 59 (2003) 0586.
- [36] L. Huang, P.-X. Xi, M. Xu, T.-H. Liu, Z.-Z. Zeng, *Anal. Sci.* 24 (2008) x289.
- [37] G.R. Willsky, L.-H. Chi, M. Godzala, P.J. Kostyniak, J. Smece, A.M. Trujillo, J.A. Alfano, D. Ding, Z. Hu, D.C. Crans, *Coord. Chem. Rev.* 255 (2011) 2258.
- [38] J.H.B. Scarpello, H.C.S. Howlett, *Diab. Vasc. Dis. Res.* 5 (2008) 157.
- [39] G.C. Graham, J. Punt, M. Arora, R.O. Day, M.P. Doogue, J.K. Duong, T.J. Furlong, J.R. Greenfield, L.C. Greenup, C.M. Kirkpatrick, J.E. Ray, P. Timmins, K.M. Williams, *Chin. Pharmacokinet.* 50 (2011) 81.
- [40] L.C.Y. Woo, The design and synthesis of vanadyl–biguanide complexes as potential synergistic insulin mimics (M.Sc. thesis), University of British Columbia, Canada, 1998.
- [41] L.C.Y. Woo, V.G. Yuen, K.H. Thompson, J.H. McNeill, C. Orvig, *J. Inorg. Biochem.* 76 (1999) 251.
- [42] A. Chatkon, Synthesis and structural study of materials combining metformin with other compounds used for diabetes therapy (Ph.D. thesis), Suranaree University of Technology, Nakhon Ratchasima, Thailand, 2012.
- [43] A. Chatkon, P.B. Chatterjee, M.A. Sedgwick, K.J. Haller, D.C. Crans, *Eur. J. Inorg. Chem.* (2013) 1859.
- [44] D.C. Crans, P.K. Shin, *J. Am. Chem. Soc.* 116 (1994) 1305.
- [45] D.C. Crans, J. Smece, E. Galidamauskas, L. Yang, *Chem. Rev.* 104 (2004) 849.
- [46] D. Rehder, *Bull. Magn. Reson.* 4 (1982) 33.
- [47] I. Correia, F. Aveçilla, S. Marcao, J.C. Pessoa, *Inorg. Chim. Acta* 357 (2004) 4476.
- [48] K. Bukietynska, K. Krot, P. Starynowicz, *Transition Met. Chem.* 26 (2001) 311.
- [49] O.W. Howarth, *Prog. NMR Spectrosc.* 22 (1990) 453.
- [50] L. Pettersson, B. Hedman, I. Andersson, N. Ingrì, *Chem. Scr.* 22 (1983) 254.
- [51] P. Ray, *Chem. Rev.* 61 (1961) 313.
- [52] G.M. Sheldrick, *Acta Crystallogr., Sect. A* 64 (2008) 112.
- [53] Bruker, *apex2* Software, Bruker AXS Inc., Madison, Wisconsin, USA, 2005.
- [54] Bruker, *smr*, Bruker AXS Inc., Madison, Wisconsin, USA, 2001.
- [55] M.N. Burnett, C.K. Johnson, *ORTEP-III Report ORNL-6895*, Oak Ridge National Laboratory, Tennessee, USA, 1996.
- [56] S.P. Westrip, *J. Appl. Crystallogr.* 43 (2010) 920.
- [57] N. Zaman, S.F. Darlow, *J. Bangladesh Acad. Sci.* 10 (1986) 79.
- [58] C. Trautwein, K. Kummerer, *Chemosphere* 85 (2011) 765.
- [59] H.H. Gadape, K.S. Parikh, *J. Chem.* 8 (2011) 767.
- [60] P.C. Bhamare, S.B. Bael, S. Natarajan, S.H. Patil, P.T. Shirode, *Int. J. Pharm. Tech. Res.* 3 (2011) 505.
- [61] F. Tache, M. Albu, *Rev. Roum. Chim.* 52 (2007) 603.

CURRICULUM VITAE

NUTTAPORN SAMART

e-mail: *nuttapornsamart@gmail.com*

Born: August 16, 1978, Nakhon Ratchasima

Citizenship: Thailand

Education

2009-2014 Doctor of Psychology, Chemistry, Suranaree University of
Technology, Nakhon Ratchasima, Thailand

2004-2007 Master Degree of Science, Chemistry, Suranaree University of
Technology, Nakhon Ratchasima, Thailand

Publications

Samart, N., Saeger, J., Haller, K. J., Aureliano, M., and Crands, D. C. (2014).
Interaction of decavanadate with interfaces and biological model membrane
system: characterization of soft oxometalates systems. **J. Mol. Eng. Mater.**
2(1): 1440007.

Samart, N., Gilmore, C., Haller, K. J., Rithner, C.D., and Crans, D. C. (2014).
Interaction of a Biguanide Compound with Membrane Model Interface
Systems: Probing the Properties of Antimalaria and Antidiabetic
Compounds. **Langmuir.** 30(29): 8697.